ABSTRACT

Title of Dissertation:	REGULATION OF MITOCHONDRIAL METABOLISM AND LIPOGENESIS IN THE LIVER
	Chaitra V. Surugihalli, Doctor of Philosophy, 2021
Dissertation directed by:	Assistant Professor, Nishanth E. Sunny, Department of Animal and Avian Sciences

Non-alcoholic fatty liver disease is one of the most common liver disorders with a global prevalence of over 25%. Fatty liver is the most common comorbidity of insulin resistance, obesity, and type 2 diabetes mellitus. During fatty liver, nutrient overload and the associated hyperinsulinemia results in elevated circulating free fatty acids and lipid accumulation in the liver. High rates of lipid accumulation in the liver is partly attributed to high rates of lipogenesis from carbohydrates, together with dysfunctional lipid oxidation. Further, these dysfunctional metabolic networks will induce oxidative stress and inflammation. Thus, understanding the metabolic mechanisms contributing towards the etiology of fatty liver and its associated morbidities is of major interest towards developing prevention and management strategies. This dissertation utilizes a combination of *in-vivo* (chicken and mice) and *in-vitro* (isolated mitochondria) systems with stable isotope-based methodologies to study metabolic regulation.

Chicken embryos utilize yolk lipids (>45%), deriving over 90% of their energy through lipid oxidation for development. However, during the last few days of incubation and immediately after hatch, there is a substantial induction of lipogenesis. Despite the hepatic lipid overload, the synergistic remodeling of hepatic metabolic networks during embryonic-to-neonatal development blunted inflammatory onset, prevented accumulation of lipotoxic intermediates, and reduced reactive oxygen species production.

Elevated plasma branched-chain amino acids (BCAAs) are a characteristic of insulin resistance and are relevant in predicting T2DM. Defects in BCAA degradation networks are also evident in several tissues during insulin resistance and associated co-morbidities. Furthermore, alterations in BCAA metabolism are associated with changes in lipogenesis and mitochondrial oxidative networks. We utilize a combination of isolated mitochondrial systems and stable isotope tracers in diet-induced mouse models of fatty liver, to determine its impact on mitochondrial metabolism and lipogenesis.

In summary, the dissertation highlights i) the importance of the natural but dynamic remodeling of hepatic mitochondrial metabolism and lipogenesis during the efficient embryonic-to-neonatal transition in chicken ii) the significance of BCAAs as important regulators of hepatic mitochondrial lipid metabolism. Thus, these studies provide a platform to modulate hepatic metabolic networks and utilize the embryonic-to-neonatal transition phase and dietary intervention of BCAAs as management strategies to alleviate metabolic dysfunctions.

REGULATION OF MITOCHONDRIAL METABOLISM AND LIPOGENESIS IN THE LIVER

by

Chaitra V. Surugihalli

Dissertation submitted to the Faculty of the Graduate School of the
University of Maryland, College Park, in partial fulfillment
of the requirements for the degree of
Doctor of Philosophy
2021

Advisory Committee:
Assistant Professor Nishanth E. Sunny, Chair
Professor Tom E. Porter
Professor Richard Kohn
Associate Professor Ganesh Sriram
Assistant Professor Sarah Kuzmiak-Glancy

Acknowledgements

First, I would like to thank my advisor Dr. Sunny for being the pillar of support and guiding me over the past 4.5 years. Thank you for being patient and training me to be the researcher I am today. Thank you being a great teacher and always being there. You are a great mentor!

I would like to thank Dr. Porter for his guidance, support and for being a wonderful collaborator. Thank you for letting me use your lab and resources and making the embryonic-to-neonatal transition project successful. I owe you all the knowledge of mammalian endocrinology, you are truly one of the best teachers.

My sincere thanks to Dr. Kohn, Dr. Glancy and Dr. Sriram for your support and guidance over the past 4 years. Also, thank you being wonderful teachers, I truly enjoyed and learned a lot from your courses.

I would also like to thank all the current and previous lab members for their help and support. A big thank you to Vaishna for her help with branched chain amino acid study, without her extensive help this project would have been difficult to complete. I also want to thank my undergraduates Angela, Kruti and David for analyzing datasets and helping me run experiments. Also, I want to thank to thank all our collaborators for helping me with the experiments.

I owe thanks to the Department of Animal and Avian Sciences for providing me with the opportunity to be a part of this wonderful department.

Last but not the least, I would like to thank my parents for their everlasting love and confidence in me. A special thanks to my husband Ajith for being patient

and understanding through the whole process, I could not have done this without your support. Thanks to my son Vihan for being a wonderful baby. Also, thank you Ronique and Jarvis for always being there for me!

Table of Contents

List of Tables

List of Figures

List of Abbreviations

Abbreviations	Name
AcAc	Acetoacetate
ACACA/ACC	Acetyl-CoA carboxylase alpha
AICAR	5-Aminoimidazole-4-carboxamide riboside
AMPK	AMP activated protein kinase
ANOVA	Analysis of variance
BCAAs	Branched-chain amino acids
BCAT	Branched-chain amino acid aminotransferase
BCAT	Branched-chain amino acid aminotransferase
BCKAs	Branched chain ketoacids
BCKDH	Branched chain alpha-ketoacid dehydrogenase complex
BHB	β-hydroxybutyrate
βHBDH	β-hydroxybutyrate dehydrogenase
Cox IV	Cytochrome c oxidase subunit 4
Cpt1a	Carnitine palmitoyltransferase 1-alpha
CS	Citrate synthase;
DAMPs	Damage associated molecular patterns
DNL	Percentage de novo lipogenesis
ELOVl6	Elongation of very long chain fatty acid elongase 6
e14	Embryonic day 14
e18	Embryonic day 18
FADS2	Fatty acid desaturase;
FAMEs	Fatty acid methyl esters
FASN	Fatty acid synthase
FFA	Free fatty acids
GAPDH	Glyceraldehyde 3-phosphate dehydrogenase
GC/MS	Gas chromatography mass spectrometry

GH	Growth hormones
GIT	Gastrointestinal tract
GSH	Glutathione
HB	High-fat diet supplemented 150% branched chain amino acids
HF	High-fat diet
HPLC	High-performance liquid chromatography
IR	Insulin resistance
IRS-1	Insulin receptor substrate
KIV	α-ketoisovalerate
KMV	α-keto-β-methylvalerate
Lac	Lactate
LC-MS/MS	Liquid chromatography-mass spectrometry
LB	Low-fat diet supplemented 150% branched chain amino acids
LDH	Lactate dehydrogenase
LF	Low-fat diet
MCAD	Medium chain acyl CoA dehydrogenase
mETC	Mitochondrial electron transport chain
mTORC1	Mammalian target of rapamycin complex 1
NAD(H)	Nicotinamide adenine dinucleotide
LDH	Lactate dehydrogenase
NAFLD	Non-alcoholic fatty liver disease
NASH	Non-alcoholic steatohepatitis
NEFA	Non-esterified fatty acids
NFkB	Nuclear factor kappa B
NLRs	Nucleotide binding oligomerization domain (NOD)-like receptors
NMR	Nuclear magnetic resonance
PC	Pyruvate carboxylase
PCK1	Phosphoenolpyruvate carboxykinase (cytoplasmic)

PCK2	Phosphoenolpyruvate carboxykinase
PEPCK	Phosphoenolpyruvate carboxykinase
PGC1a	Peroxisome proliferator-activated receptor gamma coactivator 1-alpha
ph3	Post-hatch day 3
ph7	Post-hatch day 7
PPARa	Peroxisome proliferator-activated receptor alpha
Pyr	Pyruvate
RCR	Respiratory control ratio
ROS	Reactive oxygen species
SCD1	Stearoyl-CoA desaturase 1
SEM	Standard Error of Means
SLC25A	Mitochondrial citrate carrier protein
SOD1	Superoxide dismutase
SREBP-1c	Sterol regulatory element binding protein
T2DM	Type 2 diabetes mellitus
TAG	Triacylglycerol
TCA cycle	Tricarboxylic acid cycle
TFAM	Mitochondrial transcription factor A
TLRs	Toll like receptors
TNFα	Tumor necrosis factor alpha
UPLC	Ultra-performance liquid chromatography
YSM	Yolk sac membrane

Chapter 1

Literature Review

1.1. Introduction

The liver is one of the critical organs weighing about ~2.5% of the body weight, but consuming around 20% of the oxygen indicative of its high metabolic activity [1-3]. The liver accommodates several central metabolic networks with dynamic shifts between states of feeding and fasting, in response to nutrient and hormonal stimuli [4,5]. Under fed conditions, the liver uptakes blood glucose, upregulates glycolysis, and synthesizes fatty acids through *de novo* lipogenesis. Whereas the fasted liver upregulates glycogenolysis (breakdown of glycogen), stimulates gluconeogenesis (new glucose synthesis), oxidizes fatty acids, and induces ketogenesis. The loss in metabolic flexibility of the liver and the concurrent failure of metabolic networks to switch efficiently between feeding and fasting can cause metabolic dysfunctions such as insulin resistance.

During insulin resistance, there is an increased flow of free fatty acids into the liver from adipose [6]. Further, a simultaneous upregulation in lipogenesis through dietary carbohydrates accumulates more lipids in the liver [7,8]. If the lipids accumulated in the liver exceed 5% of the liver weight, the condition is clinically considered as non-alcoholic fatty liver disease (NAFLD) [9-11]. NAFLD is one of the most common liver disorders with global prevalence at approximately 25% and is a common co-morbidity of insulin resistance, obesity, and type 2 diabetes mellitus (T2DM)[9,12]. NAFLD affects around 70% of T2DM patients and 90% of patients with hyperlipidemia [10,13,14]. High rates of lipid accumulation in the liver during NAFLD is partly attributed to high rates of lipogenesis, together with dysfunctional mitochondrial lipid metabolism. Chronic induction of lipogenesis in the liver and

dysfunctional mitochondrial metabolism is thought to induce oxidative stress and inflammation [13,15,16]. Therefore, understanding the metabolic and molecular mechanisms contributing towards the etiology of NAFLD is of major interest towards developing, prevention, and management strategies for the disease and its associated morbidities. In this dissertation, we utilize a combination of different in-vivo (chicken and mice) and in-vitro (isolated mitochondria) model systems to understand the factors regulating the remodeling of hepatic mitochondrial metabolism and lipogenesis.

In developing chicken embryos, the liver oxidizes yolk lipids (>45% of egg weight) as a major source of energy for embryonic development, deriving over 90% of the embryos' energy through lipid oxidation [17,18]. Further, during the last few days of incubation and immediately after hatch, there is a substantial induction of new lipid synthesis[17,19,20]. The embryonic to neonatal metabolic switch in chicken thus encompasses lipid burden from both lipid oxidation and triglyceride accumulation from lipogenesis in the liver. Interestingly, this lipid burden during embryonic to neonatal development is not associated with symptoms of inflammation or cellular stress, which is expected to be a side effect of such a metabolic milieu. In fact, the liver of mice models and human patients with non-alcoholic fatty liver disease presents an environment that accommodates high rates of fat oxidation and lipid synthesis like in embryos and neonatal chicken but is accompanied by cellular stress and onset of inflammation[15,21]. The results from this study would help us identify the molecular and metabolic adaptations in mitochondrial networks and lipogenic

machinery to prevent hepatocellular stress and inflammation during NAFLD and related dysfunctions.

Due to over-nutrition and subsequent insulin resistance, the liver loses its flexibility to remodel and adapt to nutrients and hormones favoring lipid accumulation. This failure leads to metabolic disturbances such as obesity, Type-2 diabetes (T2DM), and non-alcoholic fatty liver disease (NAFLD) [22,23]. During the initial stages of insulin resistance, there is a compensatory induction in metabolic networks. But, with the progression of the disease to a more severe stage, the metabolic networks fail to respond to hormonal cues and become inefficient leading to hepatocellular stress and inflammation. Therefore, understanding the molecular and metabolic parameters leading to metabolic dysfunction could be beneficial towards developing therapeutic and prevention strategies. Elevated levels of circulating branched-chain amino acids (BCAAs) are considered metabolic markers of insulin resistance and are predictors of T2DM onset in humans and rodent models [24-26]. The elevation in the levels of BCAAs are further linked to defects in their catabolic networks [24,27,28] and are considered as biomarkers of dysregulated lipid metabolism [29]. Further, the catabolic defects of BCAAs could cause anaplerotic stress to mitochondria and fail to induce TCA cycle leading to mitochondrial dysfunction[24,25]. The elevated BCAAs due to their catabolic defects could also contribute to impaired mitochondrial lipid metabolism [28]. Therefore, we utilize a combination of isolated mitochondrial systems and stable isotope tracers to establish the link between BCAAs and their degradation network to mitochondrial oxidative metabolism and lipid synthesis. The results from these studies will show the

relevance of BCAAs as molecular regulators of mitochondrial lipid metabolism and lipogenesis.

1.2. Overall Hypothesis

Co-ordinated and optimal remodeling of mitochondrial oxidative function and lipogenesis are central towards maintaining hepatic insulin sensitivity and preventing the onset of inflammation and hepatocellular stress.

We will test this hypothesis using the following two objectives:

Objective 1: Using 'embryonic to neonatal phase' in chicken as model to understand mitochondrial dynamics during lipid overburden in liver

Hypothesis: The onset of hepatocellular stress and inflammation is prevented during embryonic-to-neonatal development in chicken because of the optimal coupling between mitochondrial oxidative networks and lipogenesis.

Objective 2: To understand the impact of branched chain amino acids (BCAAs) on mitochondrial metabolism and lipogenesis

Hypothesis: The crosstalk between BCAAs and mitochondrial metabolism is mediated through the ability of BCAAs to alter hepatic lipid oxidation and, this alteration occurs independent of BCAAs being anaplerotic substrates to the mitochondria.

Towards profiling hepatic metabolism, we utilized stable isotope based approaches coupled with mass spectrometry (GC/MS) based metabolic flux analysis and metabolomics. Gene and protein expression profiles along with functional analysis of

circulating and tissue biomarkers were determined to obtain a snapshot of hepatic metabolism.

1.3. Hepatic insulin resistance and NAFLD

Insulin regulates cellular macronutrient homeostasis by signaling various anabolic processes during fed state [30]. Insulin is required for glucose disposal into peripheral tissues such as muscle and adipose [30,31],however the liver utilizes glucose independent of insulin action [31,32]. In muscle insulin supports storage of glycogen and in adipose insulin aids with lipid synthesis and storage [33,34]. Whereas, in the liver, insulin signals metabolic processes such as glycolysis, glycogen storage and lipid synthesis [30,32,34]. When peripheral tissues fail to respond to insulin actions, there is an increase in the circulating levels of glucose [35] and is referred as insulin resistance or 'impaired insulin-stimulated glucose disposal'. Moreover, insulin resistance is also believed to be the result of post-receptors defects in the insulin signaling network. In tissues like the liver, where insulin is not essential for glucose disposal, the attenuated response of insulin dependent metabolic networks suggests insulin resistance[36]. In normal conditions, the liver switches from a highly anabolic fed state (lipogenesis and glycolysis) to a catabolic fasted state (fat oxidation and gluconeogenesis). However, during over nutrition and subsequent insulin resistance, the liver loses its plasticity to adapt to nutrients and hormones favoring lipid accumulation leading to metabolic disturbances such as obesity, T2DM and NAFLD[23,37,38].

Insulin resistance is a common reason for lipid accumulation in the liver. Insulin mediated suppression of adipose lipolysis is subdued during insulin resistance

causing an increased flow of free fatty acids into the liver [15,36,39]. Further, i) increased expression of transcription factor sterol regulatory element binding protein-1c (SREBP-1c) and iii) suboptimal β-oxidation in the liver. All these metabolic events contribute towards triglyceride accumulation leading to NAFLD [15,16,40]. Clinically, NAFLD is associated with more than 5% fat in the liver. The sources of triglycerides include dietary fat, free fatty acids from lipolysis and hepatic lipogenesis from dietary carbohydrates [44]. Further, the excess lipid predisposes the liver to reactive oxygen species (ROS) due to impaired mitochondrial function and inflammatory cytokines worsening the disease condition [15,21,40].

NAFLD is the most common liver disease worldwide and is prevalent in over one-third adults in the united states [16,41]. It commonly co-exists with insulin resistance, T2DM and obesity [10,13,14]. During conditions of nutrient overload and/or high-fat diet induced obesity the liver accumulates excess triglycerides leading to fatty liver or simple steatosis [15,42,43]. Further, around 25% of patients with simple steatosis can develop a severe condition of hepatic inflammation, fibrosis and cellular damage called non-alcoholic steatohepatitis (NASH) [39,44]. NASH can further progress to a more severe condition of fibrosis which can result in cirrhosis and eventual liver failure [45]. Pathogenesis of NAFLD is stated as the "two-hit" hypothesis by Day and James in 1988 [46]. According to them the first hit was the metabolic disturbance such as insulin resistance leading to NAFLD and the second hit was the hepatic inflammation and injury that could lead to NASH [46].

In summary, insulin resistance during NAFLD fails to prevent lipolysis in adipose tissue causing elevated levels of free fatty acids in the plasma [6]. But, there is also a

concurrent induction in hepatic lipid synthesis from increased substrate flow to the liver [22,47]. This inability of insulin to suppress lipolysis and increased hepatic lipogenesis along with increase inflammatory response can aggravate the condition of NAFLD and progress towards NASH [21,40].

1.3.1. Mitochondrial metabolism during NAFLD

Mitochondrial dysfunction is a central feature of insulin resistant liver making it a potential target for treatment. Mitochondria plays an important role in responding to changes in cellular energy demands by integrating metabolic pathways such as ketogenesis, TCA cycle, β-oxidation, lipid synthesis and ATP production. Under normal conditions, the TCA cycle flux is coupled to mitochondrial respiration and ATP synthesis resulting in minimal ROS and cellular inflammation. However, in models of simple steatosis/ NAFLD, there is an immediate induction of ketogenesis in response to FFA overload and insulin resistance [15,16,21,40]. Further, there is a concurrent induction in β-oxidation, TCA cycle flux and mitochondrial respiration (**Figure 1.1**) [15,16,40] suggesting a compensatory mechanism of liver to dispose excess acetyl-CoA either via ketone production or complete oxidation to CO_2.

Moreover, insulin resistance fails to suppress adipose lipolysis and elevates free fatty acid flow into the liver resulting in lipid accretion [16,37,40,48]. As a compensatory mechanism to the lipid overload, the liver upregulates mitochondrial β-oxidation and ketogenesis. However, with the progression of the disease, the process become inefficient accumulating lipotoxic intermediates such as ceramides and diacylglycerols [15,21]. These toxic intermediates can further negatively regulate insulin signaling and can also activate several inflammatory pathways (eg., c-Jun N-terminal

kinase, toll-like receptor-4) [49]. Despite inefficient β-oxidation, TCA cycle remain sustained and continue complete oxidation of acetyl-CoA to support the cellular energy demands by further upregulating gluconeogenesis [16]. The chronic induction in TCA cycle can uncouple from mitochondrial respiration and ATP synthesis leading to excess ROS generation and tissue inflammation (**Figure 1.1**). But, NAFLD is also linked with reduced electron transport chain complexes, mitochondrial DNA copy number and mega mitochondria [40]. In fact, the defects in mitochondrial morphology and electron transport chain fuels oxidative stress and tissue inflammatory markers causing disease progression to NASH. This represents the eventual failure of liver to compensate for nutrient overload and to dispose excess lipids.

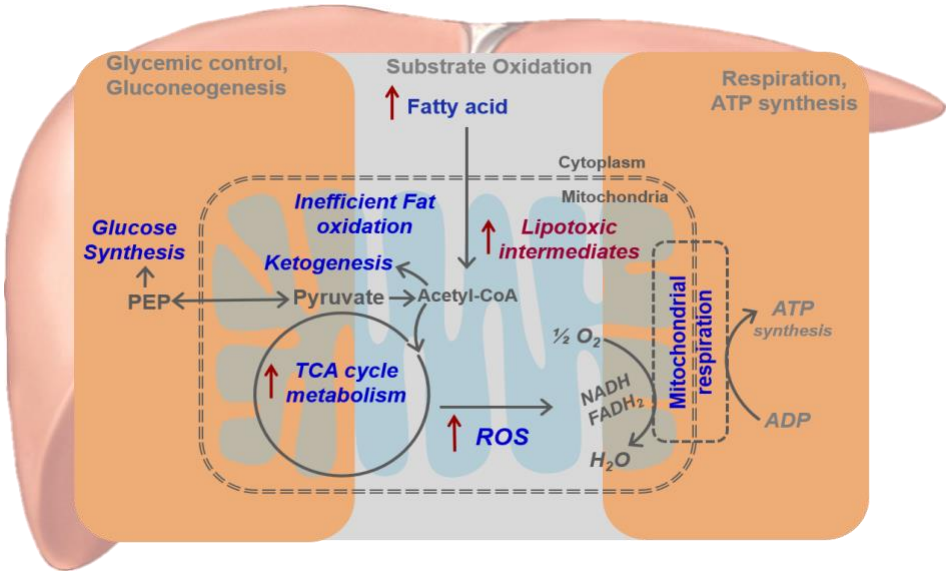

Figure 1.1. Mitochondrial dysfunction is a central feature of NAFLD. The increased free fatty acid flow into the liver i) induces mitochondrial β-oxidation and which with the progression of the disease becomes inefficient accumulating lipotoxic intermediates ii) shunts the excess acetyl-coa towards ketogenesis and iii) sustains a elevated TCA cycle metabolism which in turn uncouples from mitochondrial respiration and ATP synthesis causing ROS generation and tissue inflammation.

1.3.2. Mitochondrial metabolism, oxidative stress and inflammation

Mitochondria is one of the major sites for ROS production, a byproduct of normal cellular function other than peroxisomes and endoplasmic reticulum [50]. Complex I and III of mitochondrial electron transport chain (mETC) are contributors of ROS within the mitochondria [50-53]. However, when produced in excess, they can cause oxidative stress and inflammation.

Elevated levels of ROS can oxidize membrane lipids, proteins, and cause damage to DNA and other nucleic acids, leading to cellular stress and damage. ROS produced by a cell initiates the host defense system by inducing ROS-dependent inflammatory cytokines (TNFα), interleukins (IL6, IL18, etc.,) and various other pro-inflammatory factors such as NFkB and NLRP3 [54,55]. Mitochondrial ROS regulate redox-sensitive inflammatory pathways via NF-kB and NLRP3 [54]. Activation of damage associated molecular patterns (DAMPs) [56] by triggering toll like receptors (TLRs) and nucleotide binding oligomerization domain (NOD)-like receptors (NLRs) [55,56]. Activated NLRP3 can further stimulate caspase-1 which induce maturation of pro-inflammatory cytokines such as IL1β and IL18 [54,55,57]. Pro-inflammatory cytokines can also activate NF-kB to induce inflammatory response. Increased free fatty acids during NAFLD can also induce inflammatory pathways by directly interacting with TLRs and NLRP3 [58].

These activated inflammatory and pro inflammatory pathways (**Figure 1.2**) can further induce more ROS formation increasing the cellular damage and stress. Thus, mitochondria can be a novel target for treating metabolic diseases to alleviate ROS and control inflammation.

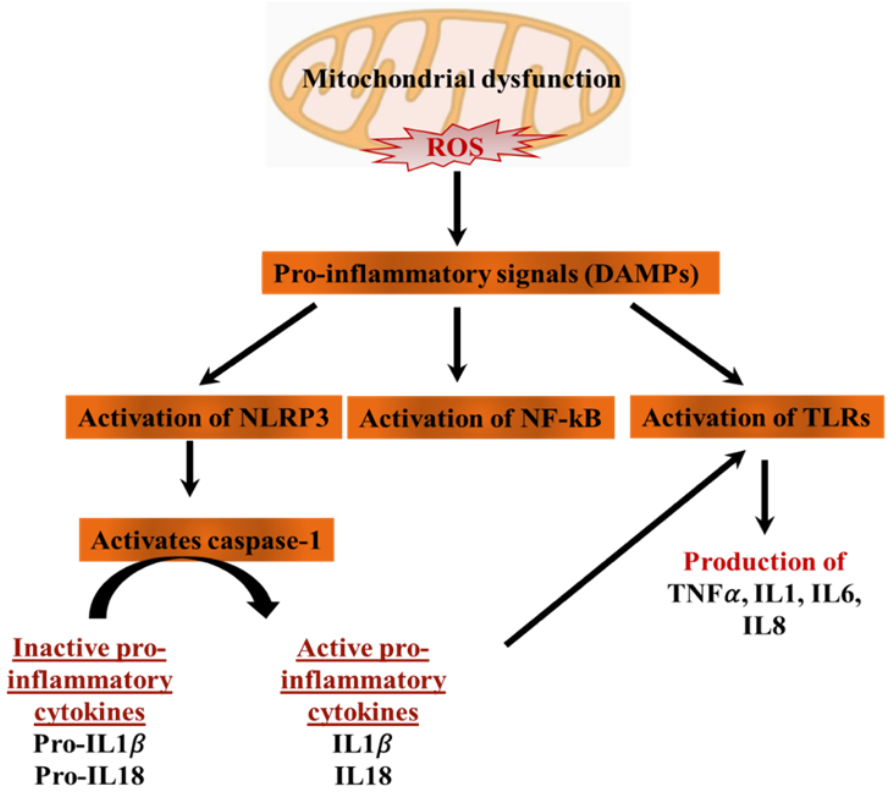

Figure 1.2. Mitochondrial ROS activates of pro-inflammatory networks contributing towards elevated interleukins and cytokines during NAFLD. Excess ROS generation during metabolic dysfunctions can signal pro-inflammatory pathways activating NLRP3, NF-kB and TLRs. Activated NLRP3 can further activate pro-inflammatory cytokines such as IL1β and IL18 via caspase-1. Active IL1β and IL18 can in turn activate TLRs which can also induce formation of other interleukins and inflammatory markers

1.4. Embryonic-to-neonatal transition in chicken: a unique model to study hepatic mitochondrial metabolism and lipogenesis

An embryo utilizes the nutrients available in the egg, which primarily include fats (>45% by dry weight) and proteins. However, the neonatal chickens are provided with >30% carbohydrates through the starter diet [59-61]. This change in substrate utilization during embryonic to neonatal development in chicken initiates a switch in hepatic lipid metabolism. The embryonic liver primarily utilizes yolk lipids, whereas the neonatal chicken liver catabolizes carbohydrates and accumulates lipids [59-61]. The embryo derives >90% of its energy from β-oxidation of yolk lipids and upregulates lipid synthesis after hatching from a high carbohydrate diet. This metabolic transition in chicken from higher rates of lipid oxidation (in embryos) to higher lipid synthesis (in neonates), accompanies hepatic lipid accumulation. A similar metabolic milieu of lipid overburden in human and rodent models of obesity or hepatic steatosis accompanies oxidative stress and inflammation. Interestingly, the liver of embryos and neonatal chicken do not display any symptoms of metabolic dysfunctions despite increased lipid accumulation. Therefore, the embryonic to neonatal transition phase provides a unique window to understand the optimum remodeling of metabolic networks to avoid hepatocellular stress and inflammation.

1.4.1. The avian egg

An avian egg comprises of the nutrients required for the normal development of the chicken embryo. The egg comprises of i) protective shell: 9-14 % ii) albumin or egg white: 52-58% and iii) vitellus or egg yolk: 32-35% [64]. The eggshell is predominantly made of calcium carbonate, foamy layer of protein (cuticle) stabilized

by matrix of interwoven protein fibers [64-66]. The water insoluble cuticle contains 90% proteins, which forms a protective layer on the shell surface [65]. The albumen or egg white is mostly comprised of water, proteins, lipids (0.03%), carbohydrates (>1%) and minerals required for the development. The yolk is considered as the nutrient rich fraction of the egg with 33% lipid, 17% protein and relatively smaller amounts of carbohydrates, vitamins and minerals[64]. **Table 1.1** lists the total composition of egg and is adapted from Romanoff, A. L *et al*., 1949).

Table 1.1: Overall composition of an egg [64]

Shell Composition		
Mineral	**Percentage (%)**	
Calcium Carbonate	98.2 %	
Magnesium	0.9 %	
Phosphorous	0.9%	
Egg composition		
Nutrients (%)	**Albumen**	**Yolk**
Water	84.3 - 88.8	48
Protein	9.7 - 10.6	15.7 - 16.6
Lipid	0.03	31.8 - 35.5
Carbohydrate	0.4 - 0.9	0.2 - 1.0
Elements		
Sulphur	0.195	0.016
Potassium	0.145 - 0.167	0.112 - 0.360
Sodium	0.161 - 0.169	0.070 - 0.093
Phosphorus	0.018	0.543 - 0.980
Calcium	0.008 - 0.02	0.121 - 0.262
Magnesium	0.009	0.032 - 0.128
Iron	0.0009	0.0053 - 0.011

1.4.2. Macronutrient metabolism during embryonic development

During development, the embryos depend on the macronutrient supply from yolk and albumen. They primarily utilize lipids and proteins to meet the energy demands during various stages to ensure optimum development.

Carbohydrate metabolism

An egg contain < 3% carbohydrates in the albumen and yolk combined. During early days of development, the embryo utilizes carbohydrates via anaerobic glycolysis because of limited oxygen supply [60]. During this period, an embryo utilize glucose to produce pyruvate via glycolysis, but due to lack of oxygen, pyruvate is converted to lactate to maintain glycolysis function [67]. However, after re-establishment of oxygen supply, lactate is recycled in liver to glucose through cori cycle [67,68]. However, the limitation in carbohydrates initiate the metabolic switch to fat utilization/oxidation once oxygen supply is established around day 11-14 of incubation[18,69].

The embryonic development is associated with continuous rise in plasma glucose concentration from <100 mg/dl in early embryos to 150-160 mg/dl in late embryos [69,70]. The low levels of glucose in the egg at the start of incubation and the steady increase in blood glucose concentration during development, suggests an active gluconeogenesis. Also, the activity of gluconeogenic enzymes such as pyruvate carboxylase (PC), phosphoenolpyruvate carboxykinase (PEPCK) reaches peak around 17-20 days of incubation and decreases thereafter [71]. The major gluconeogenic substrates utilized are lactate, pyruvate, dihydroxyacetone, glycerol and amino acids [72,73]. The glucose produced from these substrates are mostly stored in liver and

muscle as glycogen through glycogenesis and serves as an important source of energy for late embryo survival [67,72,73]. When the embryo approaches the plateau stage of O_2 consumption (day 19-21), the energy supply switches to glycolysis utilizing the glucose mobilized by gluconeogenesis from glycogen stores [68]. Further, glycolysis and gluconeogenesis play an important role in late embryonic development, piping and early post-hatch days.

Lipid metabolism

Lipids are the main components of egg yolk and contribute to >90% of energy during mid-late embryonic development. In fact, a respiratory quotient of 0.7 during mid-late embryonic stages confirms the lipid utilization/oxidation by embryos [74,75]. Triacylglycerols (TAGs) represents the major form of lipids in the yolk (67% w/w), phospholipids accounts for about 25% of yolk lipids and cholesterol forms about 5% of yolk lipids [64]. Whereas, cholesteryl ester and free fatty acids are found in trace amounts. TAGs entering the embryo is hydrolyzed into free fatty acids and glycerol via lipoprotein lipase. Glycerol is used as a gluconeogenic substrate and free fatty acids are used as substrate for β-oxidation through TCA cycle [68,73].

During the first half of incubation, the embryo take up only small proportions of yolk lipids [76]. However, around day 12 of incubation, the embryo significantly increases uptake of yolk contents through yolk sac membrane [17,76] and accounts for 15% increase in the embryonic liver weight between day 15 to 18. Additionally, carnitine palmitoyl transferase-1 (CPT-l), the enzyme responsible for the translocation of acyl groups into the mitochondria, is highly expressed in yolk sac membrane and the liver of late embryos, suggesting an increased fat oxidation via mitochondrial[76-79]. Also,

most of the enzymes involved in lipid metabolism are highly expressed in chicken embryos (one or more folds) compared to an adult bird or mammals [76,78]. However, the embryo utilizes only 75% of yolk lipid contents by day 21 (day of hatch) and the rest is internalized by the embryo into the body cavity starting day 19[17].

Amino acid metabolism

The yolk and albumen contain fixed amount of protein for the development and the amino acids start to appear in circulation from day 3 of incubation. An active amino acid transport system in the embryos during day 6 of incubation support the transport of amino acids to the embryo [80]. The free albumen is orally consumed by the embryo until day 19 of incubation from amniotic sac.

The amino acids profile of the egg remains the same throughout development and the amino acids are utilized at a constant rate from yolk and albumen [81]. Despite higher rate of protein accumulation in the embryonic liver, a significant amount of essential and non-essential amino acids remains unused until day 19 of incubation [81]. However, certain amino acids (eg., glycine and proline) are utilized at much faster rate and does not seem to be sufficient to at the end of incubation. These amino acids must be synthesized from other substrates and in fact, glutamine and glutamate are the potential candidates for synthesizing proline [81].

In addition to protein synthesis, amino acids serve as important substrates for gluconeogenesis during embryonic development. Amino acids such as glutamine and glutamate play a crucial role as gluconeogenic precursors during early development [67,72]. However, in the later stages, the non-essential amino acids are synthesized from glycerol via TCA cycle metabolism [73,82]. In summary, the amino acids are involved in

variety of function such as nitrogen utilization between tissues, protein synthesis, gluconeogenesis, nucleotide synthesis and substrates for mitochondrial TCA cycle.

1.4.3. Nutrient metabolism during embryonic to neonatal development

The embryo utilizes only 75% yolk lipids, and starting day 19 the yolk sac membrane (YSM) and its enclosed yolk are gradually taken up into the body cavity of the embryo [20,78]. Residual yolk and YSM uptake is completed before the chick is hatched and serve as energy reserve for newly hatched chick until they are fed. The residual yolk contains 50% lipids and accounts for 15% of hatchlings body weight [20,83] and 90% of which is used within 2 days after hatch. The yolk provides about 30% of the nutrients for initial growth and maintenance of the neonates [84].

The new hatchlings are provided with a diet containing ~ 30% carbohydrates and since the chicken lack glycogen at hatch, the diet help increasing liver glycogen gradually [85]. Also, carbohydrate diet feeding upregulates lipid accumulation in the neonatal chicken liver [20] associated with elevated hepatic triglycerides around 5-7 days post-hatch [84,86]. In summary, the neonatal chicks display high rates of lipogenesis and simultaneous triglyceride accumulation and suppressed lipid oxidation as an adaptation to high carbohydrate diet.

The post-natal development of chicks depends on the residual yolk, glycogen reserves, access to feed, maturity of gastrointestinal tract (GIT) and nutrient content of the feed [60,86]. Contribution of GIT to plasma glucose is low at hatch but increases after 3 days. Further, the lipoprotein levels are reduced by day one indicating a reduction in lipid transport. These metabolic adaptation highlights an increased

glucose absorption while reducing lipid transport after hatch [83,87] suggesting glucose to serve as a major energy source as the yolk lipids are exhausted [87].

1.4.4. Hormonal regulation of embryonic development

The development of endocrine system begins during early days of incubation. The hormones producing cells in pituitary, hypothalamus and pancreas start to appear between 3-8 days. The variation in hormone levels closely influence different stages of embryonic growth and development.

Plasma insulin levels continuously increase from embryonic day 10 (130 pg/mL) until 10 days after hatch (1217 pg/mL) [69, 89]. The insulin peaks during day 17 (460 pg/mL) of incubation, day 1 post-hatch (717 pg/mL) and day 5 post-hatch (842 pg/mL) [69,89]. A study from Hohlweg et al., showed that insulin can control and regulate the levels of amino acids in plasma, allantoic and amniotic fluids during embryonic development [35]. Also, a strong co-relation (r=0.6311) between chicken embryo body weight and plasma insulin [69] indicates the anabolic role of insulin in promoting protein deposition. Further, the infusion of various amino acids (leucine, isoleucine, lysine or phenylalanine) into liver can induce insulin release similar to glucose, suggesting the role of insulin in promoting muscle growth and development[35].

Like insulin, glucagon levels in plasma significantly increases from day 15 of incubation until hatch (429 pg/mL) [69]. A peak in glucagon levels during e18 is associated with lower glycogen in late embryonic liver suggesting a glucagon stimulated glycogenolysis [90] by activating glycogen phosphorylase. During, late embryonic days, glucagon induces gluconeogenesis to support piping and hatching by

releasing glucose[70, 90, 91]. A positive co-relation (r=0.6334) between plasma glucagon levels and embryo body weight [69] reflects a growth stimulating effect of glucagon[92]. The ratio of insulin to glucagon is significantly higher in the embryos during day15-17 (2 - 4), and drops during hatching and elevates after feeding (2 - 5.2). These data indicate the interactive role of insulin and glucagon in stimulating embryonic growth.

Corticosterone is the major glucocorticoid in birds and start to appear in plasma during embryonic day 4 and peaks right before hatch (49 ng/mL) [93,94]. Glucocorticoids stimulate hepatic gluconeogenesis by mobilizing extrahepatic amino acids. Also, they induce lipogenesis and glycogen deposit in the liver.

The catecholamines such as dopamine, norephinephrine and epinephrine are the adrenal hormones synthesized from tyrosine [95], and can be detected in plasma of day 9 embryos. However, their levels continue to increase until the time of hatch [96]. Catecholamines support glycogenolysis and lipolysis which result in the elevation of blood glucose and free fatty acids. Norepinephrine is the dominant hormone during embryonic development whereas at hatch adrenaline play a major role. However, despite the similar metabolic effects, adrenaline is less potent in chicken.

Growth hormones (GH) in the plasma are required for normal growth and development of the embryos and new chicks. GH is detected in neural tissue of the embryos during first week of incubation and is supplied to other tissues in the later days (Harvey 2001). Embryos have higher levels of circulating GH, which continue to rise until post-hatch day 5 and gradually plummets in the later days [97]. GH promotes lipolysis of the adipose and aid glycerol release and can induce gluconeogenesis and protein synthesis.

The thyroid hormones such as thyroxine (T_4) and triiodothyronine (T_3) are required to maintain normal body temperature. Plasma T_3 can be detected in the embryos from day 9 and the levels do not vary during mid incubation [69]. However, T_3 levels peaks during piping and hatching (897 pg/mL) and these levels increase with age of hatched chicks [69,98]. Whereas, the plasma T_4 levels increases during mid-incubation and peaks during hatching (day 19; 6.2 ng/mL). Further, the elevation in thyroid hormone receptors in the liver and brain during embryonic development parallels with T4 [69,98]. And, both T_3 and T_4 has a significant positive co-relation with embryo body weight [69], suggesting their role in maintaining normal growth and development.

1.4.5. Comparing chicken and mammalian lipid metabolism

Various studies in mammals and avian species suggests an existence of related metabolic pathways. In most mammals, lipogenesis takes place in both liver and adipose with adipose being the major site [99-101]. Also, the adipose tissue contributes for at least 50% of fatty acid synthesis and may contribute up to 95% in some occasions [101]. Conversely, in humans and chicken, the liver contributes around 90-95% towards de novo lipogenesis [102,103,104]. Although, the chicken adipose tissue can incorporate both acetate and glucose into fatty acids, the rate of incorporation is much greater in chicken liver [105,106] suggesting a higher rates of lipid synthesis in the liver.

The plasma insulin levels remain pharmacologically elevated in chicken and most other birds compared to mammals [107,108]. In rats, insulin exhibits antilipolytic action on glucagon stimulated adipose tissue lysis, causing a fall in plasma free fatty acid and glucose, but supports lipogenesis [109-111]. In chicken, insulin supports

glucagon induced lipolysis in the adipose but it remains either poorly sensitive or insensitive to lipogenic action of insulin [111]. In liver, insulin can stimulate lipogenesis and lipogenic enzyme activity in chickens and other avian species, but however they require relatively larger doses of insulin compared to humans or rodents [112,113].

1.5. Branched chain amino acids and metabolic health

Branched chain amino acids (BCAAs) include valine, leucine and isoleucine are essential for protein synthesis, cellular growth and glucose homeostasis [114]. BCAAs make up to 15-20% of total protein intake and form ~35% of the amino acid content in the muscle [114]. Insulin has an inhibitory action on amino acid release from muscle, hence their metabolic network is altered during conditions of insulin resistance [34,115]. BCAAs specially leucine is known to regulate insulin signaling by promoting activation phosphorylation of insulin receptor substrate (IRS-1) [116-118]. However, some research highlights negative feedback regulation of the insulin signaling network via BCAA mediated activation of the mammalian target of rapamycin complex 1 (mTORC1) [116,119].

Metabolic disorders such as insulin resistance are associated with elevated levels of circulating BCAAs and are considered predictors of type-2 diabetes onset[24,26,27,120]. The increased levels of circulating BCAAs are co-related to defects in their metabolic network [24,27]. Further, with confounding evidence in literature, it is still unclear if the elevated BCAAs are causal or causative agents of insulin resistance.

1.5.1. Branched chain amino acids catabolism

The increased levels of BCAAs and their degradation products branched chain keto-acids (BCKAs) are linked to defects in their catabolic network [24,27]. This highlights BCAA catabolic network as an important target of interest during onset and progressive stages of insulin resistance.

All three BCAAs share a common first step in their catabolic network. BCAAs are converted to their respective keto acids by reversible transamination reaction via branched-chain amino acid aminotransferase (BCAT) [121,122]. The transamination reaction occurs in-pair with interconversion of α-ketoglutarate and glutamate. Leucine produces α-ketoisocaproate (KIC), isoleucine forms α-keto-β-methylvalerate (KMV) and valine forms α-ketoisovalerate (KIV) [121,122]. The second step involves irreversible oxidative decarboxylation of BCKAs into CoA moeities, catalysed by branched chain alpha-ketoacid dehydrogenase complex (BCKDH) [121,122]. The following steps are unique to each BCAAs; Valine forms propionyl-CoA, leucine yields acetoacetate and acetyl-CoA and isoleucine can form both propionyl-CoA and acetyl-CoA. The propinoyl-CoA generated from valine and isoleucine catabolism is converted into methylmalonyl-CoA and succinyl-CoA. The CoA moieties are either completely metabolised into CO_2 or fuel mitochondrial TCA cycle by being carbon source or anaplerotic substrates for new glucose formation [27].

Tissue localization of BCAA catabolism

All the steps of BCAA catabolism occur in the mitochondria of the cell[27,121]. BCAT, the first enzyme involved in BCAA catabolism, is expressed in most organs of the body[123,124]. BCATm (mitochondrial isoform) minimally or not expressed in

liver but highly expressed in other tissues specially skeletal muscle[125,126] . Whereas the BCKDH activity is highest in the liver and low in muscle. In the skeletal muscle of humans and rat, the ratio of measured BCAT to actual BCKDH activities is ≥90[27,127]. The high ratio of BCAT: BCKDH in skeletal muscle i) allow transfer of BCAA nitrogen into BCKAs ii) favors release of BCKAs rather than their oxidation[27]. However, higher BCKDH activities and limited BCATm in the liver allows degradation of BCKAs[27].

BCAA Catabolism during metabolic diseases

Adipose tissue of humans with insulin resistance, T2DM and obesity was associated with significantly lower expression of genes involved in BCAA catabolism including BCATm, BCKDHA/B leading to increased levels of circulating BCAAs [27,125,128]. Similarly, BCAAs catabolic genes in muscle and liver of insulin resistant, obese and T2DM humans were lower compared to normal individuals [27,125,128]. The liver of an insulin resistant human was found to have lower expression of BCKDH gene and protein causing elevated levels of BCAAs in circulation [27]. These events suggest a dysregulated BCAA catabolism during metabolic syndrome such as insulin resistance leading to increased circulating BCAAs.

1.5.2. Interaction between BCAAs and mitochondrial metabolism

BCAAs can either have a catabolic or anabolic outcome based on signals from cellular requirements. These signals direct BCAAs to be either i) substrates for mitochondria and fuel TCA cycle or ii) initiate protein synthesis and aspects of lipid metabolism via mTOR[25,27].

BCAAs interact with hepatic mitochondria by being anaplerotic substrates and fuel TCA cycle [26]. In conditions, such as starvation or hormonal stimuli by glucagon, adrenaline, cortisol and growth hormone increase cellular uptake of BCAAs and favor their complete oxidation to CO_2 and/or conversion to glucose prior to complete oxidation [24]. BCAA degradation produce their respective BCKAs which further produce CoA moieties that can enter hepatic mitochondria as substrates. Carbons from leucine, a ketogenic amino acid enters TCA cycle as acetyl-CoA whereas carbons from isoleucine (ketogenic and gluconeogenic) and valine (gluconeogenic) form acetyl-CoA and/or succinyl-CoA[24,27]. These CoA moieties can in turn fuel TCA cycle as substrates and get completely oxidized or become carbons for glucose prior to complete oxidation[24,27].

BCAAs can also signal aspects of mitochondrial metabolism independent of being substrates. BCAAs and their degradation products BCKAs can interact with mTORC1 and regulate the downstream signaling network. Activated mTORC1 regulates i) PGC1a, a gene involved in mitochondrial biogenesis and ii) PPARa, a master regulator of lipid oxidation[24]. These signaling molecules in turn regulate various aspects of mitochondrial biogenesis, maintenance, and mitochondrial networks such as β-oxidation and electron transport chain.

1.6. Metabolic approaches to study hepatic oxidative metabolism and lipogenesis

We will primarily utilize the combination of stable isotope tracers and gas chromatography-mass spectrometry (GC-MS) to probe the hepatic mitochondrial oxidative function and lipogenesis. Utilizing an effective combination of analytical

and molecular techniques would to help us understand the hepatic lipid metabolism at the level of gene, protein and individual metabolites.

Metabolic pathways are complex and they integrate gene, environmental and tissue factors [129]. Metabolites include a distinct collection of varied molecular weight structures such as lipids, amino acids, peptides, nucleic acids and organic acids [129,130]. The analysis and identification of metabolites is a challenge, but can be accomplished by using analytical techniques including gas chromatography (GC), high-performance liquid chromatography (HPLC), ultra-performance liquid chromatography (UPLC), capillary electrophoresis (CE) coupled to mass spectrometry (MS) or nuclear magnetic resonance (NMR) [129-131]. The GC separation requires chemical modification of the metabolites (called derivatization) prior to analysis, which is well studied and works efficiently towards analyzing small molecules [130]. Due to high sensitivity and wide range of metabolites covered under GC, it is indeed a choice for biochemical analysis [132].

Various approaches can be used to investigate nutrient utilization via different metabolic pathways. In this dissertation, we utilize i) Stable isotope based metabolic profiling ii) Targeted analysis of metabolic intermediates by mass spec iii) Gene and protein expression profiles along with circulating and tissue biomarkers of mitochondrial oxidative metabolism, lipogenesis and oxidative stress.

1.7. Use of stable isotopes to study mitochondrial oxidative metabolism

Mass spectrometric analysis of stable isotope incorporation into metabolic intermediates can be precisely used to understand nutrient fluxes in tissue or in whole animal level. The stable isotopes such as ^{13}C, ^{2}H, ^{15}N, ^{18}O, and ^{34}S are particularly

useful in biological studies due to their natural occurrence [129,133]. The stable isotopes will allow us i) to predict the fragments of derivatized isotope-enriched molecules and ii) to obtain an identical ion spectrum signature of the unlabeled (naturally abundant) compound when using GC-MS. The mass isotopomer pattern, or distribution, can be analyzed using a combinatorial probability model by comparing measured abundances to theoretical distributions.

The activity of metabolic pathways can be analyzed in two ways: i) calculating the isotope enrichment into their intermediates and ii) quantifying the concentration of metabolites. As an example., [$^{13}C_6$]glucose can be used in several studies to quantify glycolysis and Krebs cycle activity [67,134,135]. Uniformly labelled glucose is labelled with ^{13}C at all carbons and thus is heavier by six mass units [M+6]. The glucose enters TCA cycle as a 3-carbon pyruvate molecule, and since all the carbons are derived from glucose, it would be labelled with ^{13}C at all carbons resulting in [M+3] pyruvate [67,134]. This information could be used to understand the carbon turnover in glycolysis and further in TCA cycle.

In this dissertation we utilize [$^{13}C_3$]pyruvate and other stable isotope tracers to analyze the different aspects of mitochondrial lipid metabolism. For example: uniformly labelled pyruvate [M+3] can be used to analyze the TCA cycle activity via isotopomer patterns of labeled carbon (M+1, M+2, M+3 etc.,) into its intermediates (e.g., [M+2]acetyl CoA, [M+2]citrate etc.,) by incubating the isolated mitochondria with [U^{13}C]pyruvate [136-138]. Measurement of ^{13}C labelling in TCA cycle intermediates and their transamination partners (**Figure 1.3**) provides a good comparison of the nutrient fluxes and insights into compartmentalization of these metabolites [67]. Also,

comparing isotopomer patterns of two intermediates can be used to derive relative contributions of metabolites to the respective pathway [67,135,139]. For example, the relative labeling patterns of isotopomer in citrate, can provide us with an insight of the activity of TCA cycle. An increased incorporation of ^{13}C from pyruvate can generate in [M+2] citrate suggesting an increased movement of the tracer carbon and thus a higher activity of Krebs cycle [139].

Stable isotope labeled standards can be used to quantify the relative pool sizes of the metabolic intermediates to calculate their abundance in tissue or plasma or isolated mitochondria. For example., A known concentration of [U^{13}C] citrate [M+6] can be spiked into the samples to find the concentration of unlabeled citrate [M] pool. The relative abundance of [M]citrate to [M+6]citrate would give us the concentration/pool size of citrate. A combination of information from stable isotope enrichment pattern and pool sizes of metabolites can be used to retrieve the information of carbon turnover and fluxes of the metabolic pathways.

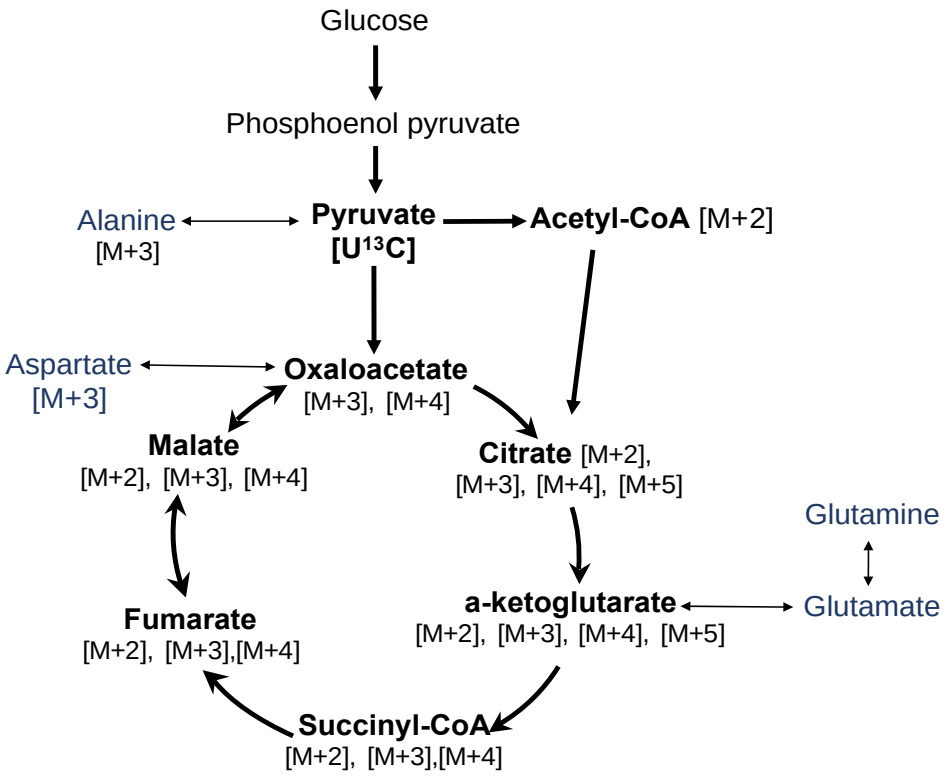

Figure 1.3. Expected isotopomer pattern of ^{13}C incorporation into TCA cycle intermediates from [$^{13}C_3$]pyruvate. Stable isotope labeled biomarker such as [$^{13}C_3$]pyruvate creates a isotopomer patterns in TCA cycle intermediates. The incorporation of ^{13}C into TCA cycle intermediates results in a major M+2 ion peak of TCA cycle intermediates. These footprints can be used to analyze the activity of mitochondrial TCA cycle.

1.8. Summary

It is clear from the available literature that the embryonic to post-hatch transition phase involves a dynamic switch from fatty acid utilization to lipid synthesis, which accompanies triglyceride accumulation in the liver. Despite high rates of fat oxidation and lipid synthesis, the embryo develops into a healthy chick without metabolic discrepancies. Therefore, this unique and natural phase can be probed to understand the interaction between mitochondrial oxidative metabolism and lipogenesis to minimize oxidative stress and inflammation. Literature also highlights the importance of BCAAs and their role in regulating aspects of cellular metabolism and protein synthesis. Although there is some recent evidence of interaction between BCAAs and lipid metabolism, their specific interaction with hepatic mitochondrial metabolism and lipogenesis needs attention. Literature highlights hepatic mitochondrial dysfunction as a comorbidity of insulin resistant and associated metabolic diseases. Further, literature also links elevated levels of circulating BCAAs as a marker of onset and progression of insulin resistance. Therefore, it is important to understand the interaction of BCAAs with mitochondrial metabolism during metabolic diseases.

To further understand the regulation of hepatic mitochondrial metabolism during metabolic diseases, this dissertation will focus on i) developing a new in-vivo model of 'embryonic to neonatal developmental phase' as unique window to study hepatic mitochondrial metabolism and aspects of lipid metabolism ii) Utilizing BCAAs as dietary intervention and highlighting their regulatory role in hepatic lipid metabolism and mitochondrial function.

Chapter 2

Hepatic Mitochondrial Oxidative Metabolism and Lipogenesis Synergistically Adapt to Mediate Healthy Embryonic-to-Neonatal Transition in Chicken

2.1. Abstract

During the normal embryonic-to-neonatal development, the chicken liver is subjected to intense lipid burden from high rates of yolk-lipid oxidation and from the accumulation of the yolk-derived and newly synthesized lipids from carbohydrates. High rates of hepatic lipid oxidation and lipogenesis are also central features of non-alcoholic fatty liver disease (NAFLD) in both rodents and humans, but is associated with impaired insulin signaling, dysfunctional mitochondrial energetics and oxidative stress. However, these adverse effects are not apparent in the liver of embryonic and neonatal chicken, despite lipid burden. Utilizing comprehensive metabolic profiling, we identify that steady induction of hepatic mitochondrial tri carboxylic acid (TCA) cycle and lipogenesis are central features of embryonic-to-neonatal transition. More importantly, the induction of TCA cycle and lipogenesis occurred together with the downregulation of hepatic β-oxidation and ketogenesis in the neonatal chicken. This synergistic remodeling of hepatic metabolic networks blunted inflammatory onset, prevented accumulation of lipotoxic intermediates (ceramides and diacylglycerols) and reduced reactive oxygen species production during embryonic-to-neonatal development. The natural but dynamic remodeling of hepatic mitochondrial oxidative flux and lipogenesis during the healthy embryonic-to-neonatal transition in chicken provides a road map to modulate hepatic metabolic networks and alleviate metabolic dysfunction during NAFLD.

2.2. Introduction

The prevalence of NAFLD is approximately 30% in the general population and over 70% in patients with type 2 diabetes mellitus (T2DM) [140,141]. Dysfunctional mitochondrial energetics, sustained lipogenesis, hepatocellular stress and inflammation are all central features of NAFLD and T2DM [40,142,143]. However, the metabolic mechanisms leading to these hepatic dysfunctions remain elusive. Hepatic mitochondrial oxidative function encompasses central pathways including β-oxidation, TCA cycle, respiratory chain and ketogenesis, which are vital in supporting gluconeogenesis and lipogenesis. As an inherent response to nutrient and hormonal overstimulation, these networks adapt and remodel during the progression of hepatic insulin resistance [144,145]. Thus, a compensatory induction in 'mitochondrial oxidative function' is shown to accompany early stages of hepatic insulin resistance [145-147]. However, with progressive severity of NAFLD and T2DM, certain networks (e.g. ketogenesis, mitochondrial respiratory chain and ATP synthesis) are impaired[40,143,148,149], while others (e.g. TCA cycle, lipogenesis) stay sustained [148,16,21]. Furthermore, chronic induction of oxidative flux through β-oxidation or TCA cycle can aggravate hepatocellular stress and inflammation in NAFLD [150-153]. Understanding the factors responsible for the optimal relationship between mitochondrial oxidative function, lipogenesis, hepatocellular stress and inflammation is of significant interest towards the management of NAFLD.

During the embryonic-to-neonatal development period in chicken, the liver presents a rapidly adapting and highly plastic metabolic environment, which transitions from fatty acid oxidation in the embryo to lipogenesis in the neonate

[70,17,60,62]. While the existence of this metabolic switch is known, the role of the hepatic mitochondrial networks in modulating this process is not clear. Furthermore, despite high rates of lipid oxidation during the embryonic stages and high rates of hepatic lipid accumulation in the neonate (from yolk lipids and lipogenesis), a healthy embryonic-to-neonatal transition ensues with no apparent symptoms of metabolic dysfunction, cellular stress or inflammation in the liver. This is unlike rodent models or humans with NAFLD, where high rates of lipid oxidation and hepatic lipid accumulation is concurrent to hepatocellular stress and inflammation [40,16,150]. We hypothesized that the onset of hepatocellular stress and inflammation is prevented during embryonic-to-neonatal development in chicken because of the optimal coupling between mitochondrial oxidative networks and lipogenesis. Targeted profiling of mitochondrial oxidative function and lipogenesis illustrate that the dynamic remodeling of metabolic networks in the liver, which in synergy with antioxidant defense deterred hepatic insulin resistance to mediate healthy embryonic-to-neonatal development.

2.3. Materials and methods

2.3.1. Study design. Experiments were conducted in accordance with the Institutional Animal Care and Use Committee protocols approved at the University of Maryland, College Park. Eggs (64 g ± 0.6 standard error of means; SEM) were obtained from Perdue Farms Inc. (Salisbury, MD) from a broiler flock (Ross 708; ~25-30 weeks old), and were incubated at 37°C, at 45% relative humidity. On the day of hatch (day 21), neonatal chicken were transferred to floor pens maintained at 37°C and were provided a starter diet (Diet S-G 5065; ASAP Feed and Bedding, Quakertown, PA)

ad libitum. Embryonic day 14 and 18 (e14 and e18) and post-hatch days 3 and 7 (ph3 and ph7) were selected for the experiments, with the following rationale. The late term embryonic liver rely predominantly on yolk-lipid oxidation and immediately post-hatch upregulate new lipid synthesis. Thus, the liver during e14 and e18 has high rates of lipid-oxidation and low lipid synthesis, while that of ph3 and ph7 has high lipogenesis and low lipid oxidation. For the studies, embryos were sacrificed by decapitation and, the neonatal chicken were decapitated following isoflurane anesthesia. Blood samples were centrifuged at 1500 X g for 10 min to separate serum. Liver samples were utilized for mitochondrial isolation and a section of the liver was flash-frozen in liquid nitrogen and stored at -80°C for future analysis.

2.3.2. Studies on isolated hepatic mitochondria

Mitochondrial isolation. Fresh livers were washed with ice cold phosphate buffered saline (PBS; 1X). Tissue (0.5-1g) was then minced in 2-4 mL MSHE buffer (70 mM sucrose, 210 mM mannitol, 5mM HEPES, 1 mM EGTA and 0.5% bovine serum albumin (BSA); pH 7.2) and homogenized in a Dounce homogenizer. The homogenate was diluted with 4mL of MSHE buffer and centrifuged at 800 X g for 10 mins at 4°C. The supernatant was then passed through a double layered cheese cloth and centrifuged at 8000 X g for 10 mins at 4°C, to obtain the mitochondrial pellet. This pellet was refined by re-suspending in 3 mL MSHE buffer and centrifuging at 8000 X g for 10 mins at 4°C, for two times. The final pellet was suspended in 100 µL MSHE buffer without BSA for estimation of mitochondrial protein using Pierce protein assay kit (Thermo Fischer Scientific. Waltham, MA).

Isolated hepatic mitochondrial incubations to determine changes in TCA cycle metabolism. Mitochondria (250 µg) was incubated with 1mM [$^{13}C_3$]pyruvate in 1mL MAS-3 buffer (115 mM KCl, 10 mM KH2PO4, 2 mM MgCl2, 3 mM HEPES, 1 mM EGTA and 0.2% fat free BSA; pH 7.2) containing 5 mM glutamate and 2.5 mM malate. Mitochondrial aliquots from each liver were incubated for 0, 5 and 10 min at 37 °C, following which the mitochondrial pellets were collected and stored at -80°C for determining the incorporation of ^{13}C into the TCA cycle intermediates by gas chromatography- mass spectrometry (GC-MS).

Another set of the mitochondrial samples (250 µg) were incubated as described above without the addition of the stable isotope tracer, to determine the changes in pool sizes of the TCA cycle intermediates. Levels of TCA cycle intermediates in the mitochondria were determined by GC-MS in relation to a known amount of stable isotope labeled internal standards.

Hepatic mitochondrial respiration. An oxygraph oxygen electrode (Hansatech Instruments, Norfolk, England) was utilized to measure oxygen consumption by isolated mitochondria (250 µg) suspended in 1-ml of MAS-3 buffer containing 5 mM glutamate and 2.5 mM malate. Basal (state II), ADP stimulated (with 100 µM ADP; state III) and ADP depleted (state IV) respiration rates were determined. Respiratory control ratio (RCR) was calculated as the ratio of state III to state IV respiration [40,172].

ROS generation by isolated hepatic mitochondria. Amplex Red reagent (10-acetyl-3,7-dihydroxyphenoxazine) in combination with HRP (horseradish peroxidase) was used to detect hydrogen peroxide (H_2O_2) released by the isolated mitochondria, by recording the real-time oxidation of Amplex red to the florescent resorufin.

Mitochondria (15 µg) was incubated with HRP (0.2 U/mL) and amplex red reagent (100 µM) prepared in MAS-3 buffer with glutamate and malate and the changes in fluorescence were detected at 585 nm using a Cytation 5 spectrophotometer (BioTek Instruments, Inc. Winooski, VT).

2.3.3. Metabolomic analysis

GC-MS analysis of mitochondrial and serum metabolites. TCA cycle intermediates were extracted from the mitochondrial pellet or the liver tissue in 750 µL chloroform: methanol (2:1) plus 250 µL water. The aqueous phase was dried and the metabolites were converted to their oximes with 2% methoxamine hydrochloride in pyridine (W/V) by microwaving for 90 sec, and then converted to their respective TBDMS (Tert-butyldimethylsilyl) derivatives [173].

Serum (25µL) spiked with [$^{13}C_4$]β-hydroxybutyrate (500µM; Cambridge isotopes, MA) were deproteinized with cold acetonitrile, dried and converted to its TBDMS derivative. All the metabolites were separated on a HP-5MS UI column (30 m × 0.25 mm × 0.25 µm; Agilent, CA) and fragmented under electron ionization and detected using single ion monitoring (SIM) on a GC-MS (5973N-Mass Selective Detector, 6890-Series GC, Agilent, CA) [21,173].

GC-MS analysis of triglyceride-free fatty acids. Frozen liver (~ 20-25 mg) was homogenized with 750µL chloroform: methanol (2:1) after addition of mixed U^{13}C fatty acid standard (Cambridge isotopes, MA). The lipid layer was dried and saponified with 0.5 N methanolic NaOH for 30 mins at 50°C. Fatty acid methyl esters (FAMEs) were generated with 1 mL of 2% methanolic sulphuric acid and incubation at 50°C for 2 h, then extracted with 2 mL hexane, dried and re-suspended in 50-100

µL hexane for GC-MS analysis. The FAMEs were separated on a VF 23ms column (30m × 0.25mm × 0.25µm; Agilent, CA) and fragmented under electron ionization under SIM on a GC-MS (5973N-Mass Selective Detector, 6890-Series GC, Agilent, CA). Concentrations were determined relative to their isotope-labeled internal standard.

GC-MS analysis of serum glucose and liver glycogen. Serum (25µL) and labeled internal standard ([$^{13}C_6$] glucose; 5.37 mM; Cambridge isotopes, MA) were mixed and deproteinized with 500µL acetonitrile and dried. The glucose was converted to its Di-O-isopropylidene derivative and separated on a HP-5MS UI column (30 m × 0.25 mm × 0.25 µm; Agilent, CA) under electron ionization (5973N-Mass Selective Detector, 6890-Series GC, Agilent, CA) [173].

For liver glycogen analysis [173], frozen liver (~ 20-25 mg) was deproteinized with 8% sulphosalicylic acid and glycogen was precipitated with cold ethanol. The glycogen pellet was washed with ethanol (2-3 times) to remove residual glucose and the pellet was air dried. The glycogen pellet was incubated with amyloglucosidase in acetate buffer with pH 5.0 (250 µL; 1 unit enzyme/ mg glycogen) for 1 h at 55°C. The released glucose was spiked with $^{13}C_6$ glucose internal standard and processed for GC-MS analysis.

LC-MS/MS analysis of serum and liver acylcarnitines. Serum (50 µL) and liver (20-25 mg) were homogenized and deproteinized with cold acetonitrile containing a known amount of stable isotope-labeled acylcarnitine internal standard (Cambridge Isotopes, MA), dried and reconstituted in 90:10 methanol-water for liquid chromatography-mass spectrometry (LC-MS/MS). The data was collected using

selected reaction monitoring (SRM) mode on a Thermo TSQ Quantum Access triple-quadrupole mass spectrometer with an Accela 1200 LC pump and Heated Electrospray Ionization (HESI) source (positive ionization). Reactions fragmenting to *m/z* 85.3 were monitored following a 5-µl injection on an ACE PFP-C18 column (100 × 2.1 mm, 2 µm particle size) at 40°C [26].

LC-MS/MS analysis of ceramides (Cer) and diacylglycerols (DAGs) in the liver. Livers from specific pathogen-free (SPF) leghorn chickens (layers) were obtained during the time periods - e18, ph0, ph3 and ph7 days (n=9) [21] Following pre-normalization to sample protein concentration (500 µg/ml), samples were Folch extracted and the organic layer was dried and reconstituted for LC-MS/MS analysis. Metabolomics profiling was performed on a Thermo Q-Exactive Oribtrap mass spectrometer with Dionex UHPLC and autosampler. All samples were analyzed in positive and negative heated electrospray ionization with a mass resolution of 35,000 at m/z 200 as separate injections. Separation was achieved on Acquity BEH C18 1.7 µm, 100 x 2.1 mm column for lipid metabolites [21,174].

2.3.4. **Liver histology.** Livers (~100-150 mg) from embryos and neonatal chicken were fixed in 4% neutral buffered formalin for 18-24 h, washed thrice and stored in 70% ethanol at 4°C. Hematoxylin and eosin (H&E) staining of liver tissue (n=3 per group) was performed by Histoserv, Inc., (Germantown, MD) to visualize lipid droplets and/or inflammatory foci.

2.3.5. **Gene expression analysis.** Total RNA was extracted from 20-25 mg of frozen liver using 500 µLTRIZOL reagent (Invitrogen, Carlsbad, CA) and mRNA mini prep kit (Bio-Rad Laboratories Inc., Hercules, CA) following which cDNA was prepared

from1 μg mRNA using cDNA synthesis kit (Bio-Rad, Hercules, CA). Quantitative real-time PCR was performed using 25 ng of cDNA, 150 nM of each primer, and 5 μl of SYBR green PCR master mix (Invitrogen, Carlsbad, CA) with GAPDH as housekeeping gene. Samples were run in triplicate on a Bio Rad CFX Real Time system (C1000 Touch Thermal Cycler). For genes with low expression profiles (*IL6* and *TNFA*), gene specific Bio-Rad iselect cDNA synthesis kit (Bio-Rad Laboratories Inc., Hercules, CA) was used to amplify gene expression. The list of primers is provided in the **Appendix Table 2.7**.

2.3.6. **Western blot analysis.** Total liver or mitochondrial protein was determined using pierce BCA protein assay kit (Thermo Fischer Scientific. Waltham, MA). Liver and mitochondrial proteins were separated using Bolt 8 % Bis-tris Plus gels (Invitrogen, Carlsbad, CA), transferred to a nitrocellulose membrane and incubated with primary antibodies (Akt, pAkt, COX IV, GAPDH, VDAC (Cell signaling technology Inc., Danvers, MA) and TFAM (Proteintech group, Rosemont, IL)). Total OXPHOS Rodent WB Antibody Cocktail (abcam plc., Cambridge, MA) was used to profile mitochondrial complex proteins involved in oxidative phosphorylation (Oxphos).

2.3.7. Biochemical assays. Serum non-esterified fatty acid (NEFA) concentrations were determined using HR Series NEFA-HR2 kit (WAKO diagnostics, CA). Serum insulin was determined by enzyme-linked immunoassay (Cusabio Biotech Co., Ltd., Houston, TX). Liver triglycerides (Serum triglyceride determination kit, Sigma Aldrich, St. Louis, MO) and catalase activity (Catalase Activity Assay kit; abcam plc., Cambridge, MA) were measured according to the manufacturer's protocol.

2.3.8. Statistical analysis

All the data reported is presented as mean ± standard error of means (SEM). Results were analyzed using one-way ANOVA, followed by a Tukey's multiple comparison test. Means were considered significantly different at $p \leq 0.05$. Linear regression and correlation analysis were conducted to calculate rates of ROS production (**Fig. 2.14A**) and determine the relationship between ROS and ADP stimulated respiration (**Fig. 2.14B**). All statistical analysis were conducted and the graphs were plotted utilizing Prism 7 (GraphPad software Inc., San Diego, CA).

2.4. Results

2.4.1. Remodeling of liver physiology with robust induction of hepatic insulin signaling during embryonic-to-neonatal development. Appendix Table 2.1 details the phenotypic characteristics during embryonic (e14 and 18) and the neonatal stages (ph3 and ph7) in chicken. As the liver size (g ± SEM) increased rapidly from e14 (0.2 ± 0.0) to ph7 (5.7± 0.5), the color of the liver grew pale, together with increased accumulation of lipid droplets, evident from the liver histology (**Fig 2.1A**). Furthermore, the transition from embryonic to neonatal stage was characterized by a several fold increase in circulating insulin (μIU/mL ± SEM; e14, 3.1 ± 0.1; ph7, 9.3 ± 1.1) (**Fig 2.2A**) and glucose (mM ± SEM; embryonic, 8.3 ± 0.4; neonatal, 12.2 ± 0.9) (**Fig 2.2B**), and also an increase in liver glycogen stores (**Fig 2.1B**), which peaked at ph3 period. These adaptations paralleled an induction of hepatic insulin signaling reflected by the higher phosphorylation of AKT from the embryonic to neonatal stages (**Fig 2.2C**). These results illustrate an ideal anabolic environment for the healthy metabolic development of an embryonic to neonatal liver.

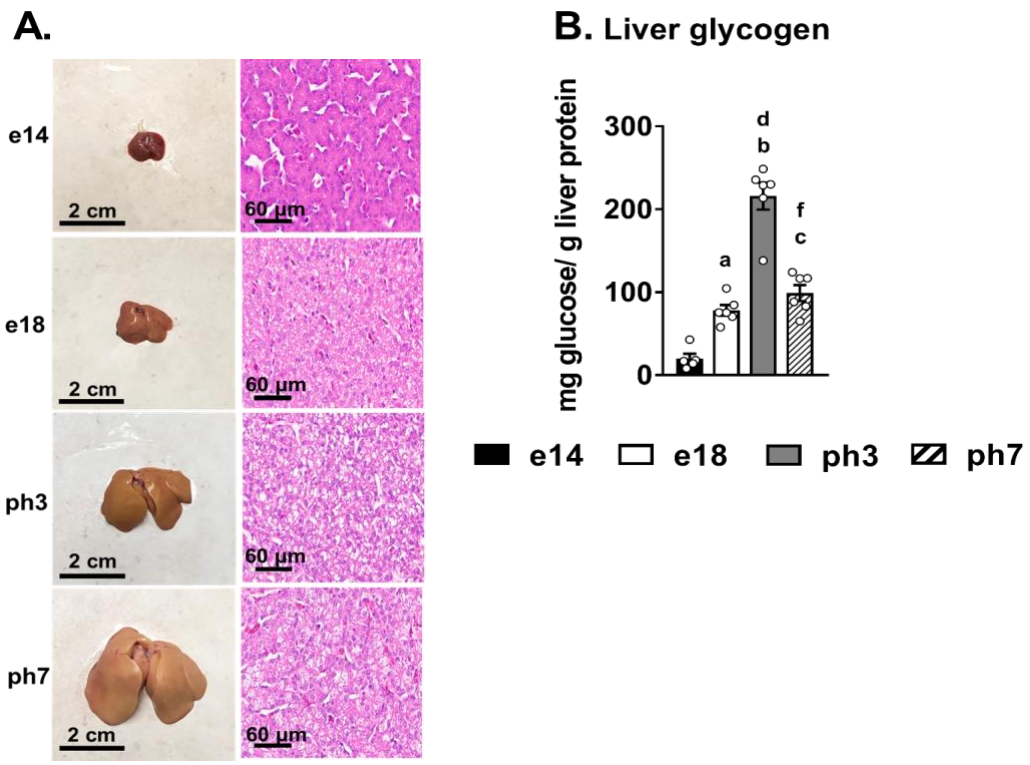

Figure 2.1. Anabolic adaptations in the liver during embryonic-to-neonatal transition in chicken. (**A**) Changes in liver size and appearance (left) and the corresponding histology (right; n = 3/group) illustrates progressive lipid accumulation. (**B**) Increase in liver glycogen content from the embryos to the neonates. Results (n = 6/group) were considered significant at $p \leq 0.05$ following pairwise mean comparisons, which are represented by the following alphabets. 'a'- e14 vs. e18; 'b' - e14 vs. ph3; 'c' - e14 vs. ph7; 'd' - e18 vs. ph3; 'e' - e18 vs. ph7; 'f' - ph3 vs. ph7.

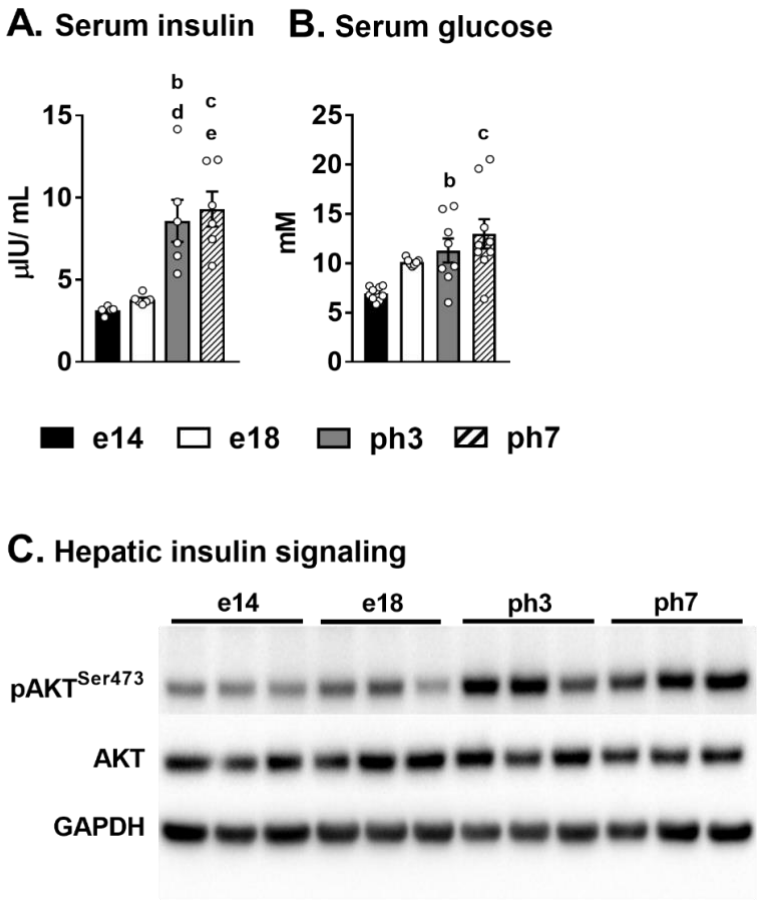

Figure 2.2. Hepatic insulin signaling during embryonic-to-posthatch transition. (A) Elevated levels of serum insulin in neonatal chicks compared to their embryonic counterparts. (B) Progressive increase in serum glucose and (C) Robust induction of hepatic insulin signaling as evidenced by higher phosphorylation of AKT, during embryonic-to-neonatal transition. Results (n = 6-9/group) were considered significant at $p \leq 0.05$ following pairwise mean comparisons, which are represented by the following alphabets. 'a'- e14 vs. e18; 'b' - e14 vs. ph3; 'c' - e14 vs. ph7; 'd' - e18 vs. ph3; 'e' - e18 vs. ph7; 'f' - ph3 vs. ph7. AKT, Protein Kinase B; GAPDH, Glyceraldehyde-3-phosphate dehydrogenase.

2.4.2. Metabolic switch from free fatty acid oxidation to triglyceride accumulation in the liver is a hallmark of embryonic to neonatal transition in chicken. Serum ketones (mM ± SEM) were high in e14 (3.2 ±0.2) and e18 embryos (3.9±0.5) but significantly dropped in ph3 (0.38 ± 0.04) and ph7 (0.30 ± .06) chicks (**Fig. 2.3A**). Hepatic triglyceride content (% of liver weight ± SEM) increased significantly from the embryonic period (0.5 ±0.0) to the neonatal period (8.9 ± 1.6) (**Fig. 2.3.A, Appendix Table 2.1**) The drop in serum ketone levels also paralleled a decrease in serum NEFA levels from the embryos to the neonates (**Fig. 2.3.B**). Further, the lower expression of genes (*CPT1A, MCAD*) (**Fig. 2.3.C**) regulating hepatic lipid oxidation together with lower plasma and hepatic carnitine and acylcarnitine profiles (**Appendix Table 2.2 & 2.3** and **Fig. 2.4A**) in the neonatal chicken signified the downregulation of hepatic lipid β-oxidation from embryonic-to-post-hatch. The changes in the AMPK protein expression parallels the extensive lipid oxidation during embryonic stages, especially embryonic day 18, as higher rates of AMPK phosphorylation is reflective of the high energy demands of the rapidly developing embryonic liver (**Appendix Fig. 2.2**).

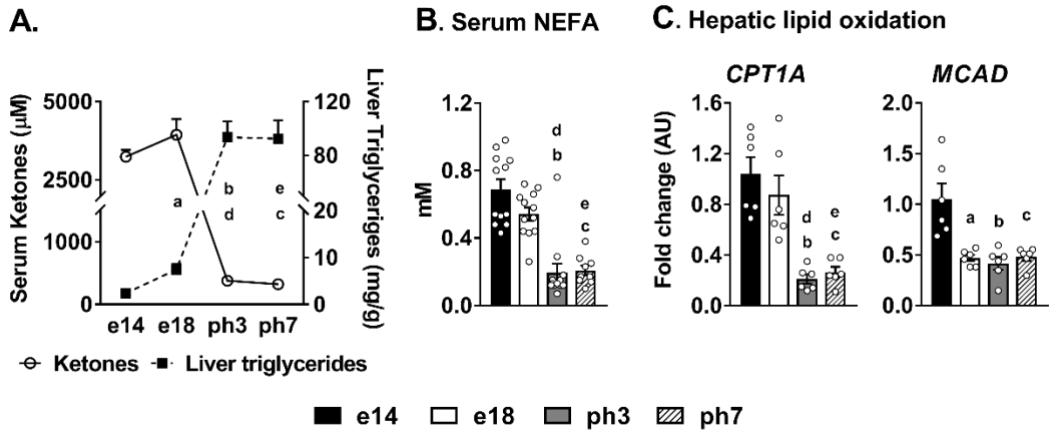

Figure 2.3. Metabolic switch from free fatty acid utilization/oxidation to triglyceride accumulation in the liver. (**A**) A dramatic reduction in serum ketones from the embryonic periods to the neonatal period, concurrent to rapid accumulation of liver triglycerides in the neonatal liver, signifies the metabolic switch from lipid utilization to accretion, (**B**) Serum NEFA levels are significantly lower in the neonatal chicken compared to their embryonic counterparts (**C**) Altered expression of genes associated with hepatic lipid oxidation (CPT1A and MCAD) substantiates the rapid metabolic switch from hepatic free fatty acid utilization in the embryos to lipid accumulation in the neonates. Results (n = 6-9/group) were considered significant at $p \leq 0.05$ following pairwise mean comparisons, which are represented by the following alphabets. 'a'- e14 vs. e18; 'b' - e14 vs. ph3; 'c' - e14 vs. ph7; 'd' - e18 vs. ph3; 'e' - e18 vs. ph7; 'f' - ph3 vs. ph7. NEFA, Non-esterified fatty acids; CPT1A, Carnitine palmitoyltransferase 1-alpha; MCAD, Medium chain acyl CoA dehydrogenase; AU, arbitrary units.

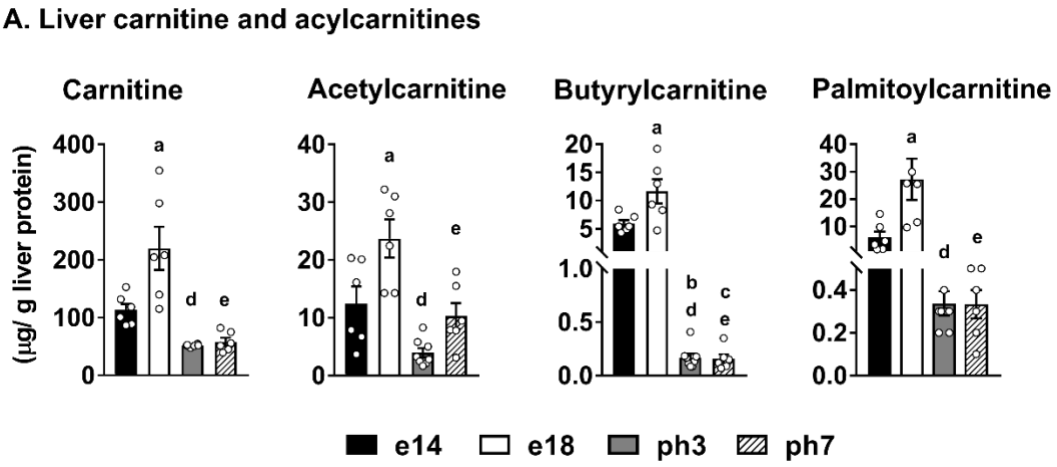

Figure 2.4. Changes in liver acylcarnitine levels. (**A**) Liver carnitine and acyl carnitines (also see **Appendix Tables 2.2** and **2.3** for all the serum and liver acyl carnitine profiles) which fuels high rates of mitochondrial β-oxidation in the embryonic liver were significantly lower in the neonatal liver. Results (n = 6/group) were considered significant at $p \leq 0.05$ following pairwise mean comparisons, which are represented by the following alphabets. 'a'- e14 vs. e18; 'b' - e14 vs. ph3; 'c' - e14 vs. ph7; 'd' - e18 vs. ph3; 'e' - e18 vs. ph7; 'f' - ph3 vs. ph7.

2.4.3. The dramatic upregulation of lipogenesis accelerates triglyceride accumulation in the liver. As there is significant upregulation of lipid accumulation in the liver of the neonate, we profiled the expression of lipogenic genes. *ACACA*, which converts acetyl CoA to malonyl-CoA and was upregulated 100 and 75-fold in ph3 and ph7 chickens, respectively (**Fig. 2.5A**). Similarly, fatty acid synthase (*FASN*) which facilitates the conversion of malonyl-CoA into palmitate was upregulated 300-fold in the neonatal chicken liver (**Fig. 2.5B**). Elongation of very long chain fatty acid elongase (*ELOVL6*), which regulates fatty acid elongation, was 200-fold higher in neonates (**Fig. 2.5D**). Moreover, fatty acid desaturases, including stearoyl-CoA desaturase 1 (*SCD1*) and the fatty acid desaturase (*FADS2*) were induced several thousand-fold in the neonatal liver (**Fig. 2.5C** & **2.5E**). These results illustrate the major role of lipogenesis towards lipid accumulation in the neonatal chicken liver. Furthermore, the triglyceride derived-palmitate, palmitoleate, stearate, oleate and linoleate were all significantly elevated in the liver of neonatal chicken (**Fig. 2.6A-E**). Most of these triglyceride derived-fatty acids are derived from the starter diet and the residual yolk lipids, but further contribute to the hepatic lipid accumulation.

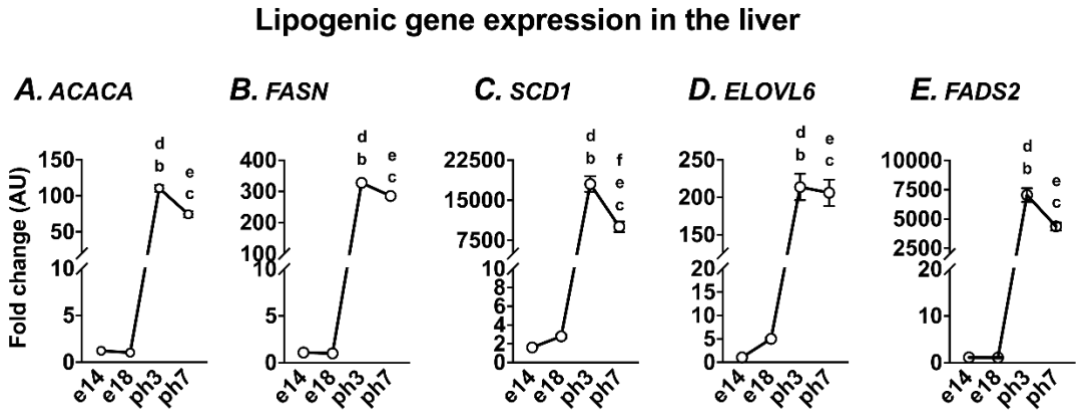

Figure 2.5. Lipogenesis is a significant contributor to triglyceride accumulation in the neonatal chicken liver. (**A**-**E**) Dramatic upregulation of lipogenic gene expression (ACACA, FASN, SCD1, ELOVL6, FADS2) provides evidence for the major contribution of hepatic lipogenesis towards lipid accretion. Results (n = 6-10/group) were considered significant at $p \leq 0.05$ following pairwise mean comparisons, which are represented by the following alphabets. 'a'- e14 vs. e18; 'b' - e14 vs. ph3; 'c' - e14 vs. ph7; 'd' - e18 vs. ph3; 'e' - e18 vs. ph7; 'f' - ph3 vs. ph7. ACACA, Acetyl-CoA carboxylase alpha; FASN, Fatty acid synthase; SCD1, Stearoyl-CoA desaturase 1; ELOVl6, Elongation of very long chain fatty acid elongase 6; FADS2, Fatty acid desaturase; AU, arbitrary units.

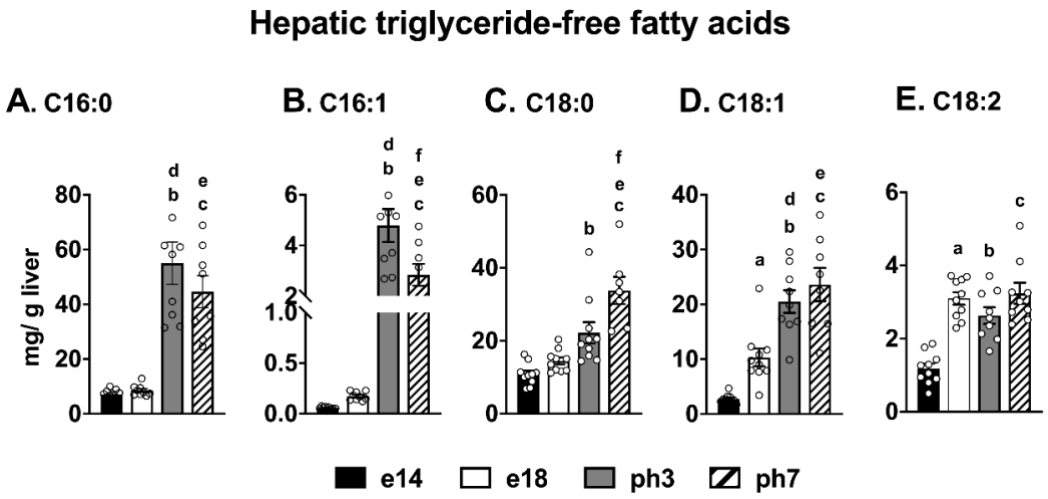

Figure 2.6. Triglyceride-derived fatty acids during embryonic-to-neonatal transition. (**A-E**) The significant increase in triglyceride-derived free fatty acids (C16:0, C16:1, C18:0, C18:1, C18:2) in neonatal chicks, typically derived from the residual yolk and the starter diet, contributes further to hepatic lipid accumulation. Results (n = 6-10/group) were considered significant at $p \leq 0.05$ following pairwise mean comparisons, which are represented by the following alphabets. 'a'- e14 vs. e18; 'b' - e14 vs. ph3; 'c' - e14 vs. ph7; 'd' - e18 vs. ph3; 'e' - e18 vs. ph7; 'f' - ph3 vs. ph7. C16:0, Palmitate, C16:1, Palmitoleate, C18:0, Stearate, C18:1, Oleate, C18:2, Linoleate.

2.4.4. Hepatic mitochondria in the embryonic and neonatal chicken are primed for substrate oxidation and maintains excellent respiratory control. We determined how high rates of lipid oxidation and lipogenesis impacted liver mitochondrial remodeling. Mitochondrial protein content, when expressed per gram liver peaked at e18 and decreased at ph3 and ph7, with the ph7 values similar to those on e14 (**Fig. 2.7A**). However, total mitochondrial content, on a whole liver basis continued to increase from e14 to ph7 (**Fig. 2.7A**). We then determined the expression patterns (per unit of liver protein) of specific mitochondrial proteins in the liver tissue, as an index of mitochondrial content of the liver (**Fig. 2.7B, Appendix Fig. 2.3A-C)**. While the voltage dependent anion channel (VDAC) protein expression showed a steady increase through e14 to ph3, the expression of the mitochondrial transcription factor A (TFAM) and cytochrome c oxidase subunit 4 (Cox IV) plateaued after an initial significant increase from e14 to e18. To evaluate efficiency and function, mitochondrial oxygen consumption [40,154] was determined under basal and ADP stimulated conditions. Basal oxygen consumption remained similar between the embryonic and neonatal liver mitochondria (**Fig. 2.8A**). However, ADP stimulated respiration (state III), resulted in the highest oxygen consumption rates during e18, which then tapered to e14 levels by ph7 (**Fig. 2.8B**). Interestingly, the respiratory control ratio (RCR), determined as the ratio of state III to state IV (**Fig. 2.8C**) respiration, did not vary and remained high (~ 4 to 6) through the embryonic-to-neonatal development (**Fig. 2.8D**). Further, the expression of the mitochondrial Oxphos complex proteins in the liver were highest during e18 and ph3, and tapered off in the ph7 mitochondria (**Figure. 2.8E; Appendix Fig. 2.3D-G**).

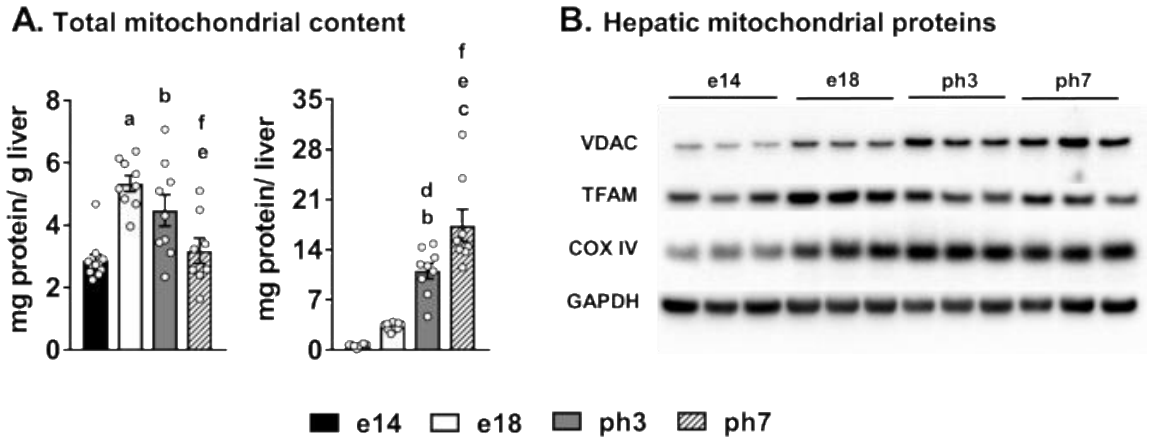

Figure 2.7. Changes in mitochondrial proteins in the liver during embryonic to neonatal transition. (**A**) Total mitochondrial protein content in the liver expressed on a per gram liver and whole liver basis. (**B**) Changes in expression of hepatic mitochondrial proteins (VDAC, TFAM and COX IV) in the embryos and the neonates. Results (n = 6-9/group) were considered significant at $p \leq 0.05$ following pairwise mean comparisons, which are represented by the following alphabets. 'a'- e14 vs. e18; 'b' - e14 vs. ph3; 'c' - e14 vs. ph7; 'd' - e18 vs. ph3; 'e' - e18 vs. ph7; 'f' - ph3 vs. ph7. VDAC, Voltage dependent anion channel; TFAM, Mitochondrial transcription factor A; COX IV, Cytochrome c oxidase subunit 4; GAPDH, Glyceraldehyde-3-phosphate dehydrogenase.

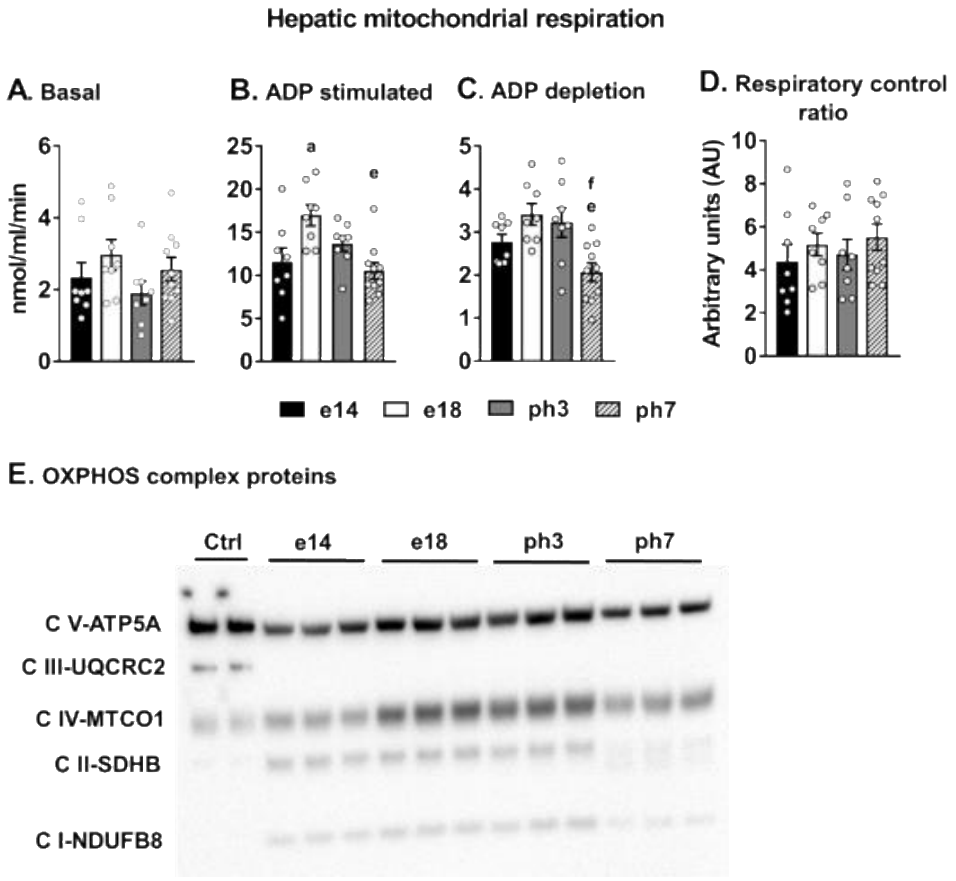

Figure 2.8. Changes in mitochondrial respiration and Oxphos proteins in the liver during embryonic to neonatal transition. Oxygen consumption by the liver mitochondria determined under (**A**) Basal, (**B**) ADP stimulated and (**C**) ADP depleted states, and the (**D**) Respiratory control ratios in the embryos and the neonates. (**E**) Western blot analysis of changes in the expression of the mitochondrial Oxphos protein complexes Graphical representation in **Appendix Fig. 2.3**). (Results (n = 6-9/group) were considered significant at $p \leq 0.05$ following pairwise mean comparisons, which are represented by the following alphabets. 'a'- e14 vs. e18; 'b' - e14 vs. ph3; 'c' - e14 vs. ph7; 'd' - e18 vs. ph3; 'e' - e18 vs. ph7; 'f' - ph3 vs. ph7. Oxphos, Oxidative phosphorylation.

2.4.5. Induction of hepatic mitochondrial TCA cycle accompanies high rates of lipogenesis. Hepatic TCA cycle plays a critical role in integrating mitochondrial function. To profile TCA cycle metabolism, we incubated isolated mitochondria (250 µg) in respiration buffer containing uniformly labeled [$^{13}C_3$]pyruvate for 10 and 20 min. The incorporation of ^{13}C from pyruvate into TCA cycle intermediates including citrate, α-ketoglutarate, succinate, fumarate and malate was determined using gas chromatography-mass spectrometry (GC-MS). First, there was significant incorporation of ^{13}C into all the TCA cycle intermediates for e14, e18, ph3 and ph7 (**Fig. 2.9A, 2.9B,** and **Appendix Tables 2.4 & 2.5**). More interestingly, the rate of incorporation of ^{13}C was significantly higher ($p<0.05$) in metabolites from e18, ph3 and ph7, compared to their e14 counterparts (**Fig. 2.9A, 2.9B,** and **Appendix Tables 2.4 & 2.5**). These results illustrate the significant upregulation of hepatic TCA cycle activity between e14 and e18 of development.

We further determined the changes in the 'pool sizes' of the TCA cycle intermediates, following 0, 5 or 10 min of incubation of the mitochondria (250 µg) in a respiration buffer. Hepatic mitochondria from ph3 and ph7 had significantly higher ($p<0.05$) levels of TCA cycle intermediates compared to their e14 and e18 counterparts (**Fig. 2.10A, 2.10B,** and **Appendix Table 2.6**). Further, changes in the pool sizes of specific TCA cycle intermediates were also observed with 5 and 10 min of incubation. For example, α-ketoglutarate levels increased steadily with the time of incubation (0 to 10 min) in e14, e18, ph3 and ph7 liver mitochondria (**Fig. 2.10A**). Considering the rate-limiting nature of α-ketoglutarate in driving TCA cycle flux [155,156] this response could point to α-ketoglutarate synthesis from other carbon sources

(e.g. amino acids). On the contrary, citrate pool size decreased from 0 to 10 min of mitochondrial incubation, and more interestingly, only in the ph3 and ph7 liver mitochondria (**Fig. 2.10B**). Considering the high lipogenic capacity of ph3 and ph7 livers (**Fig. 2.5**) and the role of citrate as a precursor for the lipogenic acetyl CoA, changes in citrate pool sizes from 0 to 10 min could reflect the export of citrate out of the mitochondria, as a potential substrate for ATP citrate lyase. A general induction in the expression of genes (e.g. *CS*, *PCK1*, and *PCK2*) involved in the regulation of mitochondrial TCA cycle was also evident from e14 to ph7 (**Fig. 2.11A**), substantiating the overall induction of the TCA cycle activity.

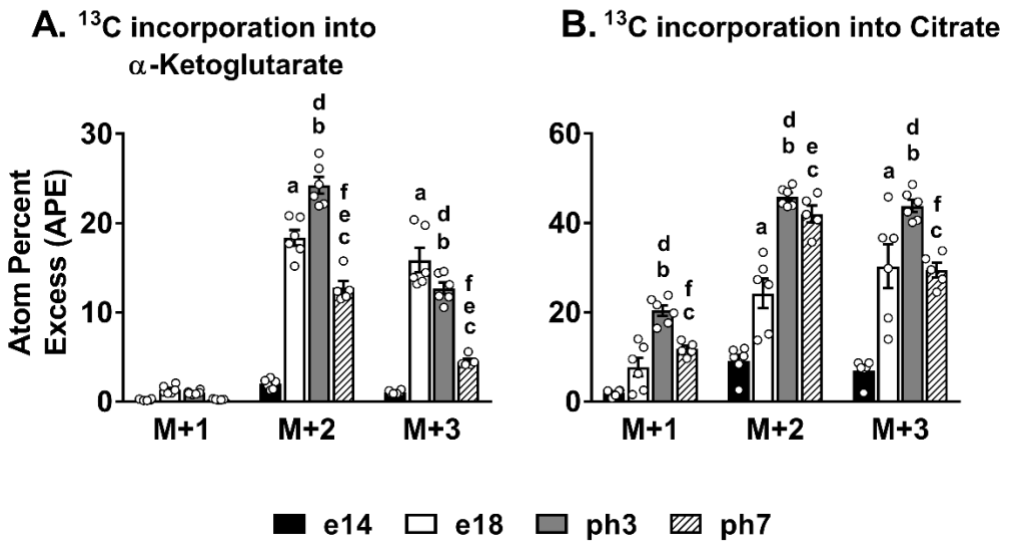

Figure 2.9. Changes in ^{13}C incorporation from [$^{13}C_3$]pyruvate into TCA cycle intermediates from during embryonic-to-neonatal transition. Increased ^{13}C incorporation from [$^{13}C_3$]pyruvate into (A) α-ketoglutarate and (B) citrate after 10 min of mitochondrial incubation in e18 and ph3 illustrate elevated mitochondrial TCA cycle activity. **Appendix Tables 2.4 & 2.5** provides the ^{13}C enrichments in all TCA cycle intermediates following 10 min and 20 min of mitochondrial incubations respectively. Results (n = 6-9/group) were considered significant at $p \leq 0.05$ following pairwise mean comparisons, which are represented by the following alphabets. 'a'- e14 vs. e18; 'b' - e14 vs. ph3; 'c' - e14 vs. ph7; 'd' - e18 vs. ph3; 'e' - e18 vs. ph7; 'f' - ph3 vs. ph7.

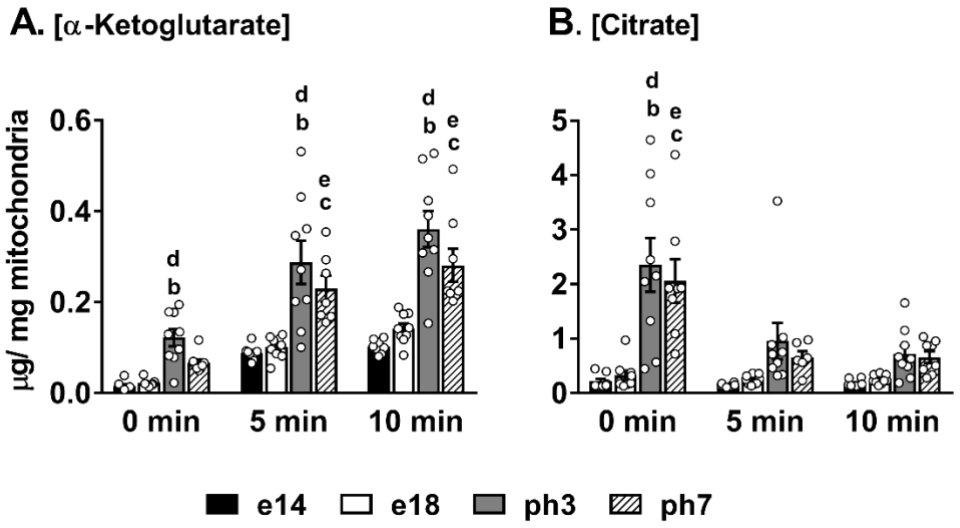

Figure 2.10. Changes in concentration of TCA cycle intermediates during embryonic-to-neonatal transition. Changes in concentrations of (**A**) α-ketoglutarate and (**B**) citrate following incubation of 250µg of mitochondrial from each group for 0, 5, and 10 minutes (**Appendix Table 2.6** for the changes in concentrations of succinate, fumarate and malate). Results (n = 6-9/group) were considered significant at $p \leq 0.05$ following pairwise mean comparisons, which are represented by the following alphabets. 'a'- e14 vs. e18; 'b' - e14 vs. ph3; 'c' - e14 vs. ph7; 'd' - e18 vs. ph3; 'e' - e18 vs. ph7; 'f' - ph3 vs. ph7.

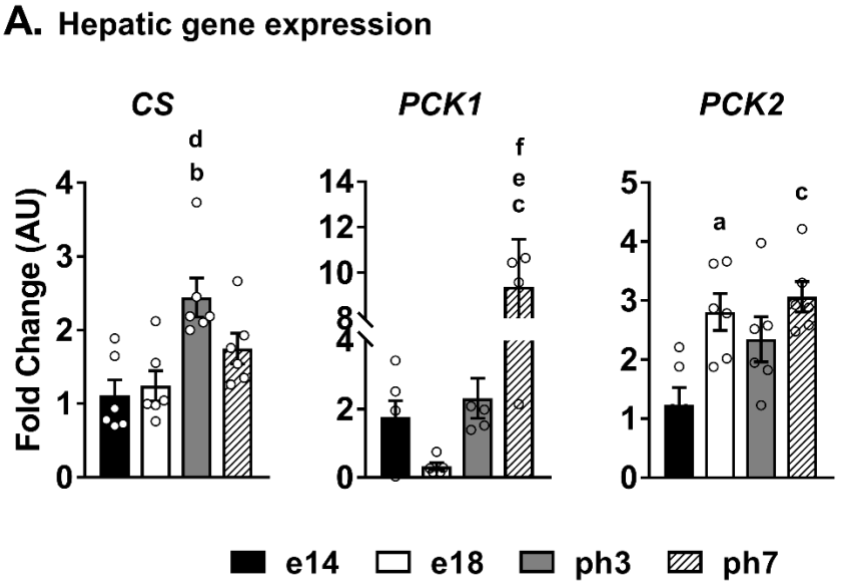

Figure 2.11. Changes in hepatic mitochondrial gene expression. (**A**) Changes in the expression of genes involved in the regulation of hepatic TCA cycle metabolism (CS, PCK1 and PCK2). Results (n = 6-9/group) were considered significant at $p \leq 0.05$ following pairwise mean comparisons, which are represented by the following alphabets. 'a'- e14 vs. e18; 'b' - e14 vs. ph3; 'c' - e14 vs. ph7; 'd' - e18 vs. ph3; 'e' - e18 vs. ph7; 'f' - ph3 vs. ph7. CS, Citrate synthase; PCK1, Phosphoenolpyruvate carboxykinase (cytoplasmic); PCK2, Phosphoenolpyruvate carboxykinase (mitochondrial).

2.4.6. Simultaneous upregulation of hepatic lipogenesis and TCA cycle did not induce inflammation or oxidative stress. High TCA cycle activity and sustained lipogenesis during NAFLD and T2DM, co-exist with inflammation and hepatocellular toxicity [21,151,152]. However, during embryonic-to-neonatal transition in chicken, despite high rates of lipogenesis and TCA cycle activity, canonical markers of inflammation (*IL6*, *TNFA*, *NLRP3*) did not display significant changes in their gene expression in the liver (**Fig. 2.12**). However, there was a statistically significant induction of hepatic *TLR4* gene expression in the ph3 group (**Fig. 2.12**). Further, ceramides and diacylglycerols, which are considered lipotoxic intermediates [21,157,158], remained similar across the groups (**Fig. 2.13A and 2.13B**). The rates of hydrogen peroxide formation (μmoles/min ± SEM) by isolated hepatic mitochondria remained similar between e14 (0.21±0.03) and e18 (0.25 ±0.04) but was significantly reduced in ph3 mitochondria (0.10±0.01) with a further reduction in ph7 (0.05±0.00) (**Fig. 2.14A**). A robust correlation between the rates of hydrogen peroxide formation and the ADP stimulated respiration (**Fig. 2.14B**; $r = 0.55$, $p<0.001$) illustrates the relationship between ROS generation and Oxphos [159].

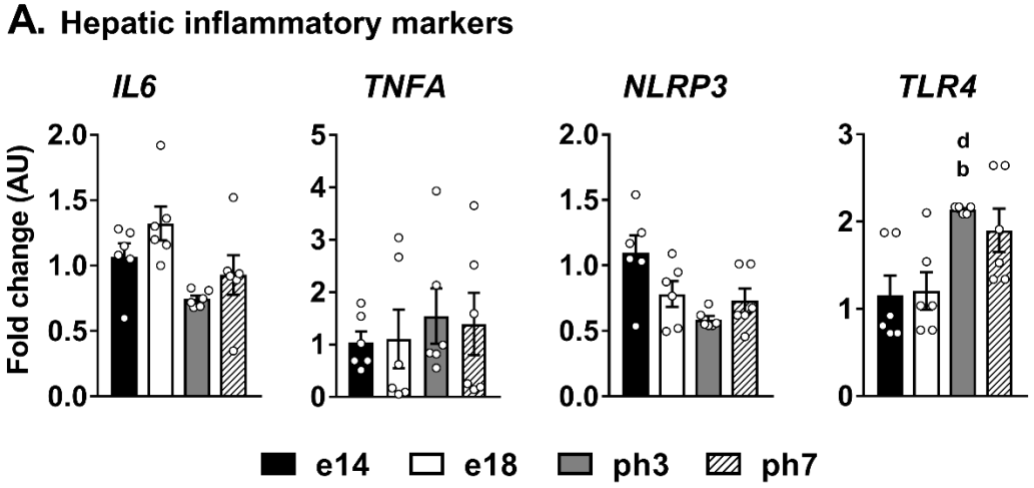

Figure 2.12. Induction of lipogenesis and mitochondrial TCA cycle, did not induce inflammation in the liver. (**A**) Expression patterns of inflammatory genes (IL6, TNFA, NLRP3 and TLR4) remained similar during embryonic-to-neonatal transition. Results (n = 6-9/group) were considered significant at $p \leq 0.05$ following pairwise mean comparisons, which are represented by the following alphabets. 'a'- e14 vs. e18; 'b' - e14 vs. ph3; 'c' - e14 vs. ph7; 'd' - e18 vs. ph3; 'e' - e18 vs. ph7; 'f' - ph3 vs. ph7; 'g' - e18 vs. ph0; 'h' - ph0 vs. ph3; 'i'- ph0 vs. ph7. AU, Arbitrary units; IL6, Interleukin 6; TNFA, Tumor necrosis factor A; NLRP3, NACHT, LRR and PYD domains-containing protein 3; TLR4, Toll like receptor 4.

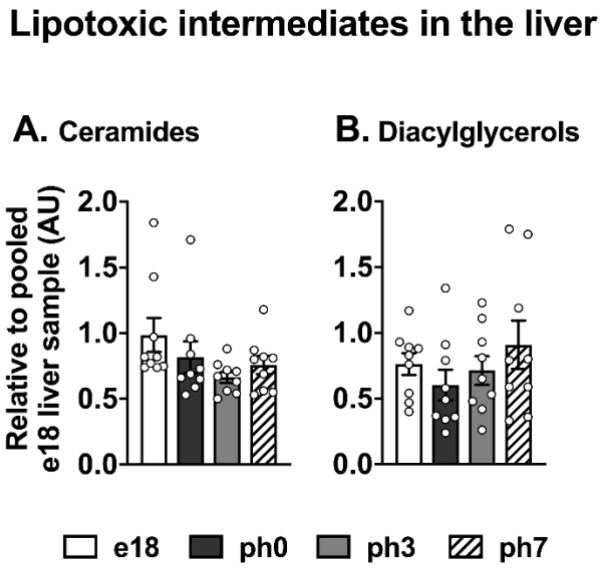

Figure 2.13. Induction of lipogenesis and mitochondrial TCA cycle, did not induce oxidative stress in the liver. Changes in hepatic lipotoxic intermediates (A) Ceramides and (B) Diacylglycerols did not increase with triglyceride accumulation in the liver. Results (n = 6-9/group) were considered significant at $p \leq 0.05$ following pairwise mean comparisons, which are represented by the following alphabets. 'a'- e14 vs. e18; 'b' - e14 vs. ph3; 'c' - e14 vs. ph7; 'd' - e18 vs. ph3; 'e' - e18 vs. ph7; 'f' - ph3 vs. ph7; 'g' - e18 vs. ph0; 'h' - ph0 vs. ph3; 'i'- ph0 vs. ph7.

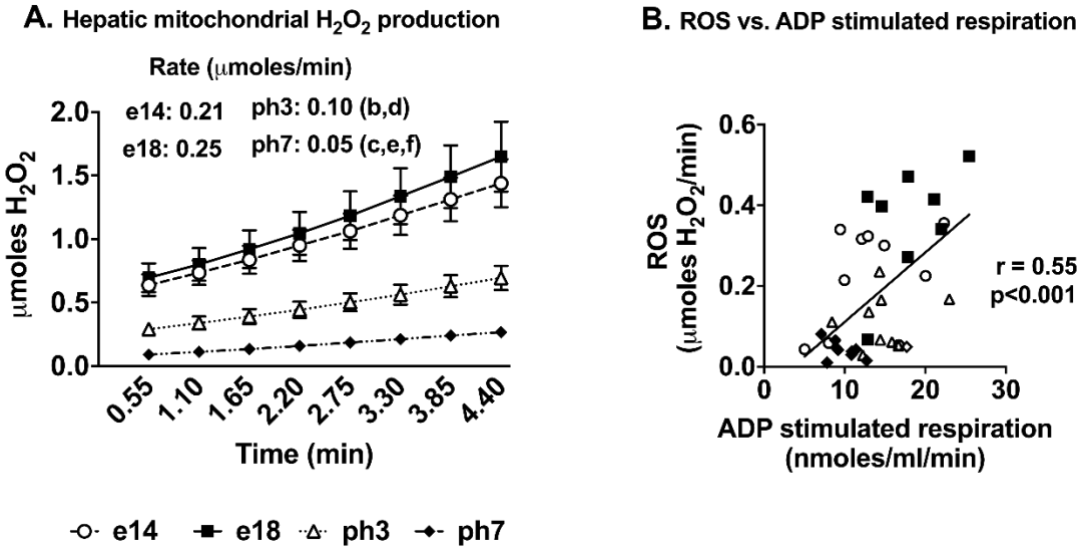

Figure 2.14. Induction of lipogenesis and mitochondrial TCA cycle, did not induce oxidative stress in the liver. (**A**) Reactive oxygen production rates, determined utilizing isolated mitochondria, were significantly lower in neonatal chicks (ph3 and ph7) compared to their embryonic counterparts. (**B**) Correlation between mitochondrial H_2O_2 production and ADP stimulated respiration in chicken embryos and neonates. Results (n = 6-9/group) were considered significant at $p \leq 0.05$ following pairwise mean comparisons, which are represented by the following alphabets. ‘a’- e14 vs. e18; ‘b’ - e14 vs. ph3; ‘c’ - e14 vs. ph7; ‘d’ - e18 vs. ph3; ‘e’ - e18 vs. ph7; ‘f’ - ph3 vs. ph7; ‘g’ - e18 vs. ph0; ‘h’ - ph0 vs. ph3; ‘i’- ph0 vs. ph7.

2.4.7. Antioxidant defense systems were upregulated during embryonic-to-neonatal transition. We hypothesized that the antioxidant mechanisms (**Fig. 2.15A**) will be upregulated to prevent oxidative stress and inflammation, under a metabolic environment favoring high oxidative activity and lipid accumulation. Indeed, glutathione (GSH), a potent antioxidant and an electron acceptor was progressively increased in the liver from e14 to ph7 (**Fig. 2.15B; p<0.0001**). Similarly, glutathione disulfide (GSSG), an oxidized form of glutathione was also elevated in the neonatal chick liver (**Fig. 2.15C; p<0.0001**). The ratio of GSH to GSSG is commonly used as an indicator of cellular oxidative stress, with a higher ratio indicating lower oxidative stress [28,29]. In fact, the ratio of GSH to GSSG was higher in the neonatal chicks compared to their embryonic counterparts (**Fig. 2.15D**), suggesting an induction of antioxidant system and efficient ROS scavenging. Similarly, the trends in superoxide dismutase (*SOD1*) gene expression, even though not statistically significant indicated a pattern of upregulation up to ph7 (**Fig. 2.16A**). Catalase activity was the highest during ph3, even though the activity was reduced ($p = 0.07$) during ph7 (**Fig. 2.16B**).

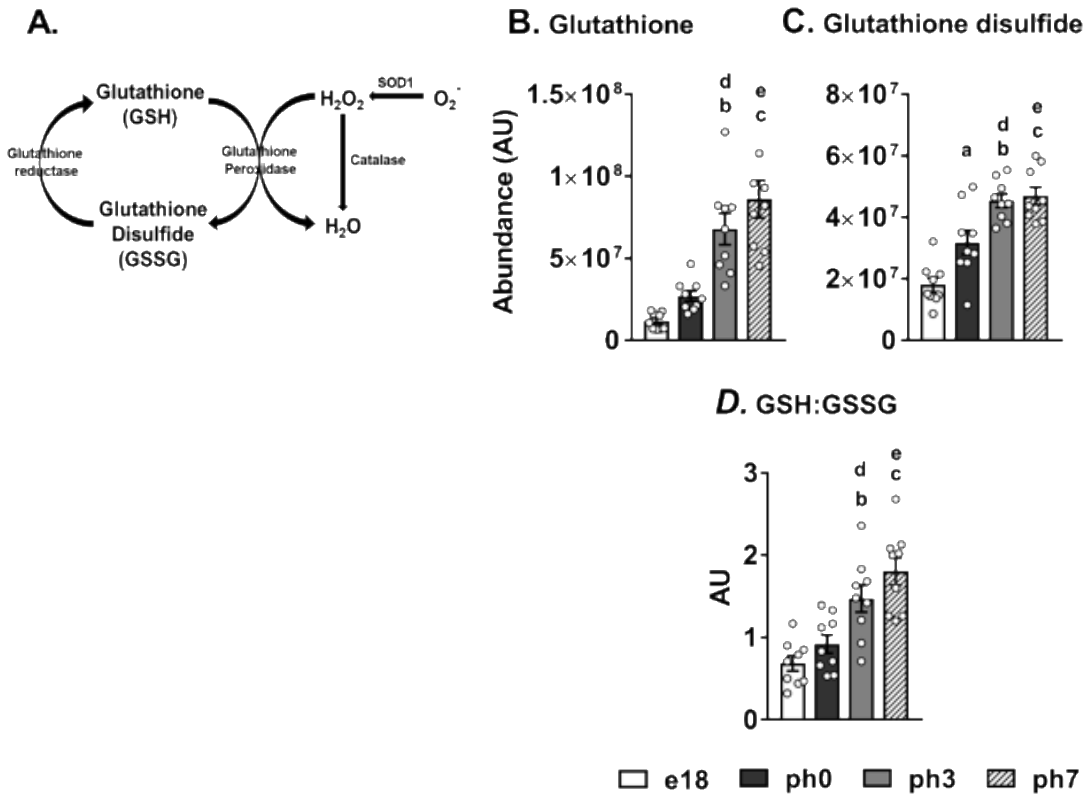

Figure 2.15. Upregulated antioxidant defense systems during embryonic to neonatal transition. (**A**) General scheme of antioxidant defense mechanism to eliminate reactive oxygen species accumulation. (**B-C**) Progressive increase in the levels of glutathione (GSH) and glutathione disulfide (GSSG), molecules involved in the process of reducing H_2O_2 to water, during embryonic-to-neonatal transition. (**D**) Ratio of GSH: GSSG in embryonic and neonatal chicken. Results (n = 6-9/group) were considered significant at $P \leq 0.05$ following pairwise mean comparisons, which are represented by the following alphabets. 'a'- e14 vs. e18; 'b' - e14 vs. ph3; 'c' - e14 vs. ph7; 'd' - e18 vs. ph3; 'e' - e18 vs. ph7; 'f' - ph3 vs. ph7; 'g' - e18 vs. ph0; 'h' - ph0 vs. ph3; 'i'- ph0 vs. ph7. GSH, Glutathione; GSSG, Glutathione disulfide.

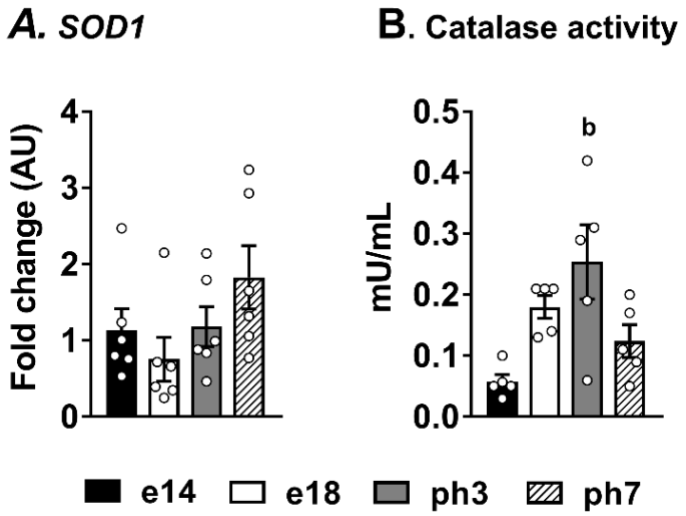

Figure 2.16. Upregulated antioxidant defense systems during embryonic to neonatal transition. (A) Expression profile of SOD1 and (B) catalase activity in embryos and neonatal chicks. Results (n = 6-9/group) were considered significant at P ≤ 0.05 following pairwise mean comparisons, which are represented by the following alphabets. 'a'- e14 vs. e18; 'b' - e14 vs. ph3; 'c' - e14 vs. ph7; 'd' - e18 vs. ph3; 'e' - e18 vs. ph7; 'f' - ph3 vs. ph7; 'g' - e18 vs. ph0; 'h' - ph0 vs. ph3; 'i'- ph0 vs. ph7. SOD1, Superoxide dismutase 1, AU, Arbitrary units.

2.5. Discussion

Dysfunctional mitochondrial networks (e.g. β-oxidation, ketogenesis, TCA cycle flux and Oxphos) and sustained lipogenesis co-exist with hepatocellular stress and inflammation in rodent models and humans with NAFLD and T2DM [151-153]. As several of these networks share biochemical and molecular mediators, it is plausible to hypothesize that synergy between these networks is required to deter hepatic insulin resistance. In embryonic and neonatal chicken, the dynamic but synergistic shifts in mitochondrial β-oxidation, ketogenesis, TCA cycle flux and lipogenesis buffer the metabolic burden from lipids in the liver. This synergy helps avoid hepatocellular stress by efficiently channeling **a)** acetyl CoA from free fatty acid oxidation towards ketone synthesis in the embryonic chicken and **b)** acetyl CoA from carbohydrate oxidation towards the TCA cycle and lipogenesis in the neonatal chicken (**Fig. 2.17**).

The liver of an embryonic chicken has a unique ability to oxidize large amounts of lipids, while the neonatal liver is primed to synthesize, accumulate and transport substantial amounts of lipids [62,70]. The rates of lipid accretion in the neonatal chicken liver (9% of liver weight three days after hatch) is above the threshold (5.5%) considered as NAFLD [14,162]. Our interest is to identify the metabolic mechanisms which allows embryonic and neonatal chicken liver to handle this lipid burden, and in turn undergo healthy development. Further, this is also a relevant question in rodents and humans with NAFLD, as their livers sustain high rates of hepatic lipid oxidation and lipogenesis, but with the side effects of hepatocellular stress and inflammation, in turn aggravating the liver disease [150,151,153].

An efficient metabolic switch from fatty acid oxidation in the embryonic chicken liver to increased lipogenesis in the neonate, is central for a healthy development [17,70,60,62]. Indeed, the embryonic liver mitochondria is primed to oxidize free fatty acids by β-oxidation, as illustrated by the high levels of plasma and hepatic acylcarnitines, higher expression of genes involved in fatty acid oxidation and the high levels of serum ketones (3-4 mM) (**Fig. 2.3 and Fig 2.4, Appendix Tables 2.2 & 2.3**). The higher levels of ketones were indicative of the fact that a significant portion of the acetyl CoA derived from β-oxidation were diverted towards the synthesis of ketones. It is also important to note that the synthesis of ketones can serve as a 'sink' for acetyl CoA, thus diverting these acetyl CoA carbons from overburdening the hepatic TCA cycle during embryonic development. We believe that this diversion of acetyl CoA towards ketogenesis is aiding the qualitative and quantitative maturation of the mitochondrial TCA cycle and Oxphos in the embryonic liver.

After hatch, along with the depletion of yolk-lipids, the neonatal chicks starts to rely on dietary carbohydrates as the primary metabolic substrates [17]. As a reflection of this, serum ketones fell from 3-4 mM in the embryos to ~ 300 μM in the neonates, accompanied by a dramatic induction of hepatic lipogenesis (**Fig. 2.5**). Circulating ketones could be serving as a substrate depot for initiating hepatic lipogenesis after hatch [163-166], though the fate of ketones were not tracked in this study. Concurrently, the hepatic TCA cycle in the neonatal chicken is now primed for the complete oxidation of acetyl CoA as indicated by the higher incorporation of ^{13}C into mitochondrial TCA cycle intermediates (**Fig. 2.9** and **Appendix Table 2.4**).

Furthermore, TCA cycle activity is optimally coupled with mitochondrial respiration as indicated by the steady and high hepatic mitochondrial respiratory control ratios (RCR) (**Fig. 2.8D)**. More importantly, the metabolic remodeling of lipogenesis and TCA cycle occurred together with the significant downregulation of β-oxidation as signified by the lower levels of plasma and hepatic acylcarnitines, serum ketones and expression patterns of fat oxidation genes in the neonates (**Fig. 2.3, Appendix Tables 2.2 & 2.3**). The above results illustrate the dynamic remodeling of hepatic mitochondrial oxidative function and lipogenesis, without initiating inflammation and oxidative stress, as discussed later.

Our results also illustrate the integrative nature of the hepatic TCA cycle, which bring together aspects of mitochondrial oxidative function and lipogenesis. For example, the citrate content of the isolated mitochondria is increasing from e18 to ph3 (**Fig. 2.10B**). Furthermore, there is higher incorporation of ^{13}C from [$^{13}C_3$]pyruvate into citrate from e18 to ph3 (**Fig. 2.9B**) indicating increased citrate synthesis by the mitochondria. Further, there was a decrease in mitochondrial citrate content from 0 to 10 min, when mitochondria from ph3 and ph7 chicken liver were incubated in a respiration media (**Fig. 2.10B**). Taken together, these results point to increased mitochondrial citrate synthesis and higher rates of citrate export from the mitochondria into the cytosol, in order to serve as the lipogenic precursor.

Our results illustrates that the mitochondrial TCA cycle activity and lipogenesis are simultaneously upregulated in the neonatal chicken liver. Interestingly, this occurred without a parallel activation of ROS production or an increase in markers of hepatocellular stress, lipotoxicity or inflammation (**Fig. 2.12,**

2.13 and 2.14). These observations are contrary to those in rodent models and human subjects with NAFLD, where the metabolic milieu favoring high rates of TCA cycle metabolism and lipogenesis coexist with inflammation, hepatocellular stress and lipotoxicity [21,143,151-153]. Increase in ROS occurs when higher amounts of reducing equivalents derived from free fatty acid oxidation (β-oxidation coupled to TCA cycle) drives the transfer of electrons through the mitochondrial respiratory chain [150,159,167]. This process is optimally coupled in embryonic and neonatal chicks, as indicated by the RCR (**Fig. 2.8D**). However, a positive correlation between ADP stimulated respiration and ROS production is also evident (**Fig. 2.14B**). Coincidently, the highest rates of ADP stimulated respiration and ROS production occurred in the e18 liver when β-oxidation rates were also maximal. These results illustrate that the high rates of reducing equivalents derived from β-oxidation could be significant drivers of ROS production. Thus, the downregulation of β-oxidation immediately post-hatch helped to relieve the oxidative burden from free fatty acids on the hepatic mitochondria, and reduce ROS generation.

During embryonic-to-neonatal development, the reduction in ROS production is associated with an upregulation of antioxidant defense (**Fig. 2.14A and 2.15**). The ratio of GSH to its oxidized form, glutathione disulfide (GSSG), a frequently used index of cellular oxidative stress [160,161] was higher in neonatal chicken (**Fig. 2.15D**). This suggests that the induction of antioxidant system and efficient ROS scavenging worked together to deter the adverse impacts of high TCA cycle flux and lipogenesis. Many of the hepatic TCA cycle intermediates have also been shown to have antioxidant activities, through their molecular interactions with antioxidant defense

systems [152,168-171]. Indeed, many antioxidant TCA cycle intermediates (e.g. malate, fumarate, citrate) in the liver were progressively higher during embryonic-to-neonatal transition (**Appendix Fig. 2.4**). Taken together, these further highlight the integrative nature of mitochondrial metabolism towards maintaining optimal cellular health and redox state. In summary, healthy embryonic-to-neonatal transition in the chicken liver is accomplished through the dynamic remodeling of key mitochondrial networks including β-oxidation, ketogenesis and TCA cycle, along with hepatic lipogenesis (**Fig. 2.17**). Here, we realize the fact that the embryonic-to-neonatal transition in chicken is an active growth phase, which could have an additional impact on modulating mitochondrial function. Further, there could also be differences in species specific insulin action and glycemic control between the chicken and their mammalian counterparts, which could be contributing to the observed differences. However, the rapid influx of yolk lipids into the liver, coupled together with the fact that liver is the primary lipogenic organ in chicken, makes it an attractive model system to test the impact of lipid overburden. This metabolic milieu is unlike any mammalian system where lipid accumulation and high rates of lipid oxidation are associated with inflammation and hepatocellular stress. Based on our overall results from this natural model, lowering the flux of free fatty acids through β-oxidation could be an effective strategy to reduce mitochondrial ROS and also to avoid the metabolic burden from acetyl CoA on the TCA cycle and Oxphos during NAFLD. Lastly, the embryonic-to-neonatal development period in chicken also presents a unique and natural physiological system to investigate mechanisms regulating hepatic mitochondrial function and lipogenesis.

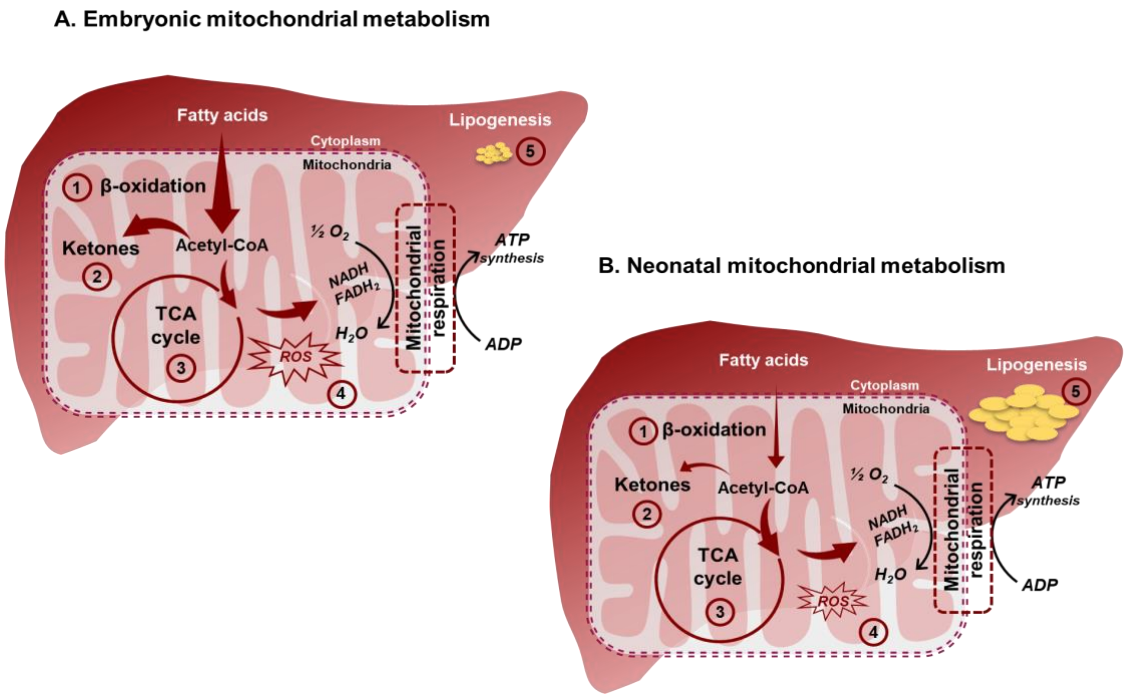

Figure 2.17. Metabolic shifts which deter hepatic insulin resistance during embryonic-to-neonatal development. Chronic inflammation and hepatic insulin resistance will ensue if the acetyl CoA derived from mitochondrial free fatty acid-β-oxidation cannot be optimally channeled to ketone synthesis or complete oxidation through the TCA cycle. This 'metabolic bottle neck' is avoided during embryonic-to-neonatal transition in chicken, through dynamic shifts in mitochondrial β-oxidation, ketogenesis, TCA cycle flux and lipogenesis in the liver. During embryonic development (**Fig. 2.17A**), high rates of β-oxidation **(1)** generates large amounts of 2-carbon units of acetyl-coA. However, simultaneous upregulation of ketone synthesis **(2)** in the embryonic liver helps to efficiently channel these acetyl-coA units towards other fates. Buffering of acetyl CoA units through ketogenesis during embryonic development occurs concurrent to the steady and progressive induction of hepatic TCA cycle metabolism **(3)**, while rates of lipogenesis remain low **(5)**. As the chicks

hatch and starts feeding (**Fig. 2.17B**), there is a dramatic downregulation of β-oxidation **(1)** and ketogenesis **(2)** in the neonatal liver. In turn, the neonatal chick, channels the acetyl CoA derived from a carbohydrate rich diet **a)** through the hepatic TCA cycle for complete oxidation and/or **b)** exports it from the mitochondria into the cytoplasm as a precursor for hepatic lipogenesis **(5)**. In summary, our results suggest that the significant downregulation of β-oxidation after hatch, helps to minimize the metabolic burden from excess acetyl CoA while maintaining high rates of lipogenesis and TCA cycle; without instigating significant side effects from mitochondrial ROS **(4)**. This optimal metabolic milieu deter the onset of hepatic insulin resistance.

Chapter 3

Branched Chain Amino Acids Modulate Hepatic Mitochondrial Oxidative Metabolism and Lipogenesis

3.1. Abstract

Mitochondrial dysfunction is a central feature of insulin resistance and associated co-morbidities. Further, elevated levels of circulating branched chain amino acids (BCAAs) are correlated to the onset of insulin resistance and are considered predictors of type-2 diabetes mellitus (T2DM). BCAAs are substrates to the mitochondrial TCA cycle, supporting anaplerotic reactions. While, defects in their catabolic network leads to anaplerotic stress and fail to induce TCA cycle leading to mitochondrial dysfunction. Although BCAAs interact with hepatic mitochondria, their impact on mitochondrial lipid metabolism remains unclear. We hypothesized that the crosstalk between BCAAs and mitochondrial metabolism is mediated through the ability of BCAAs to alter hepatic lipid oxidation. We believe, this alteration occurs independent of BCAAs being anaplerotic substrates to the mitochondria. To test our hypothesis, mice (C57BL/6) were reared on either low-fat, low-fat supplemented with 1.5X BCAAs, high-fat or high-fat diet supplemented with 1.5X BCAAs. BCAAs supplementation under normal physiological condition induced fed-to-fasted fold changes in lipid oxidation and ketogenesis, without altering TCA cycle activity. Acetyl-CoA resulting from higher rates of lipid oxidation induced ketogenesis with a concurrent suppression in lipogenesis. This metabolic milieu of higher lipid oxidation with BCAA supplementation resulted in a reduced hepatocellular environment associated with increased rates of ADP stimulated respiration with no apparent changes in reactive oxygen species (ROS) generation. The BCAAs mediated alteration in oxidative networks during fasting co-exist with a parallel increase in AMP activated protein kinase (AMPK) activity. In summary,

BCAAs altered hepatic lipid metabolism through increasing the activity of AMPK and independent of their role as substrates to the mitochondria.

3.2. Introduction

Dysfunctional mitochondrial metabolism is a central feature of insulin resistance that contributes towards onset and progressive stages of non-alcoholic fatty liver disease (NAFLD) [40,15]. In normal conditions, the mitochondrial networks including β-oxidation, ketogenesis, TCA cycle, electron transport chain and ATP synthesis are in synergy to maintain cellular energy homeostasis. However, during the progressive and severe stages of insulin resistance and associated metabolic diseases the aforementioned mitochondrial networks remodel and adapt to respond to nutrient and hormonal cues[40,145]. Initial stages of NAFLD is associated with induced mitochondrial oxidative networks such as ketogenesis and oxidative phosphorylation (Oxphos) along with higher lipogenesis followed by their impairment during severe stages [15,40]. The induction in hepatic mitochondrial oxidative networks occurs simultaneous with sustained induction of the TCA cycle [15,23,40]. Further, the remodeling of hepatic mitochondrial networks occurs along with increased lipid accumulation, oxidative stress and inflammation [21,40]. Therefore, understanding the mechanisms regulating hepatic mitochondrial metabolism and lipogenesis is significant towards developing management and prevention strategies for insulin resistance and associated metabolic disorders.

Elevated levels of circulating branched chain amino acids (BCAAs; valine, leucine and isoleucine) during insulin resistance are considered predictors of type-2 diabetes (T2DM) onset in rodent and human models[24-26]. The increase in the levels of

BCAAs occurs in association to defects in their catabolic networks[24,27,116,128,175]. Catabolism of leucine and isoleucine can fuel ketogenesis, while isoleucine and valine carbons fuel gluconeogenesis and thus form anaplerotic substrates to hepatic TCA cycle. [25, 26, 176, 177]. A positive co-relation between BCAAs and liver acyl carnitines suggests an association between BCAAs and mitochondrial lipid metabolism[8,26,25]. Also, defects in BCAA catabolism during insulin resistance contribute to anaplerotic stress and fail to induce TCA cycle metabolism, contributing towards mitochondrial dysfunction[26]. BCAA supplementation during ketogenic conditions (BCAA supplemented with high-fat calories and low carbohydrate calories) induced hepatic lipid oxidation[177]. These interesting observations in the literature suggests an interaction between BCAAs, their catabolic network and mitochondrial oxidative metabolism. Although, the induced lipid oxidation associated with BCAA supplementation in ketogenic environments projects their beneficial effects towards preventing lipid accumulation, their effects on mitochondrial oxidative metabolism needs to be further explored.

In this study, we utilized dietary intervention of BCAAs (150% excess) with (low-fat; 10 % kcal fat diet) and (high-fat; 60% kcal fat diet). Based on the observations from the literature, we hypothesized that BCAAs can modulate hepatic lipid metabolism independent of them and their catabolic end products being substrates for mitochondrial oxidative metabolism. With extensive metabolic profiling and gene and protein expression profiles, we demonstrated that BCAAs primed the liver mitochondria to induce oxidative networks (β-oxidation and

ketogenesis) along with lower rates of *de novo* lipogenesis, under normal physiological conditions.

3.3. Materials and Methods

3.3.1. Animals and diets

This study was conducted in accordance with the institutional Animal Care and Use Committee protocols approved at the University of Maryland, College Park. Male C57Bl/6NJ mice aged 4-6 weeks obtained from Jackson laboratory (Bae Harbor, ME). The mice were reared on either a low-fat (LF; 10% fat kcal), low-fat diet supplemented with BCAA (LB; LF +150% BCAAs), high-fat (HF; 60% fat kcal) or high-fat diet supplemented with BCAA (HB; 150% BCAA) for 12 and/or 24 weeks. Mice were fed ad libitum and maintained on a 12 hr light/dark cycle. Metabolic profiling was conducted under fed or overnight fasted (14-16 hrs) conditions. The dietary composition of the diets was formulated such that the HF and HB diets contribute towards onset and progression of insulin resistance and non-alcoholic fatty liver disease. The sample size for each experiment is highlighted in the legend of each figure. All the diets were custom made at Research Diets (New Brunswick, NJ, USA; **Appendix Table 3.1**).

3.3.2. Stable isotope infusion for measurement of metabolite turnover

Following a 12-week dietary treatment, mice were surgically implanted with jugular vein catheter and allowed to recover for 4 days before infusing stable isotopes. The infusions were performed under both fed and fasted conditions. The mixture containing [$^{13}C_6$]leucine (1.25mg/ml), [$^{13}C_6$]sodium 2-keto-3-methyl-pentanoate (0.5mg/mL), [$^{13}C_5$] alpha-ketoisovaleric acid, sodium salt (0.8mg/mL),

urea (3mg/mL), glucose (15mg/mL), and [$^{13}C_4$]β-hydroxybutyrate (BHB, 3 mg/mL) (Cambridge Isotope Laboratories, Inc, Tewksbury, MA) was infused as a bolus for 10 minutes at a rate of 0.3ml/hr. This was followed by continuous infusion of all the above stable isotopes at the rate of 0.12ml/hr for another 80 minutes to attain isotopic steady state. The blood and liver were collected under isoflurane anesthesia and approximately 0.8 g liver was used to isolate mitochondria as described below. The remaining liver was flash frozen in liquid nitrogen and stored at -80 °C for further gene, protein and metabolite analysis.

3.3.3. Isolation of liver mitochondria

The mice were anesthetized under isoflurane and livers were collected to isolate mitochondria. Fresh liver was washed with 1X ice cold phosphate buffered saline (1X PBS) and ~ 800mg of liver was used to isolate mitochondria. The liver was minced in 3 mL MSHE buffer (70 mM sucrose, 210 mM mannitol, 5mM HEPES, 1 mM EGTA, and 0.5% bovine serum albumin (BSA); pH 7.2) and tissue was homogenized using a Dounce homogenizer (2-4 strokes, 5-10 turns each stroke). The homogenized tissue was transferred to a 15 mL falcon tube, the homogenizer was rinsed with 4 ml of MSHE buffer and mixed with tissue homogenate. The sample was spun at 800 g for 10 min at 4 °C. The supernatant was transferred through double layered cheese cloth and was centrifuged at 8000g for 10 min at 4 °C to obtain the mitochondrial pellet. The pellet was washed and re-suspended with 3 ml MSHE and spun at 8000g for 10 min at 4 °C. Wash was repeated with 2 mL MSHE buffer. The pellet was re-suspended in 100 µL of MSHE buffer without BSA. The protein was

estimated following a 40 times dilution of mitochondrial pellet using Pierce protein assay kit (Thermo Fisher Scientific, Waltham, MA, USA).

3.3.4. Mitochondrial Incubations

Incubations with [$^{13}C_{16}$]palmitate: Isolated mitochondria was incubated with stable isotope tracers to analyze aspects of mitochondrial metabolism such as β-oxidation and TCA cycle metabolism. Isolated mitochondria (500 µg) were incubated with 1 mL of MAS-3 buffer (115 mM KCl, 10 mM, KH_2PO_4, 2 mM $MgCl_2$, 3 mM HEPES, 1 mM EGTA and 0.2% fat free BSA; pH 7.2) with 5 mM glutamate, 2.5 mM malate and 1mM carnitine along with 20µM of either U13C[palmitate] or unlabeled palmitate. The mitochondria were incubated for 5 min and 10 min at 37 °C. The mitochondria was centrifuged and pelleted at 8000 rpm for 5 minutes at 4 °C. The pellet was washed with 1X cold PBS and centrifuged at 8000 rpm for 2 minutes and the pellet was frozen at -80 °C for further analysis.

Incubations with [$^{13}C_6$]isocaproic acid: Mitochondria were isolated from a different set of mice reared on LF and LB diet for 12 weeks. The mitochondria isolated from liver was incubated with 1 mL MAS-3 buffer (115 mM KCl, 10 mM, KH_2PO_4, 2 mM $MgCl_2$, 3 mM HEPES, 1 mM EGTA and 0.2% fat free BSA; pH 7.2) with 5mM glutamate, 2.5 mM malate, 1 mM carnitine, 25 µM palmitate and 25 µM U13C[isocaproic acid] or unlabeled isocaproic acid for 10 min. The mitochondrial pellet was processed as detailed above.

The mitochondrial samples were analyzed using GC-MS to determine the incorporation of ^{13}C from [$^{13}C_{16}$]palmitate or [$^{13}C_6$]isocaproate into β-

hydroxybutyrate and/or TCA cycle intermediates to estimate activity of β -oxidation, ketogenesis and TCA cycle.

3.3.5. Analysis of organic acids, amino acids and TCA cycle intermediates

The liver tissue previously frozen (~ 10-15 mg) and isolated mitochondrial protein (~ 250 µg) were extracted for organic and amino acids with 750 µL of chloroform: methanol (2:1) and 250 µL of water. The top aqueous phase was dried under nitrogen, and the metabolites were converted to their oximes with 20 µL of 2% methoxamine hydrochloride in pyridine (w/v) by microwaving for 90 s, followed by conversion to their respective TBDMS (Tert-butyldimethylsilyl) derivatives by heating the samples at 90 °C for 1 hr.

For experiments where mitochondria was incubated with [$^{13}C_{16}$]palmitate we determined the incorporation of ^{13}C from palmitate into TCA cycle intermediates (enrichment scheme is detailed in **Fig 3.3A**). The rate of ^{13}C incorporation was determined by analyzing the mass isotopomer distribution. The TCA cycle intermediates will be (M+2) if the acetyl-CoA is derived from uniformly labeled palmitate enters the TCA cycle.

Serum (25 µL) samples were processed after deproteinization with 750 µL of cold acetonitrile and the conversion of metabolites into their oximes with 20 µL of 2% methoxamine hydrochloride in pyridine, followed by TBDMS derivatization. For the determination of metabolite concentrations, the liver tissue, mitochondria, and serum samples were spiked with a known amount of stable isotope labeled internal standards of the respective metabolites. The concentration was calculated in comparison to labeled standards. Metabolites were run on a HP-5MS UI column (30

m × 0.25 mm × 0.25 µm; Agilent, Santa Clara, CA, USA) and fragmented under electrical ionization. Fragments of interest were detected using single ion monitoring (SIM) on a GC-MS (5973N-Mass Selective Detector, 6890-Series GC, Agilent, Santa Clara, CA, USA).

3.3.6. Analysis of ketones

Serum (25 µL) and mitochondrial incubation media (250 µL) were deproteinized with 500 µL cold acetonitrile and spun at max speed for 15 min at 4 °C. The supernatant was dried under nitrogen and was derivatized with 50 µL of TBDMS by heating at 90 °C for 1 hr. For the determination of β-hydroxybutyrate (BHB) concentrations the serum and media samples were spiked with a known amount of stable isotope labeled [$^{13}C_4$]BHB as internal standard. The concentration was calculated in comparison to the labeled standard.

For experiments where mitochondria was incubated with [$^{13}C_{16}$]palmitate we determined the incorporation of ^{13}C from palmitate into BHB (enrichment scheme is detailed in **Fig 3.3A**) in the mitochondrial incubation media. The rates of reactions were determined by analysing isotopomer distribution. Based on either one acetyl-CoA or both acetyl-CoA is derived from $^{13}C_{16}$[palmitate] the ^{13}C incorporation in BHB will be M+2 and/or M+4 peak. Incubation media (500 µL) was deproteinized with 1ml cold acetonitrile and is processed as mentioned above, but without the addition of labeled standard.

Analysis of acetoacetate and β-hydroxybutyrate concentration. Serum (25 µL) was spiked with 1 M Sodium borodeuteride ($NaBD_4$) to convert unstable acetoacetate to stable BHB (M) with a deuterium (M+1). An equal volume of 500 µM

[$^{13}C_4$]BHB standard was added prior to processing. The sample mix was incubated for 5 min at room temperature followed by addition of 200 µL cold 12% sulfosalicylic acid. The samples were quickly spun for 30 sec at max speed followed by addition of 800 µL more of cold 12% sulfosalicylic acid. The samples were centrifuged at 13,000 rpm for 15 min at 4 °C and supernatant was transferred to 10 ml glass tubes. The samples were mixed with 1ml 4M HCl, 1 ml saturated NaCl and ketones were extracted with 3 ml ethyl acetate for 1 hr with continuous shaking on a shaker plate. The sample mixture was centrifuged for 10 min at room temperature and the supernatant was dried under nitrogen and derivatized with 35 µL of TBDMS derivative at 90 °C for 1hr.

Metabolites were run on a HP-5MS UI column (30 m × 0.25 mm × 0.25 µm; Agilent, Santa Clara, CA, USA) and fragmented under electrical ionization. Fragments of interest were detected using single ion monitoring (SIM) on a GC-MS (5973N-Mass Selective Detector, 6890-Series GC, Agilent, Santa Clara, CA, USA).

3.3.7. Analyzing redox state of the liver

The cellular redox state of the liver was determined by calculating NADH/NAD+ ratio in the cytoplasm and mitochondria. Mitochondrial NADH/NAD^+ was determined by plasma β-hydroxybutyrate/acetoacetate ratio. The NADH/ NAD^+ was estimated by β-hydroxybutyrate dehydrogenase equilibrium[150,179]as follows:

$$NADH/NAD^+ = [\beta\text{-hydroxybutyrate}]/[\text{acetoacetate}] \times K_{\beta HBDH}$$

$$(\text{where, } K_{\beta HBDH} = 4.92 \times 10^{-2})$$

The cytoplasmic NADH/NAD^+ was measured by liver pyruvate/lactate ratio and was estimated by lactate dehydrogenase equilibrium[150,180] as follows:

$$NADH/NAD^{+} = [lactate]/[pyruvate] \times K_{LDH}$$

(where, $K_{LDH} = 1.11 \times 10^{-4}$)

3.3.8. Determination of mitochondrial ROS

Reactive oxygen species production from isolated mitochondria was determined by Amplex red assay. Mitochondria (64 µg) was incubated with HRP (0.2 U/mL; horseradish peroxidase) and amplex red reagent (100 µM; 10-acetyl-3,7-dihydroxyphenoxazine) prepared in MAS-3 buffer with glutamate and malate. Amplex Red reagent in combination with HRP detects hydrogen peroxide (H_2O_2) released by the isolated mitochondria, by recording the real-time oxidation of Amplex red to the fluorescent resorufin detected at 585 nm using a Cytation 5 spectrophotometer (BioTek Instruments, Inc. Winooski, VT).

3.3.9. Determination of hepatic mitochondrial respiration

Mitochondrial oxygen consumption was measured using oxygraph oxygen electrode (Hansatech Instruments, Norfolk, England). Isolated mitochondria (500 µg) suspended in 1 ml of MAS-3 buffer containing 5 mM glutamate and 2.5 mM malate. Basal (state II), ADP stimulated (with 100 µM ADP; state III) and ADP depleted (state IV) respiration rates were determined.

3.3.10. *De novo* lipogenesis in the liver

Mice maintained on LF, LB, HF and HB diets for 12 weeks were intraperitoneally injected with saline D_2O (27ul/g body weight). The mice were provided with 4% D_2O in drinking water for the final 4 days. Livers were collected and ~250mg of liver was folch extracted for lipids with 10 ml of 2:1 chloroform:methanol and Add 5 mL 50 mM NaCl for 1 hr with vortex every 10-15

min. The bottom chloroform layer was transferred into glass tubes and dried and re-constituted in 600 µL of chloroform containing a pyrazine standard (2 mg/ml, 2.5% pyrazine-d4/97.5% pyrazine) and was transferred to 3mm NMR tube. Serum from each animal was run for 2H to determine body water enrichment. 5 µL serum was mixed with 495 µL of chloroform and transferred to 3 mm NMR tube to obtain 2H body water enrichment. This is with the assumption that pyruvate is the main source of acetyl-CoA, a lipogenic precursor which is equal to the body water enrichment. The samples were analyzed using Bruker Ultrashield Advance III system, equipped with CPTXI 600S3 H-C/N-D-05 Z cryoprobe. Proton and deuterium lock channel was used to acquire 1H and 2H NMR spectra respectively. The 1H spectra of lipids was acquired at 600 MHz, with 2 sec delay (d1), 64 number of scans (NS). 2H spectra was acquired at a frequency of 92.14 MHz with acquisition time of 2 s and 4096 scans. All the spectra was analyzed using TopSpin3.2 software.

Data analysis: 2H enrichment of the lipid methyl hydrogens was quantified by comparing with the pyrazine-d4 standard. 2H enrichment of serum was considered as whole body water enrichment.

De-novo lipogenesis (%) = (^{2}H methyl enrichment/^{2}H body water enrichment) × 100

3.3.11. Gene expression analysis

Frozen liver (~10-15 mg) was lysed with 600 µL TRIZOL reagent (Invitrogen, Carlsbad, CA) to isolate mRNA using mini prep kit (Bio-Rad Laboratories Inc., Hercules, CA). cDNA was prepared from 1 µg of mRNA using cDNA synthesis kit (Bio-Rad, Hercules, CA). Quantitative real-time PCR was performed using 25 ng of cDNA, 150 nM of each primer, and 5 µl of SYBR green

PCR master mix (Invitrogen, Carlsbad, CA) with cyclophilin as housekeeping gene. The samples were run in triplicates on a Bio Rad CFX Real Time system (C1000 Touch Thermal Cycler). The list of primers is provided in the **Appendix Table 3.2**.

3.3.12. Western blot analysis

Frozen liver (~ 10-15 mg) and mitochondrial pellet was lysed with 1x RIPA lysis buffer with protease and phosphatase inhibitor followed by centrifugation at 15000 rpm for 15 min at 4 °C. The total protein was measured using pierce BCA protein assay kit (Thermo Fischer Scientific. Waltham, MA). The proteins were separated using Bolt 8 % Bis-tris Plus gels (Invitrogen, Carlsbad, CA) and transferred onto nitrocellulose membrane. The membrane was incubated with primary antibody overnight followed by incubation with secondary antibody. Primary antibodies Cpt1a, Ppara, Cox IV, Acc, pAcc^{ser79}, AMPK, pAMPK^{thr172} and Gapdh (Cell Signaling Technology, Danvers MA). Lcad/ACADL (abcam, Cambridge, UK) were used for the study.

3.3.13. Biochemical assays

Serum insulin and c-peptide were measured by enzyme-linked immunoassay (Crystal Chem USA, IL). Serum non-esterified fatty acid (NEFA) concentrations were determined using HR Series NEFA-HR2 kit (WAKO diagnostics, CA). Liver triglycerides (Serum triglyceride determination kit, Sigma Aldrich, St. Louis, MO). Liver pAMPK^{thr172} levels were measured using enzyme linked immunosorbent assay (Invitrogen, Waltham, MA) and liver NADH and NAD levels was measured using NAD/NADH calorimetric assay kit (Millipore sigma, Burlington, MA). All assays were conducted per the manufacturer's protocol.

3.3.14. Statistical analysis

All the data reported is presented as mean ± standard error of means (SEM). The results from 12-weeks dietary groups (LF, LB, HF and HB) were analyzed using one-way ANOVA, followed by a Tukey's multiple comparison test. The results from 24-weeks dietary groups (HF and HB) were analyzed independently using unpaired t-test. Means were considered significantly different at $p \leq 0.05$. The means between groups were considered a trend at $p < 0.1$. All statistical analysis were conducted and the graphs were plotted utilizing Prism 7 (GraphPad software Inc., San Diego, CA).

3.4. Results

3.4.1. Branched chain amino acids supplementation induced lipid oxidation in the liver. To determine the effect of BCCAs on hepatic lipid metabolism we analyzed the expression profiles of genes and proteins involved in lipid oxidation. The lipid oxidation gene expression profiles are expressed as fed-to-fasted fold change and the values are normalized to LF fed. The fed-to-fasted fold change in gene expression profiles of long-chain and medium-chain acyl dehydrogenase enzymes (*Lcad* and *Mcad*) were significantly higher ($P<0.05$) in LB mice compared to their LF counterparts (**Fig 3.1A and 3.1B**). Carnitine palmitoyl transferase 1 (*Cpt1a*), mitochondrial enzyme responsible for the formation of fatty acylcarnitines to facilitate their transport to mitochondrial matrix was induced ~2 fold higher on fasting compared to LF diet fed mice (**Fig 3.1C**). The fed-to-fasted fold expression of *Ppara,* the master regulator of lipid oxidation and *Cd36,* a cellular importer of fatty acids, were higher with BCAA supplementation compared to their LF counterparts (**Fig 3.1D and 3.1E**). The expression profiles of all the lipid oxidation genes were

blunted after 12 and 24-wks of high-fat diet feeding (HF and HB). However, BCAA supplementation for 24-wks (HB) significantly induced fed-to-fasted fold expression in lipid oxidation genes compared to HF counterparts (**Fig 3.1A-E**). Similarly, the fed-to-fasted fold expression of hepatic lipid oxidation proteins such as (Lcad, Cpt1a and Ppara) were significantly higher in mice supplemented with LB diet compared to LF (**Fig. 3.2A and 3.2B**). However, the fed-to-fasted fold expression profiles of lipid oxidation proteins were blunted in HF and HB mice after 12 and 24-weeks of diet feeding (**Fig. 3.2A and 3.2B**). Further, the fed-to-fasted fold change (AU±SEM) in serum ketone (β-hydroxybutyrate) was trending higher (P=0.07) in LB fed mice (16.1±2.6) compared to LF fed mice (13.9±2.6) signifying the upregulation of hepatic lipid oxidation with BCAA supplementation with low-fat diet feeding (**Fig. 3.1F**). Taken together, the data demonstrate the capability of BCAA supplementation to induce hepatic lipid oxidation upon fasting in an insulin sensitive environment (Metabolic phenotype detailed in **Appendix Table 3.3 and 3.4**).

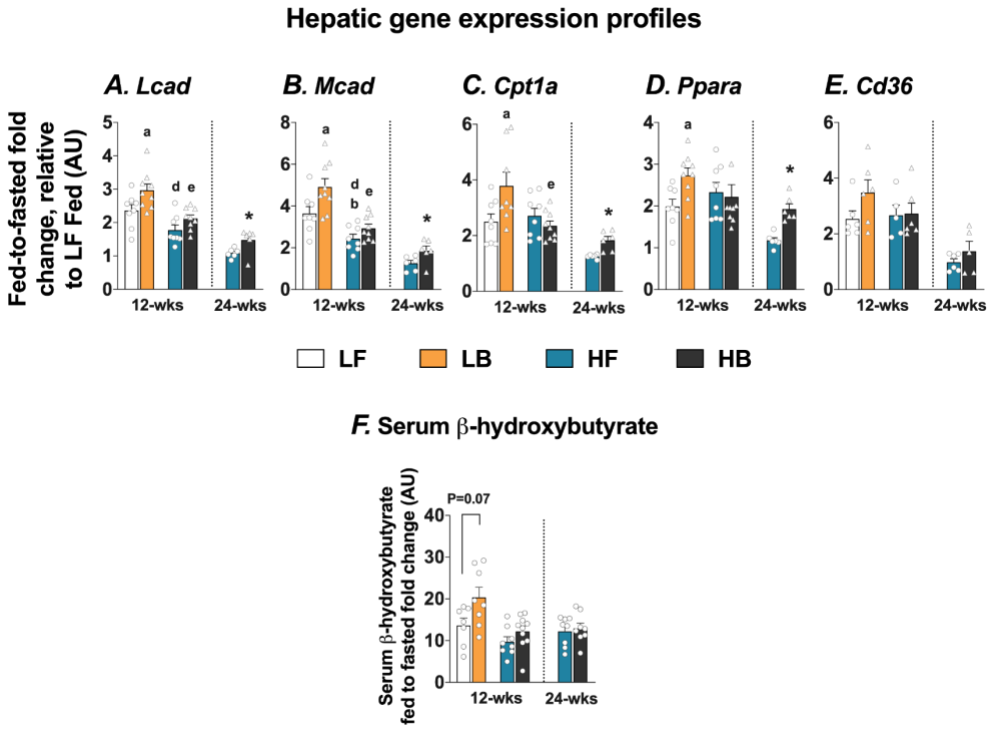

Figure 3.1. BCAA supplementation alters hepatic lipid oxidation upon fasting. Fed-to-fasted fold change in expression of lipid oxidation genes such as (**A**) Lcad, (**B**) Mcad, (**C**) Cpt1a (**D**) Ppara and (**E**) Cd36 (**F**) Fed-to-fasted fold change in β-hydroxybutyrate concentration. The values are normalized to LF fed. All the values are represented as mean ± SEM, with n=6-8/ group. Results were considered significant at $P < 0.05$ following one-way ANOVA (between 12-wk diet groups) and tukey's pairwise mean comparison which are represented by the following alphabets: "a"—LF vs LB; "b"—LF vs HF; "c"—LF vs HB; "d"—LB vs HF; "e"—LB vs HB; and "f"—HF vs HB. The significance between 24-wk HF and HB groups were analyzed following a t-test and is represented by "*". Lcad, long-chain acyl dehydrogenase; Mcad, medium-chain acyl dehydrogenase; Cpt1a, Carnitine palmitoyl transferase 1; Ppara, Peroxisome proliferator-activated receptor alpha; Cd36, Cluster of differentiation 36; AU, Arbitrary units.

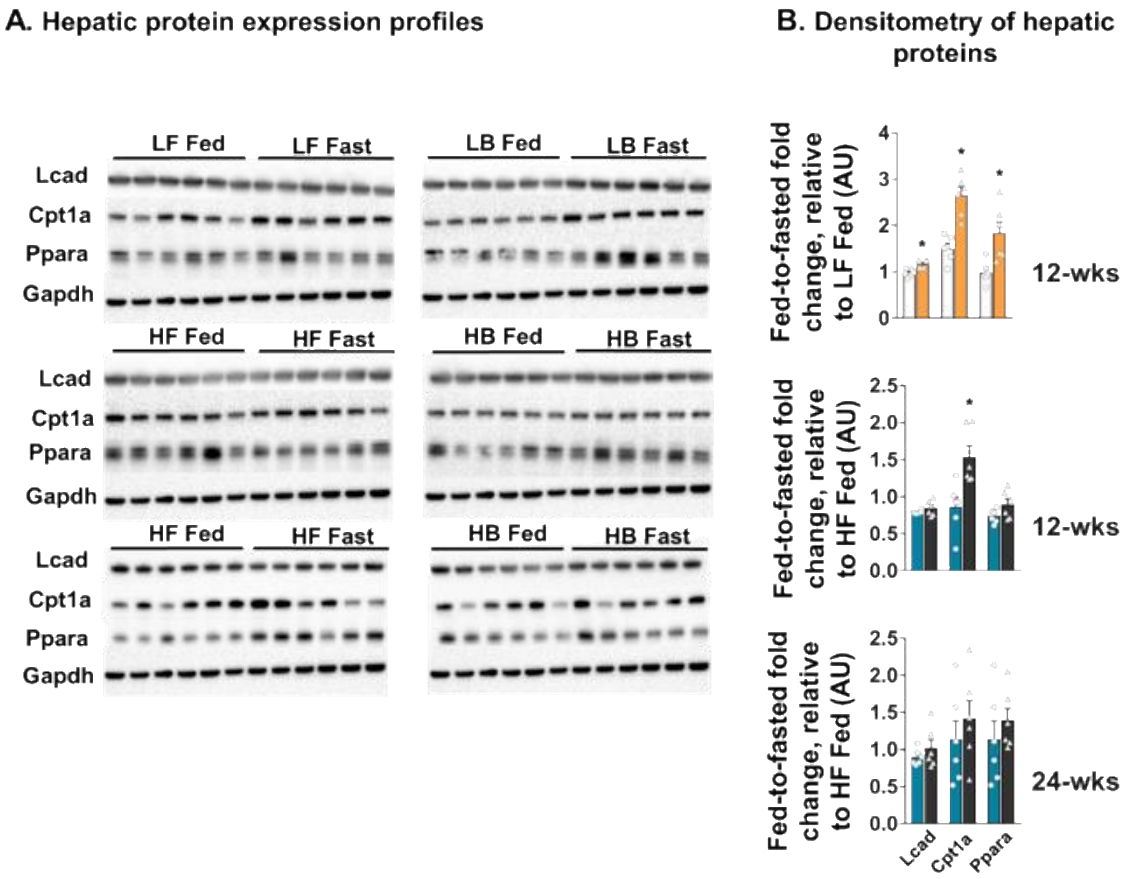

Figure 3.2. BCAA supplementation alters expression profiles of lipid oxidation proteins in the liver. (**A**) Expression profiles of lipid oxidation proteins Lcad, Ppara and Cpt1a (**B**) Densitometry analysis of lipid oxidation proteins represented as fed-to-fasted fold change. The values are normalized to their respective control fed group. All the values are represented as mean ± SEM, with n=6/ group. Results were considered significant at $P < 0.05$ following a t-test between BCAA supplemented and its control group and is represented by "*". Lcad, long-chain acyl dehydrogenase; Cpt1a, Carnitine palmitoyl transferase 1; Ppara, Peroxisome proliferator-activated receptor; Gapdh, Glyceraldehyde 3-phosphate dehydrogenase; AU, Arbitrary units.

3.4.2. Branched chain amino acid supplementation primes the hepatic mitochondria to induce β-oxidation on fasting.

The induction of hepatic lipid oxidation prompted us to investigate whether isolated mitochondria from BCAA supplemented liver retained the ability to induce lipid oxidation and ketogenesis. To test this, isolated liver mitochondria were incubated with $^{13}C_{16}$[palmitate] and the incorporation of ^{13}C from palmitate into ketones (β-hydroxybutyrate) was measured as an index of β-oxidation activity (scheme detailed in **Fig 3.3A**). The fed-to-fasted fold change in ^{13}C incorporation into β-hydroxybutyrate (M+2) significantly increased ($P<0.05$) with 12-wks BCAA supplementation (LB and HB) (**Fig 3.3B; left**). Further, BCAA supplementation increased ($P<0.1$) fed-to-fasted fold change in ^{13}C incorporation into β-hydroxybutyrate (M+4) after 12 and 24-weeks on diet (**Fig 3.3B; right**). Surprisingly, the incorporation of ^{13}C into TCA cycle intermediates (M+2) were comparable between dietary groups in both fed and fasted states (**Fig 3.3C** and **Appendix Table 3.5 and 3.6**).

The fed-to-fasted fold change in the expression of mitochondrial lipid oxidation proteins Lcad and Cpt1a were significantly higher in LB diet fed mice compared to LF (**Fig 3.4A** and **3.4B**). Further, HF diet feeding (12-wks and 24-wks) significantly induced the protein expression of Lcad but the expression of Cpt1a were comparable (**Fig 3.4A** and **3.4B**). In summary, these results demonstrate that the BCAA supplemented liver mitochondria were primed to upregulate lipid oxidation, even when BCAAs are not present in the incubation media as substrates.

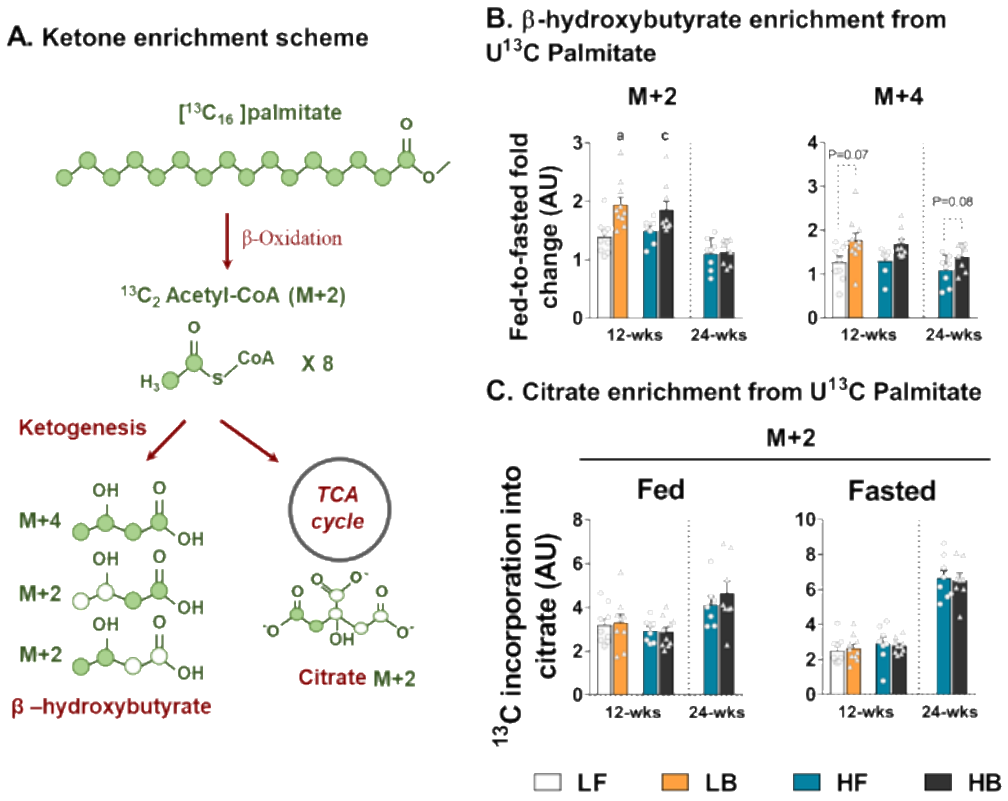

Figure 3.3. BCAA supplementation alters mitochondrial β-oxidation and ketogenesis. (**A**) Scheme highlighting ^{13}C enrichment into β-hydroxybutyrate and TCA cycle intermediates from $^{13}C_{16}$[palmitate] (**B**) Fed-to-fasted fold change in ^{13}C incorporation into β-hydroxybutyrate from U^{13}C[palmitate] (**C**) ^{13}C incorporation into citrate from U^{13}C[palmitate] in fed and fasted states. The values are normalized to their respective control fed group. All the values are represented as mean ± SEM, with n=8-10/ group. Results were considered significant at $P < 0.05$ following one-way ANOVA (between 12-wk diet groups) and tukey's pairwise mean comparison which are represented by the following alphabets: "a"—LF vs LB; "b"—LF vs HF; "c"—LF vs HB; "d"—LB vs HF; "e"—LB vs HB; and "f"—HF vs HB. The significance between 24-wk HF and HB groups were analyzed following a t-test and is represented by "*".

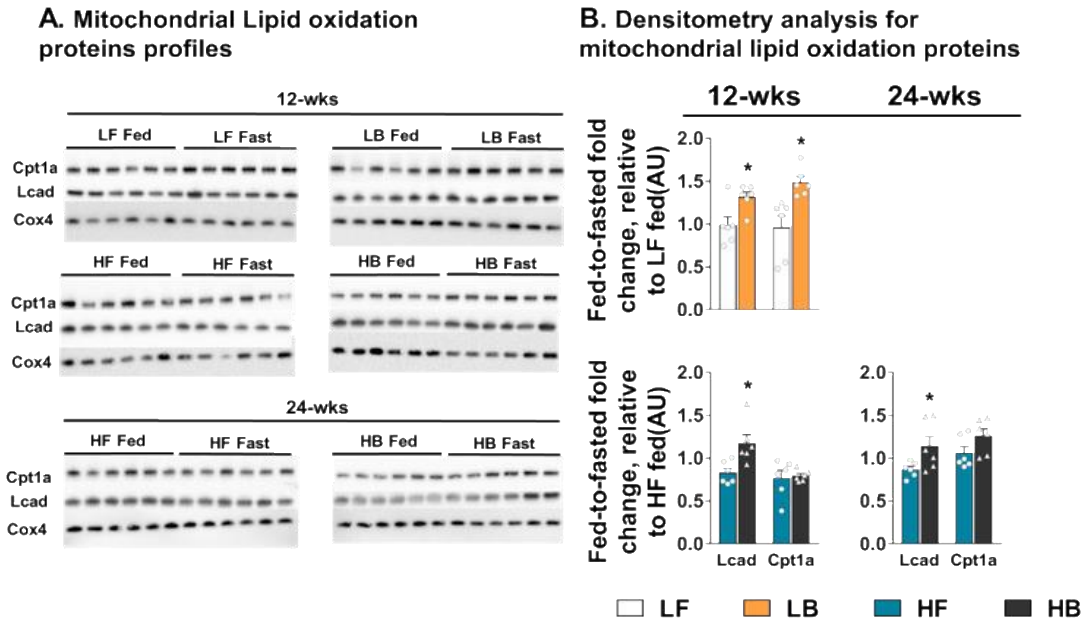

Figure 3.4. BCAA supplementation alters mitochondrial lipid oxidation protein profiles in the liver mitochondria. (**A**) Western blots of lipid oxidation proteins such as Cpt1a, Lcad and Cox4 (**B**) Fed-to-fasted fold changes in expression profiles of mitochondrial lipid oxidation proteins. The values are normalized to their respective control fed group. All the values are represented as mean ± SEM, with n=6/ group. Results were considered significant at $P < 0.05$ following a t-test between BCAA supplemented and its control group and is represented by "*". Lcad, long-chain acyl dehydrogenase; Cpt1a, Carnitine palmitoyl transferase 1; Cox4, Cytochrome oxidase subunit 4.

3.4.3. Branched chain amino acids supplementation suppressed hepatic *de novo* lipogenesis.

Lipogenesis was measured in mice after 12-wks dietary supplementation and in fed states. Deuterium enrichment into newly synthesized lipids in the liver was determined by ^{2}H NMR. Percentage de novo lipogenesis (DNL; % mean ± SEM) was significantly lower in mice fed with LB diet (28.5±2.4) compared to the LF diet (22.8±2.4) (**Fig 3.5A**). Also, the hepatic lipogenic genes such as ATP citrate lyase (*Acly*), which cleaves cytoplasmic citrate into acetyl-CoA and oxaloacetate, acetyl CoA carboxylase (*Acc*) which converts acetyl-CoA to malonyl-CoA were suppressed ~ 2 folds upon feeding LB diet compared to LF (**Fig 3.5B**). Further, genes such as fatty acid synthase (Fasn), Fatty acid elongase (Elovl6) and steroyl CoA desaturase (SCD1) were significantly downregulated in LB mice compared to LF (**Fig 3.5B**). Although the high-fat diet feeding significantly suppressed all the lipogenic genes (~4 fold) compared to LF, HB diet feeding did not alter their expression with respect to HF (**Fig 3.5B**). However, the expression of mitochondrial citrate carrier protein (SLC25A) expression was lower with BCAA supplementation although not statistically significant (**Fig 3.6A** and **3.6B**). Taken together, this data illustrates the downregulation of hepatic lipogenic machinery with BCAA supplementation under normal physiological conditions.

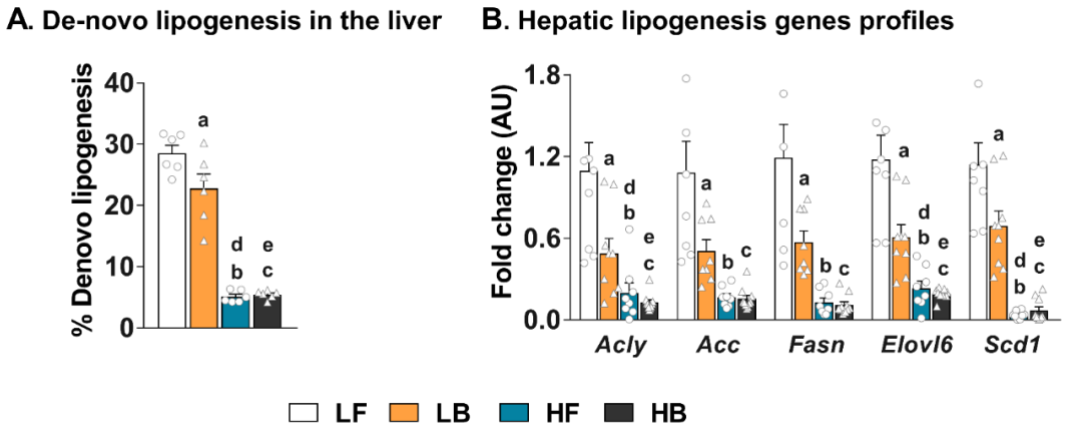

Figure 3.5. BCAA supplementation suppressed hepatic de novo lipogenesis. (**A**) Percentage de novo lipogenesis in the liver (**B**) Expression profiles of genes involved in lipogenesis such as Acly, Acc, Fasn, Elovl6 and Scd1. All the values are represented as mean ± SEM, with n=6-10/ group. Results were considered significant at $P < 0.05$ following one-way ANOVA and tukey's pairwise mean comparison which are represented by the following alphabets: "a"—LF vs LB; "b"—LF vs HF; "c"—LF vs HB; "d"—LB vs HF; "e"—LB vs HB; and "f"—HF vs HB. Acly, ATP citrate lyase; Acc, Acetyl-CoA carboxylase alpha; Fasn, Fatty acid synthase; ELOVl6, Elongation of very long chain fatty acid elongase 6; Scd1, Stearoyl-CoA desaturase 1; AU, arbitrary units.

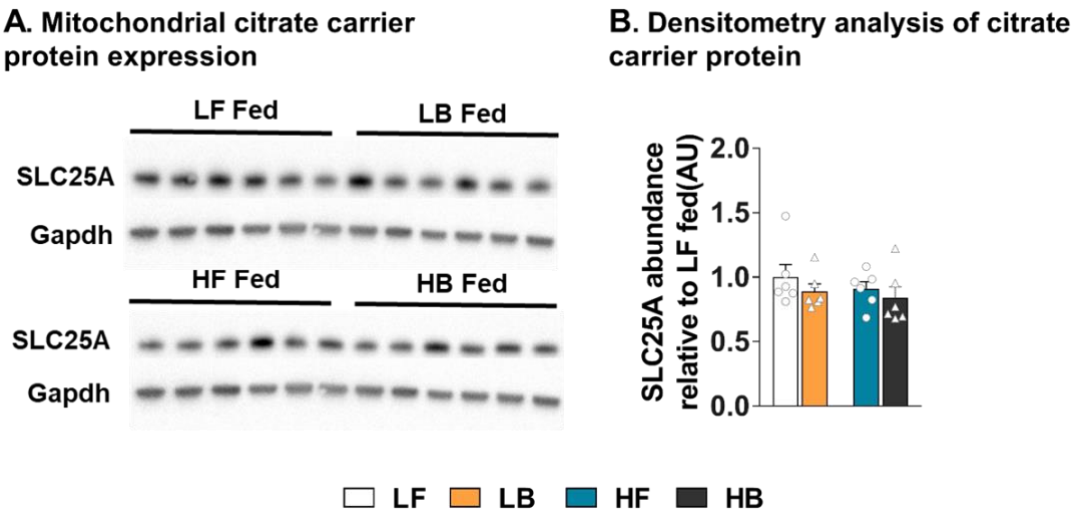

Figure 3.6. Expression profiles of mitochondrial citrate carrier protein (SLC25A). (**A**) Western blots of citrate carrier protein in isolated mitochondria (**B**) Densitometry analysis of mitochondrial citrate carrier protein expression. All the quantification was in relative to LF fed. All the values are represented as mean ± SEM, with n=6/ group. Results were considered significant at $P < 0.05$ following one-way ANOVA and tukey's pairwise mean comparison which are represented by the following alphabets: "a"—LF vs LB; "b"—LF vs HF; "c"—LF vs HB; "d"—LB vs HF; "e"—LB vs HB; and "f"—HF vs HB. SLC25A, The solute carrier family 25; Gapdh, Glyceraldehyde 3-phosphate dehydrogenase; AU, Arbitrary units.

3.4.4. The induction of hepatic lipid oxidation in the BCAA supplemented livers occurred despite a decrease in BCAA and BCKA carbons during fasting. The fed circulating concentrations of BCAAs (μM± SEM) did not increase after 12-wks dietary supplementation, but HB diet feeding for 24-wks significantly ($P \leq 0.05$) increased fed plasma concentration of BCAAs (**Fig 3.7A-C**; Valine: 432 ± 34; Leucine, 270 ± 24; and Isoleucine, 216 ± 18) compared to HF counterparts (Valine, 311 ± 38; Leucine, 190 ± 22; and Isoleucine, 176 ± 21). Similarly, the fed circulating concentrations of BCKAs did not vary between groups after 12-wks dietary treatment (**Fig 3.8A-C**). But, the plasma concentrations of BCKAs were significantly higher ($P \leq 0.05$) in HB diet fed groups compared to HF after 24-wks dietary treatment (**Fig 3.8A-C**). As expected the fasted concentrations of BCAAs (**Fig 3.7D-F**) and their respective BCKAs (**Fig 3.8D-F**) were lower compared to the fed levels, but the concentrations remained similar between dietary treatments. The lower concentration of BCAAs during fasted states was associated with increased expression of BCAA degradation enzymes such as BCKDHA, BCKDHB and PP2Cm during fasting (**Fig 3.9A-C**). Moreover, the fed turnover rates (μmoles/min ± SEM) of leucine after 12-wks dietary supplementation increased with BCAA supplementation (LB: 0.34 ± 0.03; HB: 0.39 ± 0.05) compared to their LF and HF counterparts (LF: 0.31 ± 0.03; HF: 0.30 ± 0.05) (**Appendix Fig 3.1A**). Also, the fed turnover rates of α-ketoisovaleric acid, ketoacid of valine and α-keto-β-methylvalerate, keto-acid of isoleucine increased with BCAA feeding (**Appendix Fig 3.1B-C)**. However, the fasted turnover rates of valine, α-ketoisovaleric acid and α-keto-β-methylvalerate decreased compared to the fed state but the rates remained similar between groups after 12 and 24-wks dietary treatment (**Fig 3.10A-C**).

In summary, concentrations and turnover rates of BCAAs and BCKAs reduced in fasted conditions within all treatment groups compared to the fed states. The depleted levels of BCAA derived carbons in circulation during fasted state and lower fasted turnover rates was associated with significantly higher fed-to-fasted fold induction in hepatic lipid oxidation (**Figure 3.1** and **Fig 3.2**) suggests an independent role of BCAAs in altering the hepatic lipid oxidation than being substrates to the mitochondria.

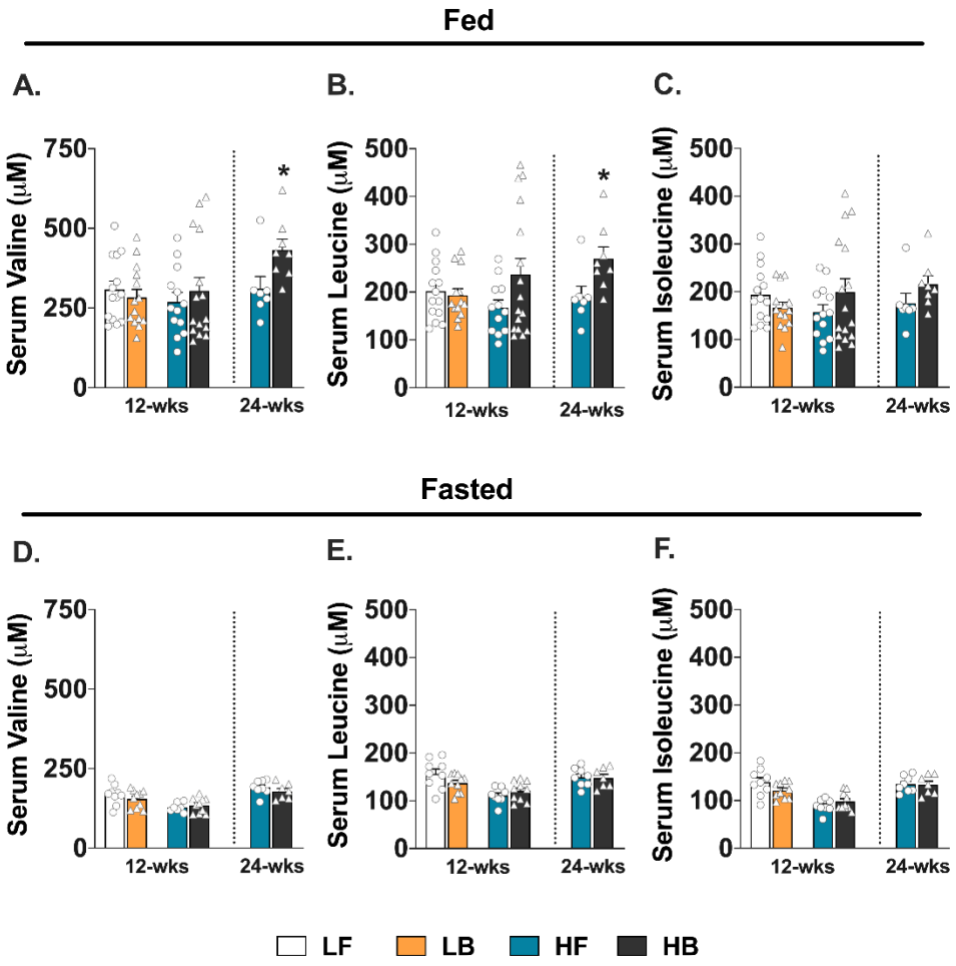

Figure 3.7. Fasting significantly reduced the circulating concentrations of BCAAs. Circulating fed concentrations of (**A**) Valine (**B**) Leucine (**C**) Isoleucine. Fasted concentrations of (**D**) Valine (**E**) Leucine (**F**) Isoleucine. All the values are represented as mean ± SEM, with n=8-14/ group. Results were considered significant at $P < 0.05$ following one-way ANOVA (between 12-wk diet groups) and tukey's pairwise mean comparison which are represented by the following alphabets: "a"—LF vs LB; "b"—LF vs HF; "c"—LF vs HB; "d"—LB vs HF; "e"—LB vs HB; and "f"—HF vs HB. The significance between 24-wk HF and HB groups were analyzed following a t-test and is represented by "*".

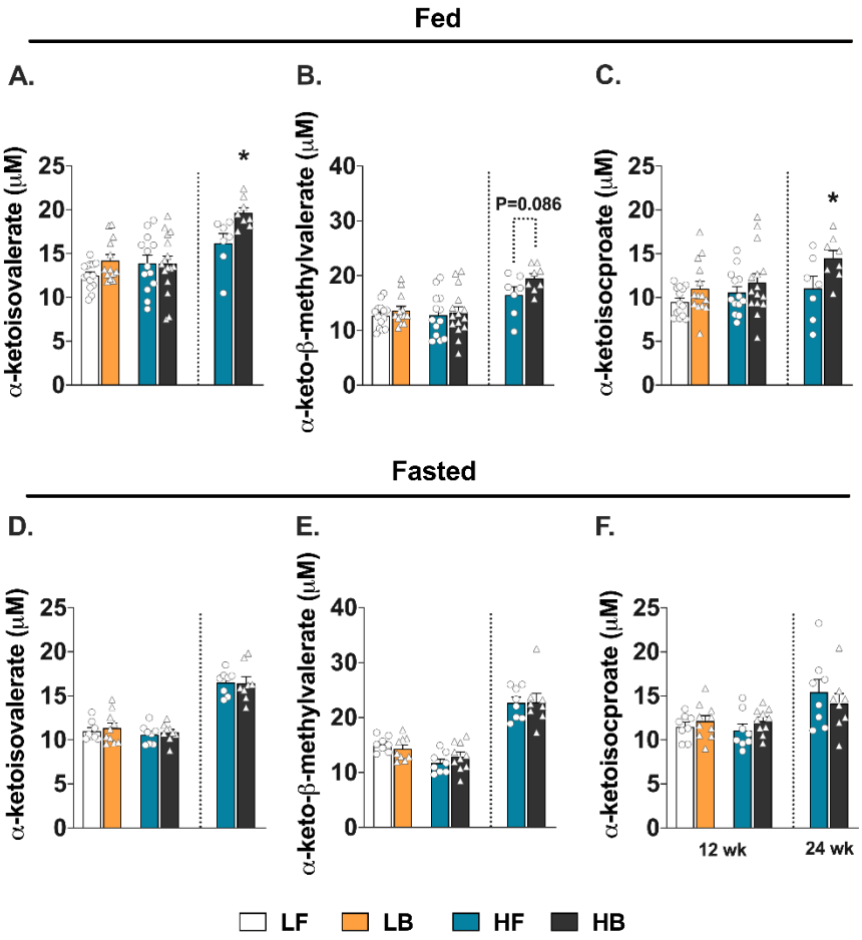

Figure 3.8. Serum concentrations of BCKAs decreased with fasting. Circulating fed concentrations of (**A**) α-ketoisovaleric acid (**B**) α-keto-β-methylvalerate (**C**) α-ketoisocaproate. Fasted concentrations of (**D**) α-ketoisovaleric acid (**E**) α-keto-β-methylvalerate (**F**) α-ketoisocaproate. All the values are represented as mean ± SEM, with n=8-14/ group. Results were considered significant at $P < 0.05$ following one-way ANOVA (between 12-wk diet groups) and tukey's pairwise mean comparison which are represented by the following alphabets: "a"—LF vs LB; "b"—LF vs HF; "c"—LF vs HB; "d"—LB vs HF; "e"—LB vs HB; and "f"—HF vs HB. The significance between 24-wk HF and HB groups were analyzed following a t-test and is represented by "*".

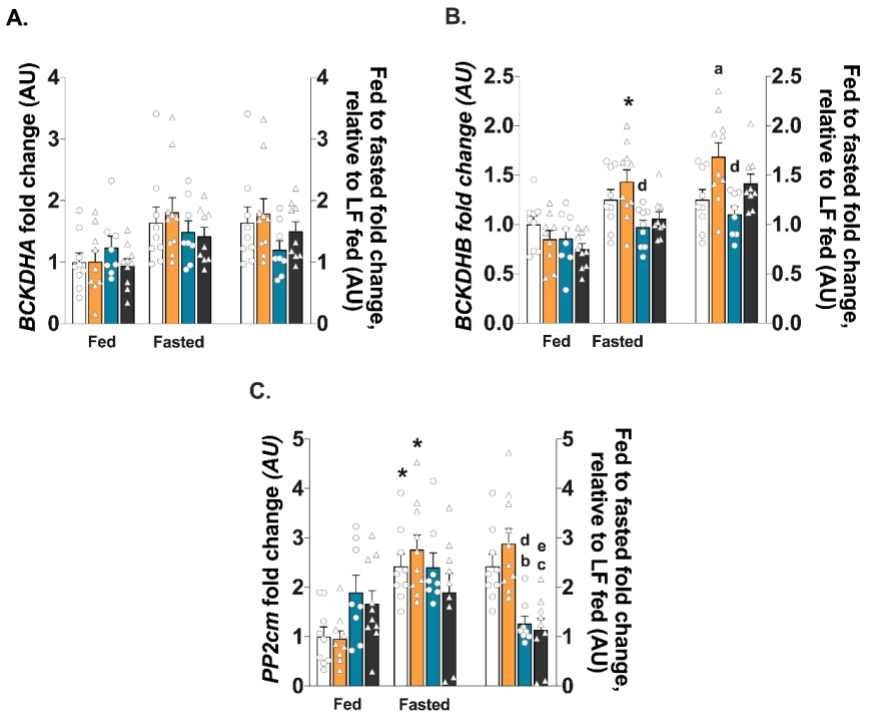

Figure 3.9. Expression profiles of hepatic genes involved in BCAA degradation increased with BCAA supplementation on fasting. Genes expression profile of (**A**) Branched-chain keto acid dehydrogenase E1 subunit alpha (**B**) Branched-chain keto acid dehydrogenase E1 subunit beta and (**C**) Mitochondrial protein phosphatase 2C. The expression profiles were measured in fed and fasted states and are normalized to LF fed. All the values are represented as mean ± SEM, with n=7-10/ group. Results were considered significant at $P < 0.05$ following one-way ANOVA and tukey's pairwise mean comparison (fed and fasted groups were analyzed separately) which are represented by the following alphabets: "a"—LF vs LB; "b"—LF vs HF; "c"—LF vs HB; "d"—LB vs HF; "e"—LB vs HB; and "f"—HF vs HB. The significance between fed and fasted states of same groups are represented by "*". BCKDHA/B, Branched chain keto acid dehydrogenase E1 subunit alpha and beta; PP2Cm, Protein phosphatase 2C mitochondrial; AU, Arbitrary units.

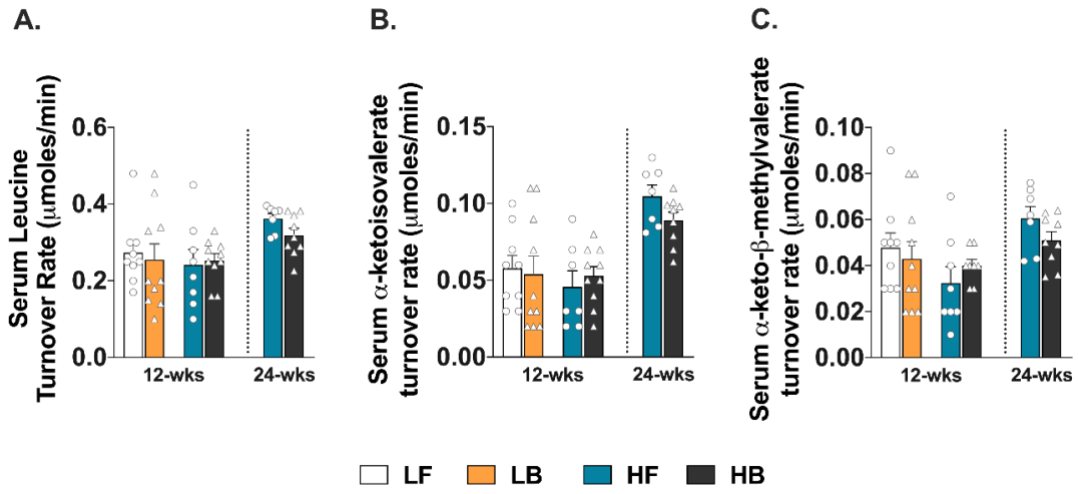

Figure 3.10. BCAA mediated induction in lipid oxidation during fasting was associated with lower turnover rates of BCAAs and BCKAs. Whole body fasted turnover rates of (A) leucine (B) α-ketoisovalerate and (C) α-keto-β-methylvalerate. All the values are represented as mean ± SEM, with n=8-10/ group. Results were considered significant at $P < 0.05$ following one-way ANOVA (between 12-wk diet groups) and tukey's pairwise mean comparison which are represented by the following alphabets: "a"—LF vs LB; "b"—LF vs HF; "c"—LF vs HB; "d"—LB vs HF; "e"—LB vs HB; and "f"—HF vs HB. The significance between 24-wk HF and HB groups were analyzed following a t-test and is represented by "*".

3.4.5. Incorporation of BCKA carbons into ketones were higher in BCAA supplemented liver mitochondria, only under fed conditions.

To determine if the BCKAs carbons fuel hepatic mitochondrial lipid oxidation and mitochondrial metabolism, we incubated the isolated hepatic mitochondria with U^{13}C[isocaproate] and tracked the incorporation of ^{13}C into ketone (β-hydroxybutyrate) and TCA cycle intermediates. The ^{13}C enrichment scheme of ketone and TCA cycle intermediates from U^{13}C[isocaproate] is detailed in **Fig 3.11A**. The ^{13}C incorporation into ketone (M+3) was significantly higher in LB diet fed mice compared to LF during fed conditions, however the fasting enrichments were similar between groups (**Fig 3.11B**). However, the ^{13}C enrichments (M+2) into citrate (**Fig 3.11C**) and other TCA cycle intermediates (**Appendix Table 3.7**) did not vary between the dietary treatments during fed or fasted states.

To summarize, higher ^{13}C enrichment into β-hydroxybutyrate during fed states were associated with no significant changes in citrate enrichment suggesting that BCKAs induced ketone formation independent of their role as substrates to the TCA cycle.

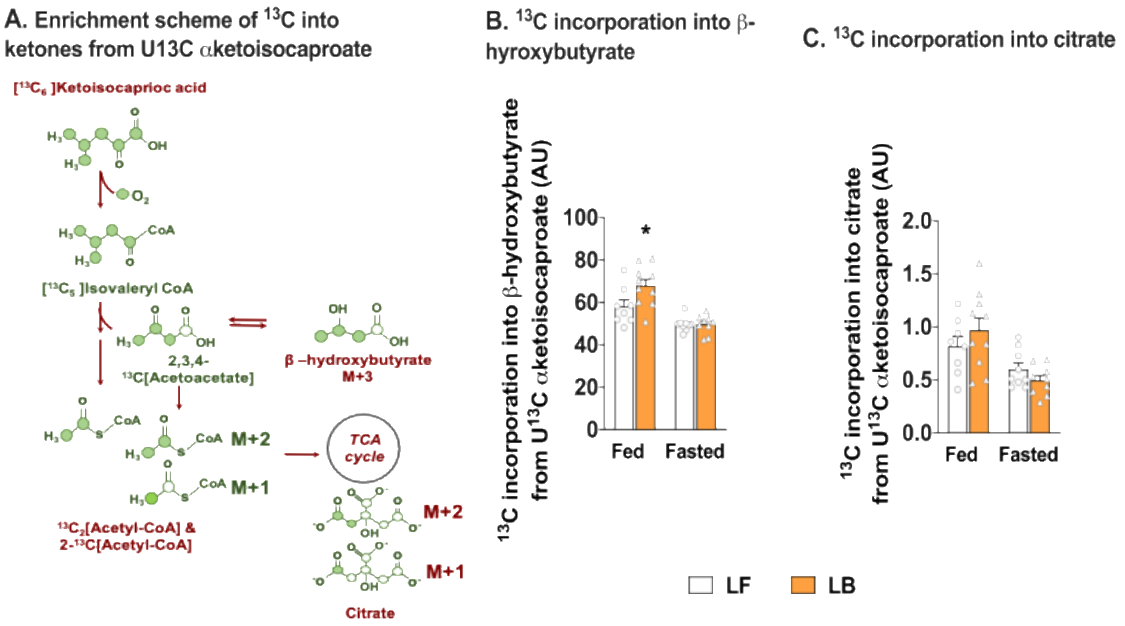

Figure .3.11. BCAA mediated induction in ketogenesis occurred independent of substrate mediated effects of BCAAs. (A) Enrichment scheme of ^{13}C enrichment into ketones and TCA cycle intermediate citrate from $^{13}C_6$[α-ketoisocaproate] (**B**) ^{13}C enrichment into β-hydroxybutyrate (**C**) ^{13}C enrichment into citrate (^{13}C enrichment into other TCA cycle intermediates in **Appendix Table 3.7**). All the values are represented as mean ± SEM, with n=7-10/ group. Results were considered significant at $P < 0.05$ following following a t-test between LF and LB and is represented by "*". Fed and fasted groups were analyzed individually. TCA, Tricarboxylic acid cycle; AU, Arbitrary units.

3.4.6. BCAA supplemented liver mitochondrial had higher ADP stimulated respiration without any changes in mitochondrial ROS generation.

BCAA supplementation induced ADP stimulated respiration (normalized to their basal respiration) in fed and fasted states compared to LF counterparts (**Fig 3.12A**). The increase in ADP stimulated respiration in BCAA supplemented mice was associated with no changes in reactive oxygen species (ROS; hydrogen peroxide) formation compared to LF counterparts in fed or fasted states (**Fig 3.12B**). In summary, the significant increase in ADP stimulated oxygen consumption with BCAA supplementation (LB) occurred in simultaneous with induction in fed-to-fasted fold change in lipid oxidation without any apparent changes in ROS production.

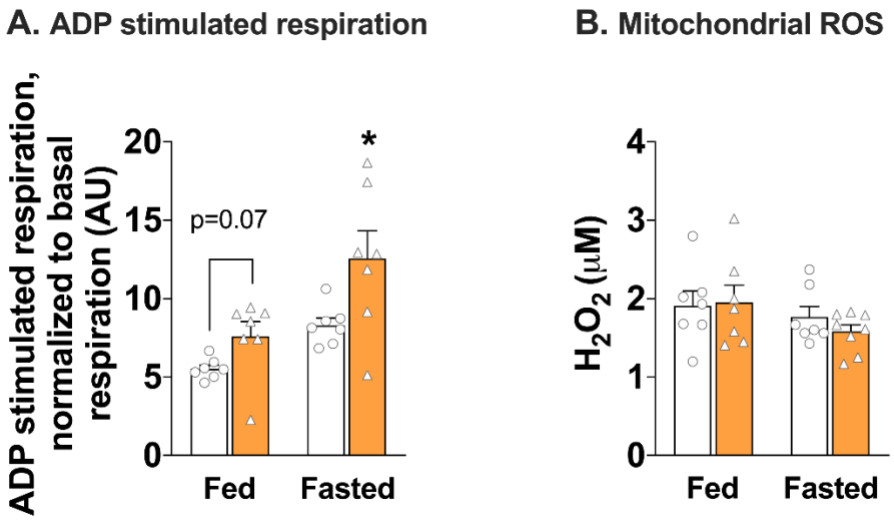

Figure 3.12. BCAA induced mitochondrial respiration without apparent changes in ROS formation. (A) ADP stimulated respiration, normalized to basal respiration in fed and fasted states (**B**) Mitochondrial ROS concentration in fed and fasted states. All the values are represented as mean ± SEM, with n=7/ group. Results were considered significant at $P < 0.05$ following a t-test between LF and LB and is represented by "*". Fed and fasted groups were analyzed individually. ADP. Adenosine diphosphate; ROS, Reactive oxygen species; AU, Arbitrary units.

3.4.7. The redox state of the BCAA supplemented livers were more favorable for sustained lipid oxidation.

Alteration in hepatic lipid metabolism with BCAA supplementation (LB) prompted us to determine the redox state of the liver. The levels of NADH is important towards maintaining cellular redox homeostasis and cellular metabolism. We measured liver lactate to pyruvate (lac/pyr) ratio as a proxy for cytoplasmic NADH/NAD+. The fasted lac/pyr ratio was higher in BCAA supplemented mice, while the fed ratio was comparable (**Fig 3.13A**). Similarly, the fasted liver $NADH/NAD^+$ ratio was significantly induced ($P<0.05$) with BCAA supplementation (LB), while the fed ratio remained elevated in LB mice (**Fig 3.13C**). Mitochondrial $NADH/NAD^+$ was calculated to using serum acetoacetate to β-hydroxybutyrate (AcAc/BHB) ratio (AU ± SEM). The fed AcAc/BHB ratio were similar between groups, however the fasted ratio was significantly higher with BCAA supplementation (**Fig 3.13B**; LF, 3.59 ± 0.15; LB, 4.40 ± 0.15).

In summary, BCAA supplementation maintained a reduced hepatocellular environment (higher $NADH/NAD^+$) in fasted states, which occurs in association with fed-to-fasted induction in hepatic mitochondrial lipid oxidation.

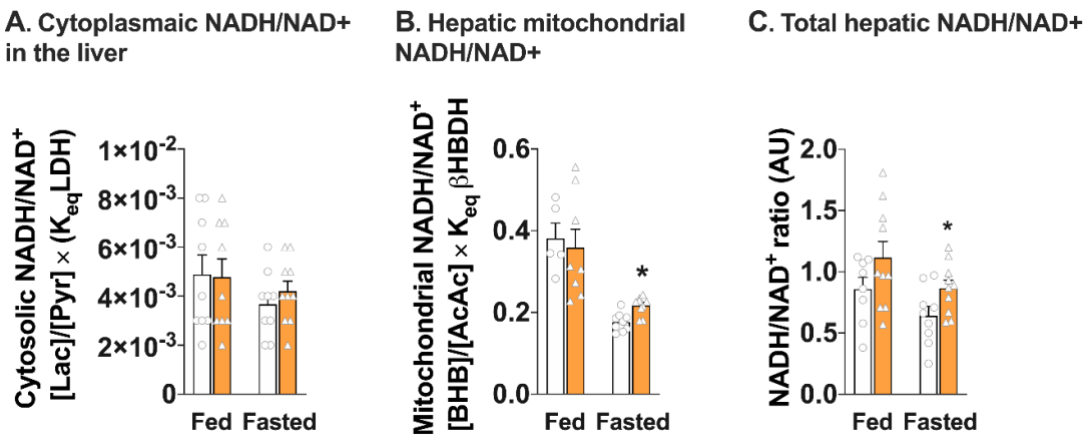

Figure 3.13. **BCAA supplemented mice maintained reduced environment in the liver. (A)** Cytosolic NADH/NAD$^+$ measured as lactate/pyruvate ratio (**B**) Mitochondrial NADH/NAD$^+$ was measured as β-hydroxybutyrate/acetoacetate ratio (**C**) Total liver NADH/NAD$^+$ ratio. All the values are represented as mean ± SEM, with n=7-10/ group. Results were considered significant at $P < 0.05$ following a t-test between LF and LB and is represented by "*". Fed and fasted groups were analyzed individually. NAD, Nicotinamide adenine dinucleotide; βHBDH, β-hydroxybutyrate dehydrogenase; Lac, Lactate; Pyr, Pyruvate; LDH, Lactate dehydrogenase; BHB, β-hyroxybutyrate dehydrogenase; AcAc, Acetoacetate; AU, Arbitrary units.

3.4.8. BCAA supplemented livers demonstrated higher AMPK activity. BCAA mediated induction in hepatic lipid metabolism and mitochondrial oxidative network in fasted states occurs in association with increased NADH/ NAD^+ ratio. We measured hepatic activity of AMPK, a master regulator of cellular energy homeostasis and AMPK mediated cellular networks. BCAA supplementation increased AMPK activity (pAMPK/AMPK ratio) with fasting (**Fig 3.14A and Fig 3.14B**). Further, the fed-to-fasted fold changes in concentration of pAMPK protein was also higher in the livers fed with the LB diet compared to LF (**Fig 3.14C**). The fed-to-fasted fold induction in the hepatic AMPK activity was associated with induced expression of PGC1a and Ppara, which are involved in mitochondrial metabolism and lipid oxidation (**Fig 3.15C**).

AMPK regulates phosphorylation of ACC at ser 79 to inhibit lipogenesis and LB diet feeding significantly induced the phosphorylation of ACC at ser 79 (**Fig 3.15A** and **Fig 3.15B**). Our data demonstrates a possible mechanism of BCAA mediated increase in AMPK activity in fasted states and associated increase in mitochondrial lipid oxidation. Also, the increased phorphorylation of ACC at ser 79 with BCAA supplementation in fed states occurs simultaneous to reduced rates of lipogenesis (**Fig 3.5A**).

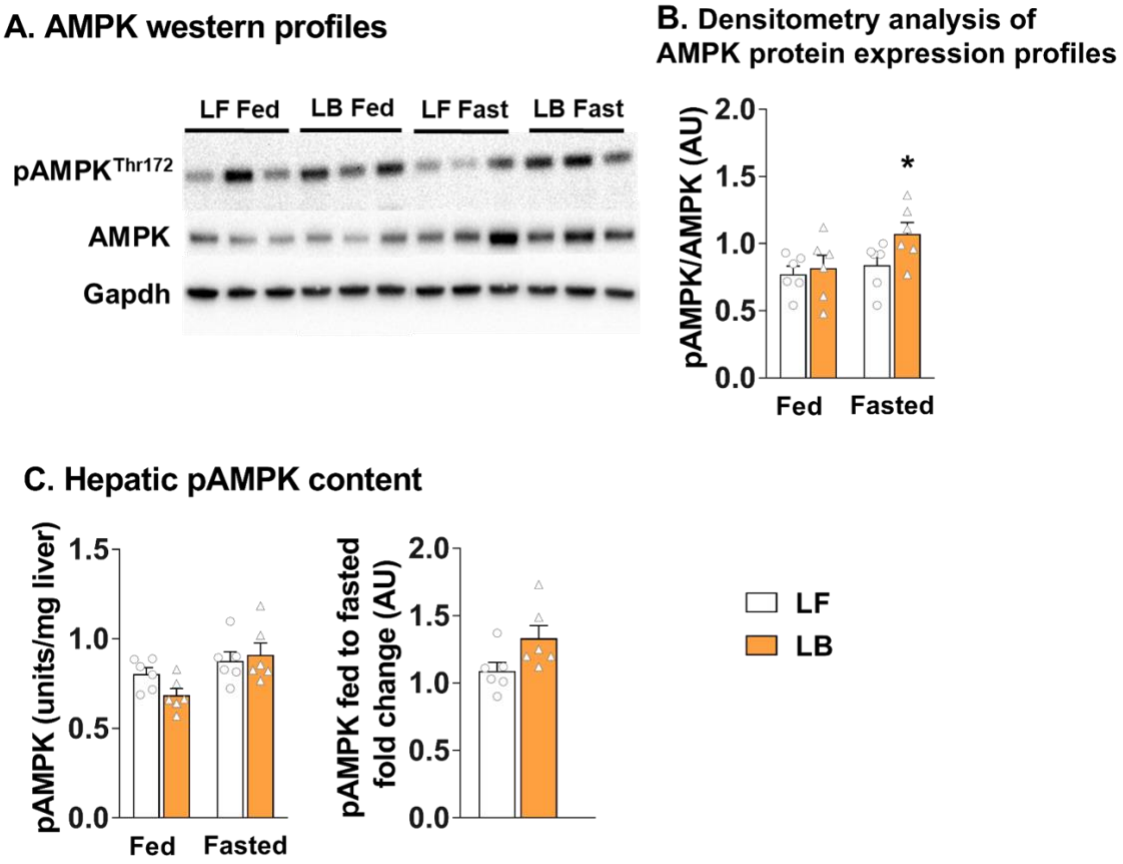

Figure 3.14. BCAA supplementation induced AMPK activity with fasting. (**A**) western blot analysis of liver AMPK and phorphorylated AMPK at Thr 172 site (**B**) Densitometry analysis of pAMPK/AMPK ratio (**C**) Hepatic pAMPK content, normalized to mg liver. All the values are represented as mean ± SEM, with n=6/ group. Results were considered significant at $P < 0.05$ following a t-test between LF and LB and is represented by "*". Fed and fasted groups were analyzed individually. AMPK, Adenosine mono phosphate-activated protein kinase; Gapdh, Glyceraldehyde 3-phosphate dehydrogenase; AU, Arbitrary units.

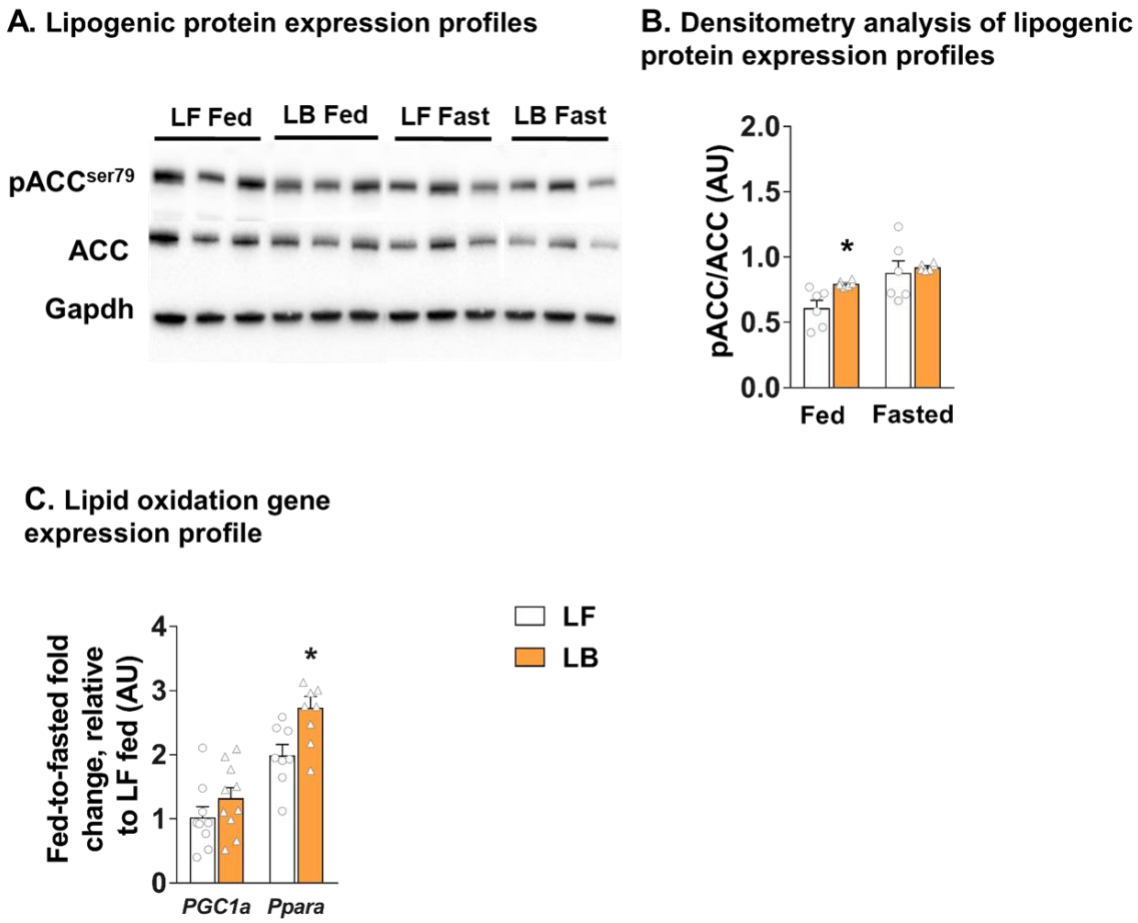

Figure 3.15. BCAA mediated increase in AMPK activity occurred simultaneous to increased lipid oxidation and lower lipogenesis. (**A**) Western blot analysis of liver ACC and phorphorylated ACC at Ser 79 site (**B**) Densitometry analysis of pACC/ACC ratio (**C**) Fed-to-fasted fold change in mitochondrial lipid metabolism genes. All the values are represented as mean ± SEM, with n=6-10/ group. Results were considered significant at $P < 0.05$ following a t-test between LF and LB and is represented by "*". Fed and fasted groups were analyzed individually. ACC, Acetyl CoA carboxylase; GAPDH, Glyceraldehyde 3-phosphate dehydrogenase; AU, Arbitrary units.

3.5. Discussion

Synergistic coupling of mitochondrial oxidative networks such as β-oxidation, ketogenesis and TCA cycle with Oxphos and ATP synthesis is required for normal mitochondrial function with minimal ROS generation as a byproduct[150,181]. However, during insulin resistance and associated metabolic diseases the mitochondrial oxidative networks remodel and adapt to hormonal and nutrient stimuli and results in an increased ROS generation[21,23,150]. The initial stages insulin resistance and NAFLD, is associated with a compensatory induction in the mitochondrial oxidative machinery to get rid of excess lipids, but with the progression of the disease the mitochondrial networks fail to adapt and gets inefficient and dysfunctional[15,16,40]. This impairment in the mitochondrial function occurs simultaneous with increased ROS, oxidative stress and inflammation[15,16,40]. Further, the progression of insulin resistance is also correlated with an increase in circulating levels of BCAAs and defects in their catabolic network[25,26]. Elevated BCAAs are considered predictors of type-2 diabetes onset and therefore are candidate of interest during insulin resistance and related metabolic diseases[25,26]. BCAAs are known to interact with mitochondrial metabolism by being substrates for the mitochondria and fuel reactions to support ketogenesis, TCA cycle and gluconeogenesis. Also, disrupted BCAA catabolism is linked to impaired mitochondrial metabolism leading to anaplerotic stress and suboptimal TCA cycle activity which further contributes towards mitochondrial dysfunction[26]. Therefore, understanding the interaction of BCAAs and mitochondrial oxidative networks is essential to fully elucidate the cause of mitochondrial dysfunction during insulin resistance and NAFLD. We hypothesized that the crosstalk between BCAAs

and mitochondrial lipid metabolism is mediated through their ability to modulate hepatic oxidative function and lipogenesis. We also postulated that this modulation occurs independent to their role as anaplerotic substrates for the mitochondrial oxidative machinery.

Liver is a metabolically flexible organ, with dynamic shifts in metabolic networks between states of feeding and fasting in response to the changes in nutrient and hormonal cues. The fed liver stimulates uptake of glucose and induce glycolysis, stores glycogen and induce lipid synthesis [182-184]. While the fasted liver upregulates glycogen breakdown, new glucose synthesis, lipid oxidation and ketogenesis[5,185]. This flexibility of liver to transit between fed and fasted states is required to maintain metabolic homeostasis. Thus, we believe that fed-to-fasted fold changes in metabolic measurements is more physiologically relevant to study metabolism than just discrete measurements at fed or fasted states.

Supplementation of 150% excess dietary BCAAs (LB) induced hepatic lipid oxidation on fasting, represented as fed-to-fasted fold changes in gene expression (**Fig 3.1A-E**). Further, increased formation of β-hydroxybutyurate in fasted BCAA supplemented liver indicated the ketogenic capability of BCAAs (**Fig 3.1F**). Our data suggests, that excess acetyl-CoA from increased lipid oxidation to fuel ketogenesis. Further, a higher fed-to-fasted fold changes in the ^{13}C incorporation from $^{13}C_{16}$[palmitate] into β-hydroxybutyurate in the isolated mitochondria from BCAAs supplemented mice livers suggested an upregulation in the β-oxidation machinery (**Fig 3.3**). The onset/ mild insulin resistance (12-wks HF dietary treatment) blunted

the lipid oxidation machinery, but the BCAAs supplementation sustained induction of lipid oxidation during progressive stages of insulin resistance (24-wks HF dietary treatment) (**Fig 3.1** and **Fig 3.2**). Taken together, BCAAs appear to prime the liver to upregulate mitochondrial oxidative networks (β-oxidation and ketogenesis) upon fasting.

Simultaneous induction of lipid oxidation and lipogenic machinery is often co-exists with hepatocellular stress and inflammation[15,21,150]. We evaluated the impact of BCAAs on hepatic de novo lipogenesis by calculating ^{2}H enrichment of lipids from deuterated water and measuring lipogenic gene expression profiles. BCAA supplementation (LB) lowered the rates of ^{2}H enrichment into the lipids represented as % *de novo* lipogenesis (**Fig 3.5A**) and expression profiles of genes involved in lipogenesis were suppressed with LB diet feeding (**Fig 3.5B**). Taken together, our data indicates a BCAA mediated priming of hepatic mitochondria to induce β-oxidation and shunt most of the resulting acetyl-CoA towards ketogenesis and away from citrate synthase flux. This highlights certain beneficial effects of BCAAs in avoiding hepatic lipid accumulation by upregulating lipid oxidation and suppressing lipid synthesis and their possible role in alleviating hepatocellular stress during insulin resistance and NAFLD.

A major component of mitochondrial oxidative metabolism is TCA cycle, which is responsible for i) complete oxidation of acetyl-CoA into CO_2 ii) supports anaplerotic reactions towards biosynthetic pathways such as gluconeogenesis and lipogenesis. BCAAs are known substrates fueling anaplerotic reactions to support gluconeogenesis via TCA cycle. We hypothesized that the alteration in hepatic lipid

metabolism by BCAAs occurs independent of their capability to serve as anaplerotic substrates to the mitochondria. To test our hypothesis we incubated the isolated mitochondria from different dietary treatments with U^{13}C[palmitate] and U^{13}C[ketoisocaproic acid] and measured the incorporation of ^{13}C from labeled palmitate or ketoisocaproic acid into TCA cycle intermediates (**Fig 3.3C** and **Fig 3.11C** and **Appendix Table 3.7**). ^{13}C enrichment into citrate and other TCA cycle intermediates were similar between BCAA supplemented group and their control in fed or fasted states (**Fig 3.3C** and **Fig 3.11C**) suggesting minimal to no changes in TCA cycle activity compared to control groups. However, the ^{13}C incorporation into BHB from U^{13}C[palmitate] was higher in mitochondria from BCAA supplemented mice during fasting (**Fig 3.3.B**). Further the ^{13}C incorporation into BHB from U^{13}C[ketoisocaproic acid] was higher in fed state suggesting BCAA mediated induction in ketogenesis (**Fig 3.11B**). The ^{13}C incorporation into BHB during fasted states are similar between groups occurs concurrent to lower BCAA carbons in circulation (**Fig 3.7** and **Fig 3.11B**) highlighting the independent role of BCAAs in altering mitochondrial lipid oxidation. Sustained TCA cycle activity is a known phenomenon during progressive stages of insulin resistance and NAFLD. However, BCAA supplementation demonstrates certain beneficial impact of BCAAs towards lowering hepatic lipid accumulation by inducing lipid oxidation and suppressing lipogenesis but without sustained induction in the TCA cycle. Moreover, the concentration and turnover rates of BCAAs reduced upon fasting and this occurs in concurrent to higher fasting BCAA degradation enzymes. The lower availability BCAA carbons during fasting occurred simultaneous to higher fed-to fasted fold

induction in hepatic lipid oxidation hinting at the non-substrate mediated effect of BCAAs to alter hepatic mitochondrial lipid oxidation. Taken together, our data highlights an important role of BCAAs in regulating hepatic lipid oxidation independent to their role of being substrates to hepatic mitochondria.

Mitochondria is the major site for redox reactions and ROS generation[187-190]. Sustained induction of mitochondrial β-oxidation during stages of NAFLD and associated co-morbidities is usually associated higher levels of ROS and a simultaneous change in cellular redox to a more oxidized state[181,187,191,192]. Mitochondrial oxidation of lipids via β-oxidation produces reducing equivalents and acetyl-CoA and the latter can be further processed via TCA cycle for more NADH and $FADH_2$ to produce ATP. With observed changes in mitochondrial lipid oxidation, we evaluated the alteration in hepatic redox state. BCAA supplementation under normal physiological conditions, increased cytoplasmic and mitochondrial $NADH/NAD^+$ upon fasting measured as lac/pyr and BHB/AcAc ratio respectively[150,179,180] (**Fig 3.13**) as their interconversion occurs through redox reactions using NADH and NAD^+. Higher reducing equivalents in the form of NADH upregulated ADP stimulated respiration in fed and fasted states without apparent changes in superoxide formation (**Fig 3.12**). To summarize, BCAA mediated induction in fed-to-fasted fold changes in mitochondrial β-oxidation shunts the majority of acetyl-CoA towards ketogenesis and away from lipogenesis, while maintaining a reduced cellular environment. Further increase $NADH/NAD^+$ occurred concurrent to increased oxygen consumption and no apparent changes in mitochondrial ROS generation.

AMPK is a major regulator of cellular homeostasis and metabolism. Dysregulation in AMPK activity is considered as one of the pathogenesis of NAFLD[193]. But, the reactivation of AMPK activity during progressive stages of NAFLD restored normalcy in hepatic lipid metabolism by lowering hepatic lipid content through activating lipid oxidation and inhibiting lipogenesis[193-195]. BCAA supplementation increased activity of AMPK (pAMPK/AMPK) upon fasting (**Fig 3.14B**) and was associated with higher fasting lipid oxidation genes (**Fig 3.1**, **3.2** and **3.15C**) and higher phosphorylation of ACC, causing inactivation of ACC and thus suppressing lipogenesis (**Fig 3.15A** and **B**).

Metformin, an anti-diabetic drug mediates its action of lowering blood glucose via AMPK. Metformin phosphorylates AMPK at thr172 to increase its activity and alter blood glucose and hepatic lipid metabolism [196-198]. Metformin increases phosphorylation of AMPK in turn activate lipid oxidation and suppress lipogenesis via phosphorylation of ACC and thus reduces hepatic steatosis and increase insulin sensitivity[198]. Further, various other AMPK activators such as pioglitazone, 5-Aminoimidazole-4-carboxamide riboside (AICAR) are used in combination with other AMPK activation drugs to improve hepatic steatosis and insulin sensitivity[197,199]. Our data highlights a similar activation in AMPK activity mediated via BCAAs under normal physiological conditions.

In summary, our results suggest that BCAA supplementation primed the liver under the setting of insulin sensitivity to sustain higher fed-to-fasted changes in mitochondrial oxidative networks including β-oxidation and ketogenesis. Most of the acetyl-CoA generated through β-oxidation shunts towards ketogenesis and away from

lipid synthesis. This metabolic milieu of increased lipid oxidation occurred independent of BCAAs being substrates to mitochondrial TCA cycle. Overall, lower rates of lipogenesis could be beneficial when occurred simultaneous with increased lipid oxidation. In conclusion, chronic supplementation of BCAAs in the setting of insulin sensitivity, primed the liver mitochondria to induce lipid oxidation and lower hepatic lipid synthesis while maintain a reduced hepatocellular environment with a potential role in alleviating lipid accumulation without causing oxidative stress. However, the impact of BCAAs during severe stages of insulin stages and associated NAFLD needs to be further explored.

Chapter 4

Summary and Future directions

4.1. Summary

Insulin resistance and associated metabolic diseases such as obesity and T2DM are considered a public health burden with over 350 million diabetic patients worldwide[14,39,44]. With over 35% obese patients and an annual medical cost of $190 billion in US alone, obesity is considered an economic burden[14,39,44]. Over 75% patients with T2DM develop NAFLD (>5% lipids in the liver) and is a common comorbidity of T2DM and obesity[11,23,44]. Hence it is important to understand molecular and metabolic mediators regulating onset and progression of metabolic diseases.

Synergistic coupling of mitochondrial oxidative networks such as β-oxidation, ketogenesis and TCA cycle along with Oxphos and ATP synthesis is required for normal mitochondrial function with minimal ROS generation as a byproduct[53,56,192]. However, during insulin resistance and associated metabolic diseases the mitochondrial oxidative networks remodel and adapt to hormonal and nutrient stimuli and results in an increased ROS generation and dysfunctional mitochondrial metabolism[15,21,150]. Simultaneous induction of lipogenesis and dysfunctional mitochondrial metabolism during NAFLD co-exists with hepatocellular stress and inflammation[15,21,150]. Thus, dysfunctional mitochondrial metabolism is considered a central feature of insulin resistance and associated metabolic diseases. In this dissertation, we tried to decipher the metabolic and molecular mechanisms contributing towards the etiology of NAFLD. The results from our studies would contribute towards developing prevention and management strategies for metabolic diseases and associated morbidities. We hypothesized that a coordinated and optimal

remodeling of mitochondrial oxidative function and lipogenesis are central towards maintaining hepatic insulin sensitivity and preventing the onset of inflammation and hepatocellular stress. To test our hypothesis we used a combination of in-vivo (chicken and mice) and in-vitro (isolated mitochondria) model systems to understand the factors regulating hepatic mitochondrial metabolism and lipogenesis. Embryonic-to-neonatal transition phase is a natural unique window that sustains higher rates of lipid oxidation and lipogenesis without symptoms of hepatocellular stress and inflammation[62]. The liver of an embryonic chicken has a unique ability to oxidize lipids, while the neonatal liver is primed to synthesize lipids[17,18,200]. The rates of lipid accretion in the neonatal chicken liver (9% of liver weight three days after hatch) is above the threshold (5.5%) and mirrors NAFLD[200]. But, the liver sustains the lipid burden without incidence of any dysfunctions. Our results highlighted that **i**) the lowering the flux of free fatty acids through β-oxidation could be an effective strategy to reduce mitochondrial ROS and also to avoid the metabolic burden from acetyl CoA on the TCA cycle and Oxphos and **ii**) an efficient metabolic switch from fatty acid oxidation in the embryonic chicken liver to increased lipogenesis in the neonate, is important to avoid hepatocellular stress and inflammation. Overall, lowering the flux of free fatty acids through β-oxidation could be an effective strategy to reduce mitochondrial ROS and also to avoid the metabolic burden from acetyl CoA on the TCA cycle and Oxphos during NAFLD. In conclusion, the embryonic-to-neonatal development period in chicken presents a unique and natural physiological system to investigate mechanisms regulating hepatic mitochondrial function and lipogenesis.

Insulin resistance is correlated with elevated circulating BCAAs and associated defects in their catabolic networks and are considered predictors of T2DM onset[25,26]. BCAAs interact with mitochondria by being substrates for the mitochondria and fuel reactions to support anaplerotic reactions of gluconeogenesis via TCA cycle[25,26]. Further, the disrupted BCAA catabolism during insulin resistance is linked to impaired mitochondrial metabolism leading to anaplerotic stress and suboptimal TCA cycle activity which further contributes towards mitochondrial dysfunction[26]. Therefore, understanding the interaction of BCAAs with mitochondrial oxidative networks is essential to fully elucidate the cause of mitochondrial dysfunction during insulin resistance and NAFLD. Our results highlighted that the chronic supplementation of BCAAs under normal physiological conditions primed the liver to sustain higher fed-to-fasted changes in mitochondrial oxidative networks including β-oxidation and ketogenesis. The acetyl-CoA generated through β-oxidation shunt towards ketogenesis and away from citrate synthase flux thus suppressing lipogenesis. This metabolic milieu of lower rates of lipogenesis and increased lipid oxidation occurred concurrent to AMPK activation. Overall, chronic supplementation of BCAAs under normal physiological conditions, primed the liver mitochondria to induce lipid oxidation and lower hepatic lipid synthesis while maintaining a reduced hepatocellular environment. In conclusion, BCCAs supplementation could be beneficial towards avoiding hepatic lipid accumulation and play a significant a role in alleviating hepatocellular stress during insulin resistance and NAFLD.

In summary, both our studies signify the importance of synergy between hepatic mitochondrial networks and lipogenesis towards alleviating hepatocellular.

Embryonic-to-neonatal developmental period in chicken would be a unique model to probe the mechanisms regulating hepatic mitochondrial oxidative metabolism and lipogenesis. Further, the chronic supplementation of BCAAs highlighted the new role of BCAAs in regulating hepatic mitochondrial lipid metabolism and lipogenesis. Results from both our studies highlighted the importance of mitochondrial oxidative metabolism and lipogenesis as potential targets towards developing management and prevention strategies for metabolic diseases and their associated dysfunctions.

4.2. Future directions

Our results highlighted the importance of synergy between mitochondrial oxidative networks including β-oxidation, ketogenesis, TCA cycle, Oxphos and ATP synthesis to maintain cellular energy homeostasis. Embryonic-to-neonatal transition phase signified that the efficient switch from fatty acid oxidation in the embryonic chick to *de novo* lipogenesis in the neonates is central for a healthy development without hepatocellular stress and inflammation. Also, our results from chapter 3 suggests the role of BCAAs supplementation in alleviating hepatic lipid accumulation. In summary, our results from both studies highlighted the importance of mitochondrial oxidative metabolism and lipogenesis as potential targets towards developing management and prevention strategies for metabolic diseases and their associated dysfunctions. Our studies still leave various questions unanswered and thus I will be providing certain possibilities for future studies.

Since the optimal coupling between mitochondrial oxidative metabolism and lipogenesis during embryonic-to-neonatal transition appears to be one of main reason of healthy embryonic development. It would be interesting to determine *whether disruption of lipid oxidation and/or lipogenesis during embryonic to post-hatch transition, will result in symptoms of hepatic insulin resistance and NAFLD*. This objective can help us identify the 'control points' that are critical to the onset of hepatic insulin resistance and cellular stress by i) modulating lipid oxidation in embryos (eg., using inhibitors/ inducers of β-oxidation, to regulate fatty acid metabolism ii) disrupting induction of lipogenesis and/or continual induction of β-oxidation in neonatal chicken (eg., using inhibitors of lipogenesis and/or inducers of

β-oxidation). The outcome from this experiment will help establish mitochondrial oxidative metabolism and lipogenesis as a viable nutritional and/or therapeutic target to alleviate inflammation and oxidative stress during hepatic lipid burden.

Chronic supplementation of BCAAs under normal physiological conditions, primed the liver mitochondria to induce lipid oxidation and lower lipogenesis while maintaining a reduced hepatocellular environment. This metabolic milieu occurs concurrent with higher rates of ADP stimulated respiration without changes in ROS generation. However, the impact of BCAAs during severe stages of insulin resistance and associated NAFLD needs to be further elucidated. It would be interesting to test weather chronic supplementation of BCAAs during insulin resistance and/or NAFLD would be beneficial towards suppressing hepatic lipid accumulation.

Sustained induction of mitochondrial lipid oxidation machinery during NAFLD is usually associated with accumulation of lipotoxic intermediates as the process of β-oxidation become inefficient. BCAAs supplementation under normal physiological conditions is associated with upregulated lipid oxidation machinery, their impact on mitochondrial oxidative network during insulin resistance would be interesting to uncover. This objective would allow us to answer i) if continuous exposure of sustained oxidative machinery present a significant risk toward aggravating liver injury during NAFLD ii) if the suppression of lipogenesis along with induced lipogenesis alleviate hepatocellular stress and inflammation

In summary, more specific studies are required to elucidate the significance of synergy between mitochondrial oxidative metabolism and lipogenesis to maintain hepatocellular health and avoid metabolic perturbations.

Appendices

	e14	e18	ph3	ph7	p-value
Embryo weight (g ± SEM)	13.6 ± 0.32	27.04 ± 0.53			
Chick weight (g ± SEM)			60.1 ± 0.81	117.7 ± 5.28	
Liver weight (g ± SEM)	0.22 ± 0.00	0.61 ± 0.02	2.50 ± 0.09[bd]	5.70 ± 0.55[cef]	<0.0001
Liver weight (% body weight)	2.01 ± 0.04	2.29 ± 0.09	4.14 ± 0.13[bd]	4.78 ± 0.28[ce]	<0.0001
% Liver triglycerides	0.23 ± 0.05	0.74 ± 0.12	9.36 ± 1.79[bd]	9.24 ± 1.37[ce]	<0.0001
Serum insulin (µIU/mL ± SEM)	3.14 ± 0.11	3.80 ± 0.12	8.58 ± 1.28[bd]	9.30 ± 1.06[ce]	<0.0001
Serum glucose (mM ± SEM)	6.95 ± 0.21	10.13 ± 0.13	11.29 ± 1.22[b]	12.98 ± 1.49[c]	0.0007
Liver glycogen (mg glucose/ g liver protein ± SEM)	20.0 ± 6.0	78.1 ± 6.4[a]	248 ± 35.4[bd]	99.1 ± 9.6[cf]	<0.0001

Appendix Table 2.1: **Metabolic and phenotypic adaptations during embryonic to neonatal transition**. n = 6-9/ group; results were considered significant at $p \leq 0.05$ following one way ANOVA and pairwise mean comparisons, represented by the following alphabets. ‘a’- e14 vs. e18; ‘b’ - e14 vs. ph3; ‘c’ - e14 vs. ph7; ‘d’ - e18 vs. ph3; ‘e’ - e18 vs. ph7; ‘f’ - ph3 vs. ph7.

Serum Acyl carnitines (nmoles/L ± SEM)	e14	e18	ph3	ph7	p-value
Carnitine	101 ± 30.7	262 ± 31.8[a]	144 ± 11.1[d]	145 ± 10.9[e]	<0.0001
Acetyl carnitine	60.7 ± 10.2	138 ± 18.9[a]	29.1 ± 2.39[d]	27.9 ± 3.77[e]	<0.0001
Propionyl carnitine	1.16 ± 0.22	4.08 ± 0.51[a]	3.31 ± 0.72[b]	1.90 ± 0.32[e]	0.0030
n-Butyrylcarnitine	0.71 ± 0.14	4.64 ± 0.49[a]	1.07 ± 0.25[d]	0.62 ± 0.22[e]	<0.0001
Butyrylcarnitine	0.90 ± 0.07	4.64 ± 0.49[a]	1.51 ± 0.18[d]	0.93 ± 0.17[e]	<0.0001
Valerylcarnitine	0.21 ± 0.02	0.81 ± 0.08[a]	0.13 ± 0.03[d]	0.06 ± 0.01[e]	<0.0001
Isovalerylcarnitine	0.24 ± 0.03	0.72 ± 0.14[a]	0.55 ± 0.13	0.34 ± 0.06	0.0223
Hexanoylcarnitine	0.08 ± 0.01	0.26 ± 0.06[a]	0.24 ± 0.05	0.18 ± 0.02	0.0264
Octanoylcarnitine	0.03 ± 0.01	0.08 ± 0.02	0.05 ± 0.02	0.04 ± 0.01	0.0827
Myristoylcarnitine	0.63 ± 0.04	0.72 ± 0.05	0.07 ± 0.03[bd]	0.05 ± 0.01[ce]	<0.0001
Palmitoylcarnitine	7.37 ± 0.19	6.96 ± 0.45	0.80 ± 0.28[bd]	1.11 ± 0.20[ce]	<0.0001

Appendix Table 2.2. Serum carnitine and acylcarnitine levels during embryonic-to-neonatal transition. n = 6-9/ group; results were considered significant at $p \leq 0.05$ following one way ANOVA and pairwise mean comparisons, represented by the following alphabets. ‘a’- e14 vs. e18; ‘b’ - e14 vs. ph3; ‘c’ - e14 vs. ph7; ‘d’ - e18 vs. ph3; ‘e’ - e18 vs. ph7; ‘f’ - ph3 vs. ph7.

Liver Acylcarnitines (µg/ g liverprotein ± SEM)	e14	e18	ph3	ph7	p-value
Carnitine	113 ± 10.6	220 ± 37.4[a]	61.1 ± 6.23[d]	58.2 ± 6.89[e]	<0.0001
Acetyl carnitine	12.5 ± 2.98	23.7 ± 3.29[a]	3.94 ± 0.96[d]	10.3 ± 2.24[e]	<0.0001
Propionyl Carnitine	26.9 ± 2.75	28.5 ± 5.19	5.31 ± 0.56[bd]	2.22 ± 0.24[ce]	<0.0001
n-Butyrylcarnitine	5.93 ± 0.62	11.6 ± 2.14[a]	0.17 ± 0.02[bd]	0.14 ± 0.05[ce]	<0.0001
Butyrylcarnitine	5.93 ± 0.62	11.6 ± 2.14[a]	0.17 ± 0.02[bd]	0.16 ± 0.04[ce]	<0.0001
Valerylcarnitine	0.46 ± 0.04	0.70 ± 0.15	0.01 ± 0.00[bd]	0.00 ± 0.00[ce]	<0.0001
Isovalerylcarnitine	1.69 ± 0.18	1.45 ± 0.40	0.06 ± 0.01[bd]	0.04 ± 0.01[ce]	<0.0001
Hexanoylcarnitine	0.08 ± 0.03	0.28 ± 0.06[a]	0.01 ± 0.00[d]	0.02 ± 0.00[e]	<0.0001
Octanoylcarnitine	0.02 ± 0.01	0.15 ± 0.03[a]	0.002 ± 0.001[d]	0.01± 0.00[e]	<0.0001
Myristoylcarnitine	0.17 ± 0.06	0.83 ± 0.24[a]	0.02 ± 0.01[d]	0.01 ± 0.00[e]	0.0003
Palmitoylcarnitine	6.00 ± 2.10	27.2 ± 7.55[a]	0.35 ± 0.08[d]	0.33 ± 0.07[e]	0.0002

Appendix Table 2.3. Liver carnitine and acylcarnitine levels during embryonic-to-neonatal transition. n = 6-9/ group; results were considered significant at $p \leq 0.05$ following one way ANOVA and pairwise mean comparisons, represented by the following alphabets. ‘a’- e14 vs. e18; ‘b’ - e14 vs. ph3; ‘c’ - e14 vs. ph7; ‘d’ - e18 vs. ph3; ‘e’ - e18 vs. ph7; ‘f’ - ph3 vs. ph7

Citrate (APE ± SEM)						
	M+1	**M+2**	**M+3**	**M+4**	**M+5**	**M+6**
e14	1.98 ± 0.29	9.90 ± 1.39	6.99 ± 1.03	3.77 ± 0.58	2.25 ± 0.39	0.91 ± 0.17
e18	7.69 ± 2.08	24.24 ± 3.27[a]	30.26 ± 4.90[a]	33.72 ± 5.54[a]	38.59 ± 6.20[a]	33.78 ± 5.79[a]
ph3	20.37 ± 1.20[bd]	45.84 ± 0.87[bd]	43.81 ± 1.36[bd]	36.72 ± 1.10[b]	26.15 ± 1.11[bd]	17.33 ± 1.18[bd]
ph7	11.76 ± 0.69[cf]	42.01 ± 1.90[ce]	29.46 ± 1.64[cf]	17.60 ± 1.21[cef]	6.76 ± 0.58[ef]	2.09 ± 0.19[ef]
p-value	<0.0001	<0.0001	<0.0001	<0.0001	<0.0001	<0.0001
α-Ketoglutarate (APE ± SEM)						
	M+1	**M+2**	**M+3**	**M+4**	**M+5**	
e14	0.22 ± 0.03	1.98 ± 0.23	1.09 ± 0.08	0.64 ± 0.05	0.24 ± 0.03	
e18	1.34 ± 0.19	18.36 ± 0.89[a]	15.87 ± 1.35[a]	19.10 ± 1.72[a]	23.32 ± 2.42[a]	
ph3	1.01 ± 0.09	24.24 ± 0.96[bd]	12.70 ± 0.65[bd]	9.27 ± 0.55[bd]	6.74 ± 0.69[bd]	
ph7	0.25 ± 0.03	12.78 ± 0.76[cef]	4.52 ± 0.27[cef]	2.17 ± 0.14[ef]	0.50 ± 0.03[ef]	
p-value	<0.0001	<0.0001	<0.0001	<0.0001	<0.0001	
Succinate (APE ± SEM)						
	M+1	**M+2**	**M+3**	**M+4**		
e14	0.30 ± 0.04	2.60 ± 0.20	1.37 ± 0.09	1.17 ± 0.35		
e18	-0.09 ± 0.10	6.77 ± 1.03[a]	3.01 ± 0.58[a]	9.06 ± 1.82[a]		
ph3	0.56 ± 0.17	13.94 ± 0.94[bd]	5.47 ± 0.48[bd]	5.30 ± 0.53[d]		
ph7	0.99 ± 0.86	10.48 ± 0.90[cf]	3.74 ± 0.96[ce]	2.82 ± 1.63[e]		
p-value	ns	<0.0001	0.0006	0.0016		
Fumarate (APE ± SEM)						
	M+1	**M+2**	**M+3**	**M+4**		
e14	1.54 ± 0.15	2.78 ± 0.20	4.77 ± 0.19	1.42 ± 0.05		
e18	5.45 ± 1.78	14.10 ± 2.72[a]	26.22 ± 4.83[a]	23.93 ± 4.78[a]		
ph3	0.74 ± 0.17	3.52 ± 0.53[d]	4.85 ± 0.24[d]	3.42 ± 0.16[d]		
ph7	0.58 ± 0.11	1.83 ± 0.22[e]	1.31 ± 0.05[e]	0.54 ± 0.05[e]		
p-value	0.0119	<0.0001	<0.0001	<0.0001		
Malate (APE ± SEM)						
	M+1	**M+2**	**M+3**	**M+4**		
e14	1.32 ± 0.09	2.09 ± 0.15	3.87 ± 0.16	1.49 ± 0.07		
e18	4.74 ± 1.39	10.66 ± 2.92[a]	27.91 ± 5.04[a]	24.57 ± 5.29[a]		
ph3	1.61 ± 0.11	3.92 ± 0.27	6.09 ± 0.32[d]	3.87 ± 0.27[d]		
ph7	1.11 ± 0.06	2.02 ± 0.07[e]	1.37 ± 0.04[e]	0.54 ± 0.02[e]		
p-value	0.0068	0.0013	<0.0001	<0.0001		

Appendix Table 2.4. **Enrichments of TCA cycle intermediates in isolated liver mitochondria from uniformly labeled [$^{13}C_3$]pyruvate, following 10 min of incubation.** n = 6-9/ group; results were considered significant at $p \leq 0.05$ following one way ANOVA and pairwise mean comparisons, represented by the following alphabets. ‘a’- e14 vs. e18; ‘b’ - e14 vs. ph3; ‘c’ - e14 vs. ph7; ‘d’ - e18 vs. ph3; ‘e’ - e18 vs. ph7; ‘f’ - ph3 vs. ph7.

Citrate (APE ± SEM)						
	M+1	**M+2**	**M+3**	**M+4**	**M+5**	**M+6**
e14	4.93 ± 0.19	20.58 ± 0.96	15.24 ± 0.79	8.99 ± 0.52	5.49 ± 0.42	2.11 ± 0.18
e18	7.01 ± 1.57	30.77 ± 2.35^{a}	28.89 ± 3.14^{a}	31.19 ± 3.13^{a}	34.37 ± 3.90^{a}	30.55 ± 4.00^{a}
ph3	20.86 ± 1.33^{bd}	47.36 ± 0.90^{bd}	44.58 ± 1.30^{bd}	37.52 ± 0.97^{b}	26.27 ± 0.91^{b}	17.13 ± 1.18^{bd}
ph7	9.15 ± 1.63^{f}	37.06 ± 6.14^{cf}	25.84 ± 4.51^{cf}	15.87 ± 2.86^{ef}	6.37 ± 1.19^{ef}	2.17 ± 0.40^{ef}
p-value	<0.0001	0.0002	<0.0001	<0.0001	<0.0001	<0.0001
α-Ketoglutarate (APE ± SEM)						
	M+1	**M+2**	**M+3**	**M+4**	**M+5**	
e14	0.49 ± 0.04	7.03 ± 0.16	3.01 ± 0.07	1.75 ± 0.04	0.70 ± 0.02	
e18	0.91 ± 0.06	22.70 ± 1.21^{a}	13.09 ± 0.66^{a}	16.34 ± 0.90^{a}	17.86 ± 1.53^{a}	
ph3	0.87 ± 0.08	23.82 ± 0.93^{b}	12.12 ± 0.64^{b}	8.77 ± 0.54^{bd}	6.18 ± 0.62^{bd}	
ph7	0.35 ± 0.04	12.62 ± 0.30^{cef}	4.48 ± 0.10^{ef}	2.18 ± 0.05^{ef}	0.49 ± 0.01^{ef}	
p-value	ns	<0.0001	<0.0001	<0.0001	<0.0001	
Succinate (APE ± SEM)						
	M+1	**M+2**	**M+3**	**M+4**		
e14	0.81 ± 0.06	6.77 ± 0.42	2.75 ± 0.24	2.18 ± 0.41		
e18	-0.04 ± 0.18	9.93 ± 1.05^{a}	4.47 ± 0.52	9.94 ± 1.56a		
ph3	0.60 ± 0.17	15.11 ± 1.23^{bd}	5.83 ± 0.58^{b}	5.56 ± 0.60^{bd}		
ph7	0.06 ± 0.07	9.45 ± 0.32 ^{cf}	2.73 ± 0.13^{f}	1.47 ± 0.36^{ef}		
p-value	ns	<0.0001	<0.0001	<0.0001		
Fumarate (APE ± SEM)						
	M+1	**M+2**	**M+3**	**M+4**		
e14	2.04 ± 0.18	3.19 ± 0.25	4.97 ± 0.21	1.60 ± 0.07		
e18	0.82 ± 0.28	6.33 ± 0.93^{a}	15.26 ± 2.10^{a}	11.12 ± 1.76^{a}		
ph3	0.72 ± 0.11	4.37 ± 0.70	4.67 ± 0.20^{d}	3.24 ± 0.26^{d}		
ph7	0.64 ± 0.07	1.91 ± 0.12^{e}	1.30 ± 0.06^{cef}	0.49 ± 0.04^{e}		
p-value	<0.0001	0.0003	<0.0001	<0.0001		
Malate (APE ± SEM)						
	M+1	**M+2**	**M+3**	**M+4**		
e14	1.75 ± 0.11	2.75 ± 0.18	4.62 ± 0.19	1.88 ± 0.09		
e18	1.42 ± 0.18	4.25 ± 0.59	18.56 ± 3.02^{a}	12.20 ± 2.50^{a}		
ph3	1.49 ± 0.12	3.90 ± 0.30	5.95 ± 0.27^{d}	3.75 ± 0.29^{d}		
ph7	1.16 ± 0.04	2.27 ± 0.08	1.50 ± 0.06^{ef}	0.61 ± 0.03^{e}		
p-value	0.0257	0.0018	<0.0001	<0.0001		

Appendix Table 2.5. **Enrichments of TCA cycle intermediates in isolated liver mitochondria from uniformly labeled [$^{13}C_3$]pyruvate, following 20 min of incubation.** n = 6-9/ group; results were considered significant at $p \leq 0.05$ following one way ANOVA and pairwise mean comparisons, represented by the following alphabets. ‘a’- e14 vs. e18; ‘b’ - e14 vs. ph3; ‘c’ - e14 vs. ph7; ‘d’ - e18 vs. ph3; ‘e’ - e18 vs. ph7; ‘f’ - ph3 vs. ph7.

Lactate (µg/ mg mitochondria ± SEM)				
	0 min	**5 min**	**10 min**	**p-value**
e14	0.41 ± 0.08	0.56 ± 0.01	0.43 ± 0.12	ns
e18	0.58 ± 0.17	0.44 ± 0.06	0.51 ± 0.09	ns
ph3	0.76 ± 0.24	1.01 ± 0.35[d]	0.65 ± 0.20	ns
ph7	0.79 ± 0.20	0.47 ± 0.17[f]	0.67 ± 0.18	ns
p-value	ns	ns	ns	
Pyruvate (µg/ mg mitochondria ± SEM)				
	0 min	**5 min**	**10 min**	**p-value**
e14	0.14 ± 0.01	0.06 ± 0.01	0.06 ± 0.01	<0.0001
e18	0.23 ± 0.03	0.08 ± 0.01	0.09 ± 0.01	<0.0001
ph3	0.56 ± 0.07[bd]	0.30 ± 0.04[bd]	0.25 ± 0.03[bd]	0.0006
ph7	0.35 ± 0.06[cf]	0.20 ± 0.04[c]	0.17 ± 0.03	ns
p-value	<0.0001	<0.0001	<0.0001	
Citrate (µg/ mg mitochondria ± SEM)				
	0 min	**5 min**	**10 min**	**p-value**
e14	0.21 ± 0.05	0.15 ± 0.01	0.18 ± 0.02	ns
e18	0.33 ± 0.09	0.24 ± 0.03	0.25 ± 0.03	ns
ph3	2.35 ± 0.49[bd]	0.95 ± 0.33	0.72 ± 0.15	0.0066
ph7	2.06 ± 0.39[ce]	1.52 ± 0.77	0.66 ± 0.11	ns
p-value	<0.0001	ns	ns	
α-Ketoglutarate (µg/ mg mitochondria ± SEM)				
	0 min	**5 min**	**10 min**	**p-value**
e14	0.02 ± 0.00	0.09 ± 0.01	0.10 ± 0.00	<0.0001
e18	0.02 ± 0.00	0.10 ± 0.01	0.14 ± 0.01	<0.0001
ph3	0.12 ± 0.02[bd]	0.29 ± 0.05[bd]	0.36 ± 0.04[bd]	0.0005
ph7	0.07 ± 0.01	0.23 ± 0.03[ce]	0.28 ± 0.04[ce]	<0.0001
p-value	<0.0001	<0.0001	<0.0001	
Succinate (µg/ mg mitochondria ± SEM)				
	0 min	**5 min**	**10 min**	**p-value**
e14	0.38 ± 0.08	0.84 ± 0.35	0.42 ± 0.12	ns
e18	0.35 ± 0.06	0.50 ± 0.09	0.54 ± 0.09	ns
ph3	0.55 ± 0.06	0.59 ± 0.15	0.48 ± 0.07	ns
ph7	0.50± 0.07	0.46 ± 0.08	0.38 ± 0.08	ns
p-value	ns	ns	ns	

Fumarate (µg/ mg mitochondria ± SEM)				
	0 min	**5 min**	**10 min**	**p-value**
e14	0.32 ± 0.11	1.97 ± 0.16	2.11 ± 0.12	<0.0001
e18	0.69 ± 0.12	3.15 ± 0.22[a]	3.13 ± 0.22[a]	<0.0001
ph3	2.25 ± 0.22[bd]	3.23 ± 0.31[b]	3.31 ± 0.29[b]	0.0201
ph7	1.22 ± 0.17[cf]	2.38 ± 0.34[f]	2.59 ± 0.32	0.0048
p-value	<0.0001	0.0041	0.0081	
Malate (µg/ mg mitochondria ± SEM)				
	0 min	**5 min**	**10 min**	**p-value**
e14	0.17 ± 0.08	1.41 ± 0.14	1.61 ± 0.11	<0.0001
e18	0.36 ± 0.07	2.46 ± 0.35[a]	2.63 ± 0.19[a]	<0.0001
ph3	1.39 ± 0.14[bd]	2.12 ± 0.24[b]	1.99 ± 0.24	0.0541
ph7	0.73 ± 0.09	1.74 ± 0.25	1.64 ± 0.17[e]	0.0009
p-value	<0.0001	0.0458	0.0018	

Appendix Table 2.6. **Concentrations of TCA cycle intermediates in the isolated mitochondria following 0, 5 and 10 min of incubation.** n = 6-9/ group; results were considered significant at $p \leq 0.05$ following one way ANOVA and pairwise mean comparisons, represented by the following alphabets. ‘a’- e14 vs. e18; ‘b’ - e14 vs. ph3; ‘c’ - e14 vs. ph7; ‘d’ - e18 vs. ph3; ‘e’ - e18 vs. ph7; ‘f’ - ph3 vs. ph7

Gene	Forward primer	Reverse primer	Accession No.
ACACA	TGGCAGCCATGTTCAGAGAG	GGAAATTCCCTCTTCTGTGCCA	NM_205505.1
CS	AGGGATTTCATCTGGAACACACT	CACCGTGTAGTACTTCATCTCCCT	XM_015300289.2
CPT1A	TGCTCACTACCGAGACATGG	GGTACATGACCGGACGGTTT	XM_015286798.2
ELOVL6	CCGGGCCAATGAACATGT	TCATGCTCGTTGAACTGCTTCT	NM_001031539.1
FADS2	TCTTAATGGGGAGGGAACAGGT	ACCAGCTTCTTGCATTTTCACA	NM_001160428.2
FASN	GGCTACACACTAGTTGGCACT	CACTGTGTTCCCATGCCTGA	NM_205155.3
GAPDH	GATTTAATGAGCCATTCGCAGTT	CCCAGCGTGCATGTCTAAGTAC	NM. 205155.3
IL6	GCAGGACGAGATGTGCAAGA	GTCCTCCTCCGTCACCTT	NM_204628.1
MCAD	CACGCAGTAGGCACACATGAT	CGGCAGCAGCGCAAAT	
NLRP3	GGTTTACCAGGGGAA ATGAGG	TTGTGCTTCCAGATGCCGT	NM_001348947.1
PCK1	GCAGGGGTTATGATGAGAAGT	ACGGATCACAGTTTTGAAGAC	NM_205471.1
PCK2	CCTTCGCCATGAGCCCCTTTTTC	CAGCTCCGCCATGACATCCCT	NM_205470.1
SCD1	CAATGCCACCTGGCTAGTGA	CGGCCGATTGCCAAAC	NM_204890.1
SOD1	GACCAAAAGATGCAGATAGG	TCCAGCATTTCCAGTTAGTT	NM_205064
TLR4	AGTCTGAAATTGCTGAGCTCAAA T	GCGACGTTAAGCCATGGAAG	NM_001030693.1
TNFA	CCATATGACCACGCTCTTTCCG	AGCAGCAGCAGCAGCAGAGC	MF000729.1

Appendix Table 2.7. List of primers used for RT-qPCR in chapter 2.

	Low Fat Diet (LF)	Low Fat Diet + 150% BCAA (LB)	High Fat Diet (HF)	High Fat Diet + 150% BCAA (HF-BCAA)
Casein (g)	200	200	200	200
L-Cystine (g)	3	3	3	3
Isoleucine (g)	0	11.46	0	11.46
Leucine (g)	0	23.97	0	23.97
Valine (g)	0	14.11	0	14.11
Maltodextrin (g)	125	125	125	125
Cornstarch (g)	506.2	456.66	0	0
Sucrose (g)	68.8	68.8	68.8	68.8
Cellulose, BW200 (g)	50	50	50	50
Soybean oil (g)	25	25	25	25
Lard (g)	20	20	245	223
Mineral Mix S10026 (g)	10	10	10	10
DiCalcium Phosphate (g)	13	13	13	13
Calcium Carbonate (g)	5.5	5.5	5.5	5.5
Potassium Citrate (g)	16.5	16.5	16.5	16.5
Vitamin Mix V10001 (g)	10	10	10	10
Choline Bitartrate (g)	2	2	2	2
Protein (% kcal)	**20**	**25**	**20**	**25**
Carbohydrate (% kcal)	**70**	**65**	**20**	**20**
Fat (% kcal)	**10**	**10**	**60**	**55**

Appendix Table 3.1. Nutrient composition of diets used in chapter 3

Gene	Forward	Reverse
Acc1	GGACAGACTGATCGCAGAGAAAG	TGGAGAGCCCCACACACA
Acly	TGGATGCCACAGCTGACTAC	GGTTCAGCAAGGTCAGCTTC
BCKDHA	CTCCTGTTGGGACGATCTGG	CATTGGGCTGGATGAACTCAA
BCKDHB	AGTGCCCTGGATAACTCATTAGC	GCATCGGAAGACTCCACCAAA
BCKDK	ACATCAGCCAACCGATACACAC	GAGGCGAACTGAGGGCTTC
Cd36	TGGTCAAGCCAGCTAGAAA	CCCAGTCTCATTTAGCCAC
Cpt1a	CAAAGATCAATCGGACCCTAGAC	CGCCACTCACGATGTTCTTC
Elovl6	TGCCATGTTCATCACCTTGT	TGCTGCATCCAGTTGAAGAC
Fasn	GCTGCGGAAACTTCAGGAAAT	AGAGACGTGTCACTCCTGGACTT
Lcad	TCAATGGAAGCAAGGTGTTCA	GCCACGACGATCACGAGAT
Mcad	GATGCATCACCCTCGTGTAAC	AAGCCCTTTTCCCCTGAAG
PGC1a	AGACAAATGTGCTTCCAAAAAGAA	GAAGAGATAAAGTTGTTGGTTTGGC
PPARa	ACAAGGCCTCAGGGTACCA	GCCGAAAGAAGCCCTTACAG
Cyclophilin	GGAGATGGCACAGGAGGAA	GCCCGTAGTGCTTCAGCTT
PP2Cm	ATGTTATCAGCGGCCTTCATTAC	GTGGAGAAGTAGCAGGCAGG
Scd1	GCGATACACTCTGGTGCTCA	CCCAGGGAAACCAGGATATT

Appendix Table 3.2: List of primers used for RT-qPCR in chapter 3

12-wks	**Feeding status**	**LF**	**LB**	**HF**	**HFBA**
Body weight (g)	Fed	24.2 ± 0.8	28.0 ± 0.7	33.8 ± 1.5[b]	33.3 ± 1.4[c]
	Fasted	21.1 ± 0.5	23.3 ± 0.9	33.9 ± 1.5[b,d]	33.0 ± 1.2[c,e]
Liver weight (g)	Fed	1.32 ± 0.07	1.48 ± 0.05	1.41 ± 0.04	1.44 ± 0.07
	Fasted	0.92 ± 0.02	0.98 ± 0.04	1.18 ± 0.08[b]	1.17 ± 0.06[c]
Adipose weight (g)	Fed	0.35 ± 0.05	0.71 ± 0.07	1.37 ± 0.29	1.12 ± 0.20
	Fasted	0.27 ± 0.03	0.43 ± 0.09	1.61 ± 0.16[b,d]	1.59 ± 0.19[c,e]
Blood glucose (mg/dL)	Fed	123.8 ± 4.7	133.9 ± 4.1	154.3 ± 8.2[b]	141.4 ± 5.8
	Fasted	118.4 ± 6.5	112.9 ± 7.6	115.3 ± 6.2	112.0 ± 5.1
Serum insulin (ng/ml)	Fed	0.46 ± 0.12	0.52 ± 0.08	0.48 ± 0.08	0.41 ± 0.06
	Fasted	0.12 ± 0.01	0.14 ± 0.02	0.29 ± 0.07	0.22 ± 0.05
Serum c-peptide (ng/ml)	Fed	0.49 ± 0.12	0.58 ± 0.09	0.62 ± 0.11	0.52 ± 0.08
	Fasted	0.17 ± 0.05	0.16 ± 0.04	0.31 ± 0.09	0.29 ± 0.05
Serum NEFA (mM)	Fed	0.32 ± 0.03	0.64 ± 0.04[a]	0.38 ± 0.02	0.76 ± 0.07[c,f]
	Fasted	0.34 ± 0.05	0.70 ± 0.07[a]	0.36 ± 0.02	0.61 ± 0.04[c,f]

Appendix Table 3.3: Metabolic characteristics of mice reared on LF, LB, HF and HB diets for 12 weeks. All the values are represented as mean ± SEM, with n=7-10/ group. Results were considered significant at $P < 0.05$ following one-way ANOVA and tukey's pairwise mean comparison which are represented by the following alphabets: "a"—LF vs LB; "b"—LF vs HF; "c"—LF vs HB; "d"—LB vs HF; "e"—LB vs HB; and "f"—HF vs HB.

24-wks	**Feeding status**	**HF**	**HFBA**
Body weight (g)	Fed	50.3 ± 0.92	50.3 ± 0.53
	Fasted	49.2 ± 0.65	49.0 ± 0.54
Liver weight (g)	Fed	3.09 ± 0.25	2.43 ± 0.11*
	Fasted	2.26 ± 0.09	1.69 ± 0.10*
Adipose weight (g)	Fed	1.58 ± 0.11	1.74 ± 0.14
	Fasted	1.22 ± 0.10	2.12 ± 0.14*
Blood glucose (mg/dL)	Fed	200.3 ± 9.9	166.6 ± 7.3*
	Fasted	124.6 ± 8.1	126.8 ± 3.4
Serum insulin (ng/ml)	Fed	9.88 ± 1.92	6.45 ± 1.54*
	Fasted	1.06 ± 0.12	2.25 ± 0.56*
Serum c-peptide (ng/ml)	Fed	1.13 ± 0.14	0.78 ± 0.11*
	Fasted	0.22 ± 0.03	0.28 ± 0.04
Serum NEFA (mM)	Fed	0.43 ± 0.02	0.44 ± 0.02
	Fasted	0.66 ± 0.03	0.64 ± 0.03

Appendix Table 3.4: Metabolic characteristics of mice reared on HF and HB diets for 24 weeks. All the values are represented as mean ± SEM, with n=7-10/ group. Results were considered significant at $P < 0.05$ following unpaired t-test and significance is represented by "*****".

	12-wks				24-wks	
Incubation time	**LF**	**LB**	**HF**	**HB**	**HF**	**HB**
			Citrate			
0 min	1.38±0.13	1.65±0.12	1.22±0.16	1.13±0.1	0.55±0.03	0.53±0.03
5 min	0.81±0.07	0.81±0.07	0.8±0.08	0.7±0.06	0.48±0.08	0.42±0.05
10 min	0.71±0.06	0.76±0.05	0.74±0.11	0.67±0.03	0.31±0.03	0.35±0.07
			α-ketoglutarate			
0 min	0.09±0.01	0.1±0.02	0.1±0.01	0.11±0.01	0.24±0.13	0.23±0.09
5 min	0.25±0.04	1.09±0.61	0.72±0.23	0.42±0.11	0.07±0.02	0.08±0.02
10 min	0.59±0.35	0.71±0.34	0.68±0.29	0.28±0.07	0.06±0.02	0.08±0.02
			Succinate			
0 min	0.16±0.03	0.16±0.02	0.15±0.02	0.14±0.03	0.37±0.27	0.32±0.22
5 min	0.25±0.02	0.21±0.03	0.25±0.02	0.21±0.02	0.17±0.03	0.3±0.16
10 min	0.2±0.02	0.18±0.02	0.23±0.02	0.19±0.01	0.14±0.03	0.09±0.02
			Fumarate			
0 min	0.19±0.05	0.29±0.13	0.3±0.13	0.26±0.12	0.07±0.01	0.07±0.01
5 min	0.61±0.09	0.6±0.05	0.67±0.07	0.52±0.03	0.28±0.08	0.18±0.04
10 min	0.49±0.07	0.52±0.07	0.57±0.06	0.46±0.03	0.18±0.04	0.18±0.04
			Malate			
0 min	0.34±0.06	0.7±0.34	0.67±0.29	0.55±0.23	0.5±0.09	0.3±0.13
5 min	2.27±0.19	2.57±0.35	2.68±0.32	2.1±0.13	1.22±0.41	0.81±0.2
10 min	1.95±0.21	2.16±0.25	2.1±0.15	1.71±0.09	0.85±0.26	0.75±23

Appendix Table 3.5: Incorporation of ^{13}C from $^{13}C_{16}$[palmitate] into TCA cycle intermediates (M+2) following 5 and 10 min mitochondrial incubations under fed conditions. All the values are represented as mean ± SEM, with n=8-14/ group. Results were considered significant at $P < 0.05$ following one-way ANOVA (between 12-wk diet groups) and tukey's pairwise mean comparison which are represented by the following alphabets: "a"—LF vs LB; "b"—LF vs HF; "c"—LF vs HB; "d"—LB vs HF; "e"—LB vs HB; and "f"—HF vs HB. The significance between 24-wk HF and HB groups were analyzed following a t-test and is represented by "*".

	12-wks				24-wks	
Incubation time	**LF**	**LB**	**HF**	**HB**	**HF**	**HB**
			Citrate			
0 min	0.95±0.09	0.99±0.09	0.11±0.012	0.85±0.11	0.48±0.04	0.39±0.06
5 min	0.84±0.07	0.87±0.07	0.95±0.08	0.85±0.14	0.36±0.02	0.34±0.02
10 min	0.75±0.06	0.69±0.06	0.6±0.03	0.57±0.04	0.2±0.02	0.27±0.03
			α-ketoglutarate			
0 min	0.06±0.01	0.06±0	0.1±0.03	0.08±0.01	0.15±0.09	0.13±0.06
5 min	0.37±0.13	0.4±0.13	0.96±0.72	0.64±0.32	0.12±0.04	0.09±0.03
10 min	0.74±0.36	0.24±0.05	0.3±0.08	0.2±0.02	0.05±0.02	0.05±0.01
			Succinate			
0 min	0.25±0.13	0.1±0.01	0.14±0.02	0.11±0.01	0.09±0.02	0.12±0.03
5 min	0.3±0.1	0.46±0.17	0.33±0.01	0.24±0.03	0.09±0.01	0.1±0.01
10 min	0.29±0.1	0.41±0.15	0.24±0.04	0.23±0.02	0.1±0.01	0.11±0.03
			Fumarate			
0 min	0.19±0.08	0.14±0.06	0.17±0.06	0.17±0.06	0.06±0.01	0.06±0.01
5 min	0.54±0.06	0.5±0.04	0.55±0.06	0.52±0.03	0.08±0.01	0.07±0.01
10 min	0.54±0.05	0.49±0.05	0.57±0.03	0.52±0.03	0.08±0.01	0.07±0.01
			Malate			
0 min	0.35±0.16	0.26±0.08	0.32±0.06	0.34±0.09	0.15±0.02	0.13±0.01
5 min	2.36±0.2	2.43±0.21	2.41±0.26	2.32±0.2	0.2±0.03	0.17±0.02
10 min	2.4±0.22	2.25±0.18	2.32±0.14	2.15±0.14	0.16±0.02	0.14±0.01

Appendix Table 3.6: Incorporation of ^{13}C from $^{13}C_{16}$[palmitate] into TCA cycle intermediates (M+2) following 5 and 10 min mitochondrial incubations under fasted conditions. All the values are represented as mean ± SEM, with n=8-14/ group. Results were considered significant at $P < 0.05$ following one-way ANOVA (between 12-wk diet groups) and tukey's pairwise mean comparison which are represented by the following alphabets: "a"—LF vs LB; "b"—LF vs HF; "c"—LF vs HB; "d"—LB vs HF; "e"—LB vs HB; and "f"—HF vs HB. The significance between 24-wk HF and HB groups were analyzed following a t-test and is represented by "*".

M+2 TCA Cycle Intermediates 10 Minute α-ketoisocaproate Mitochondrial Incubations

Fed		Fasted	
LF	**LB**	**LF**	**LB**
Citrate			
0.82±0.09	0.97±0.12	0.60±0.06	0.5±0.05
α-ketoglutarate			
0.60±0.09	0.37±0.04	0.59±0.04	0.65±0.06
Succinate			
-0.17±0.07	-0.18±0.07	0.14±0.07	0.21±0.04
Fumarate			
-0.54±0.03	-0.61±0.02	-0.64±0.03	-0.64±0.02
Malate			
0.11±0.02	0.08±0.03	0.11±0.02	0.08±0.02

Appendix Table 3.7: Incorporation of ^{13}C from $^{13}C_6$[αketoisocaproate] into TCA cycle intermediates (M+2) following 10 min mitochondrial incubations under fed and fasted conditions . All the values are represented as mean ± SEM, with n=8-10/ group. Results were considered significant at $P < 0.05$ following a t-test and is represented by "*". Fed and fasted groups were analyzed individually.

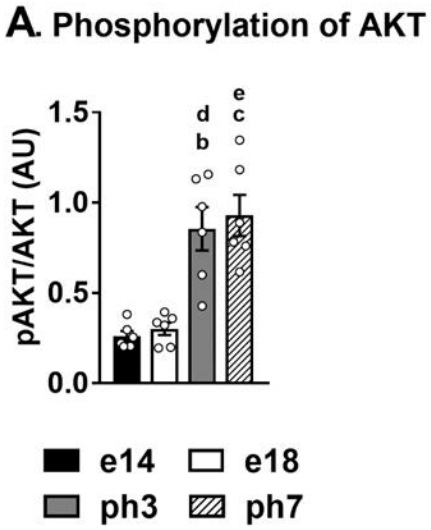

Appendix Figure 2.1. **Graphical representation of AKT phosphorylation in the liver.** Densitometry of western blots for phosphorylated AKT (Ser473) relative to total AKT (from Fig 1E). n = 6/ group; Means were considered significant at $P \leq 0.05$ following pairwise mean comparisons, represented by the following alphabets, 'a'- e14 vs. e18; 'b' - e14 vs. ph3; 'c' - e14 vs. ph7; 'd' - e18 vs. ph3; 'e' - e18 vs. ph7; 'f' - ph3 vs. ph7.

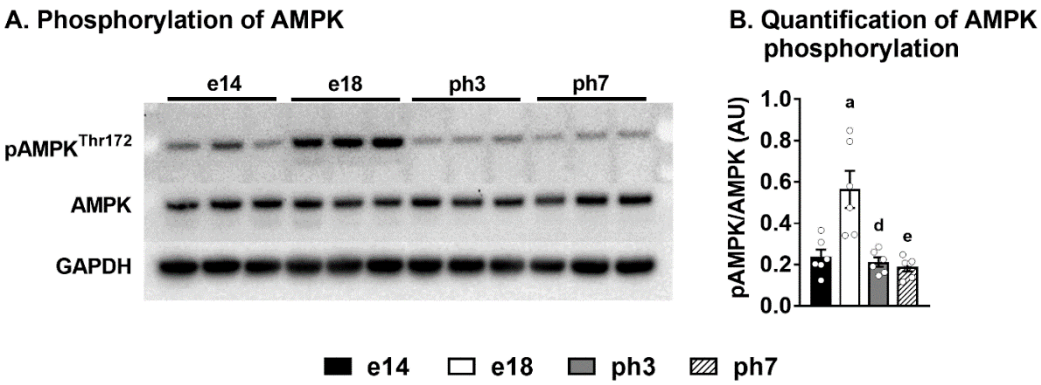

Appendix Figure 2.2. AMPK phosphorylation in the liver. (**A**) Western blot and (**B**) Densitometry of the blots for phosphorylated AMPK (Thr172) relative to total AMPK. n = 6/ group; Means were considered significant at $P \leq 0.05$ following pairwise mean comparison, represented by the following alphabets, 'a'- e14 vs. e18; 'b' - e14 vs. ph3; 'c' - e14 vs. ph7; 'd' - e18 vs. ph3; 'e' - e18 vs. ph7; 'f' - ph3 vs. ph7.

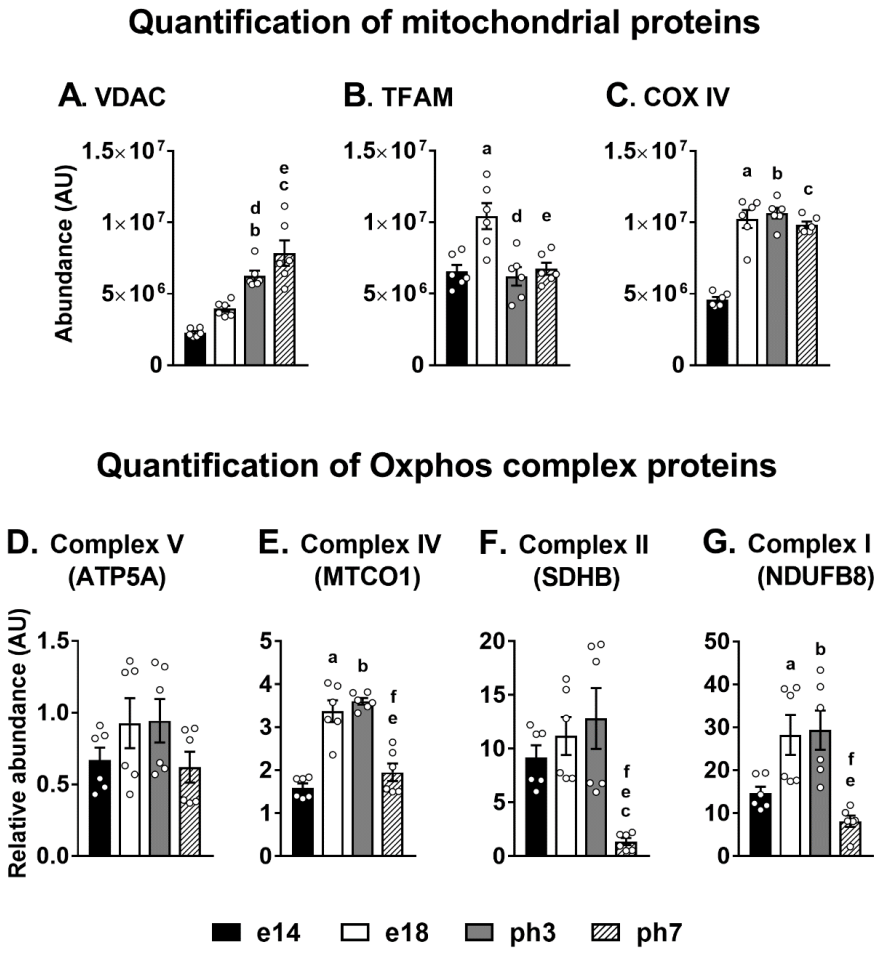

Appendix Figure 2.3. Graphical representation of mitochondrial proteins and Oxphos complex proteins. Densitometry of mitochondrial proteins (**A**) VDAC (**B**) TFAM (**C**) COX IV (from Fig 4B).and (**D**-**G**) the Oxphos complex proteins (from Fig 4G). n = 6/ group; Means were considered significant at $P \leq 0.05$ following pairwise mean comparison, represented by the following alphabets. 'a'- e14 vs. e18; 'b' - e14 vs. ph3; 'c' - e14 vs. ph7; 'd' - e18 vs. ph3; 'e' - e18 vs. ph7; 'f' - ph3 vs. ph7.

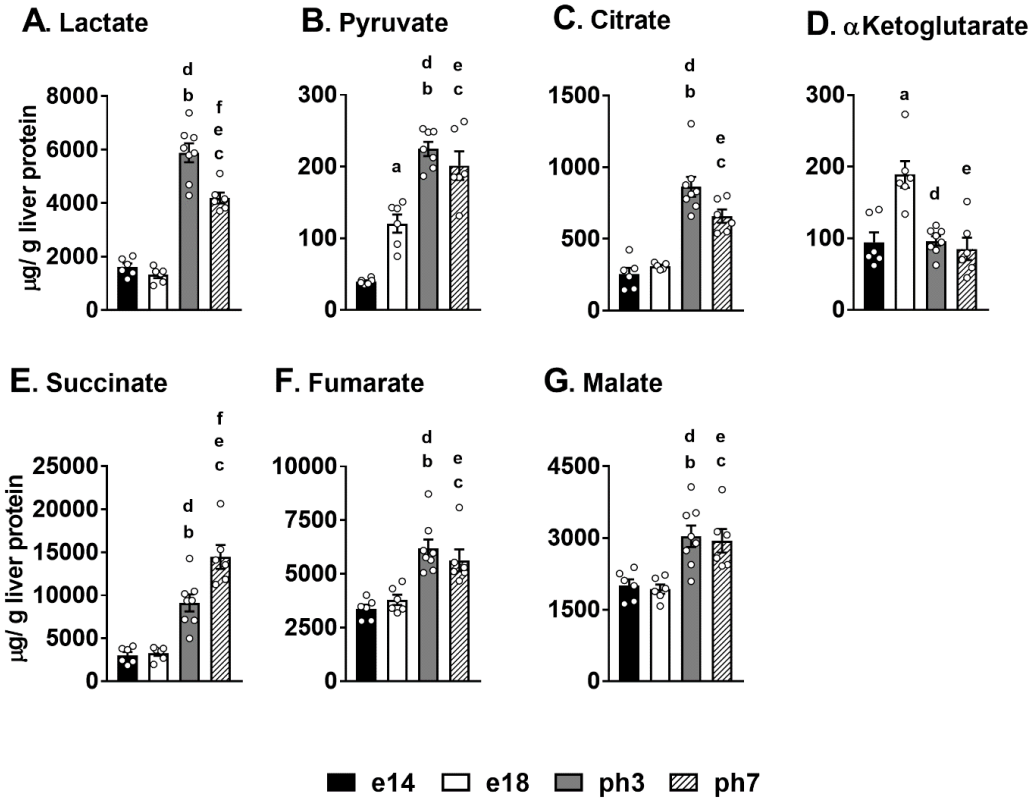

Appendix Figure 2.4. Concentrations TCA cycle intermediates in the liver.

Changes in concentrations of (**A**) Lactate (**B**) Pyruvate (**C**) Citrate (**D**) Lactate (**E**) Succinate (**F**) Fumarate (**G**) Malate. n = 6/ group; results were considered significant at $P \leq 0.05$ following pairwise mean comparisons, represented by the following alphabets. 'a'- e14 vs. e18; 'b' - e14 vs. ph3; 'c' - e14 vs. ph7; 'd' - e18 vs. ph3; 'e' - e18 vs. ph7; 'f' - ph3 vs. ph7.

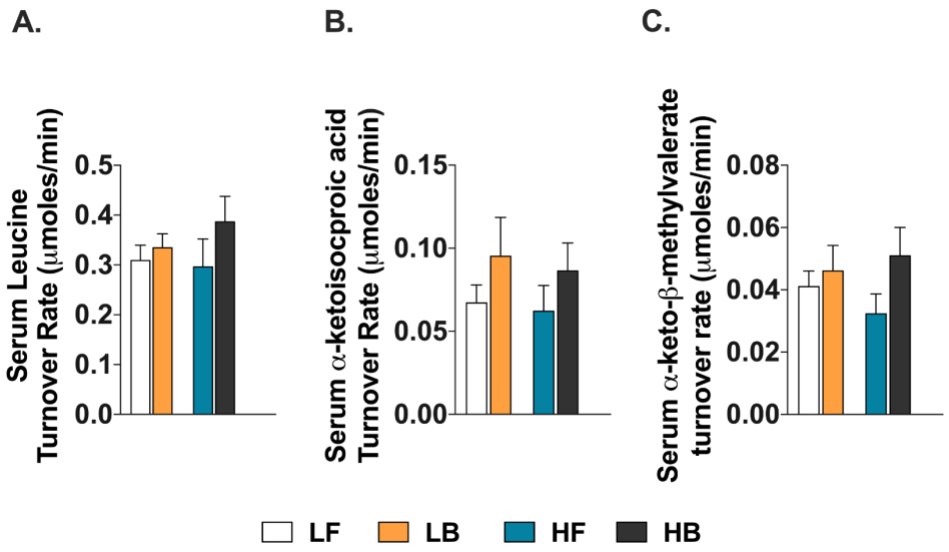

Appendix Figure 3.1. Fed turnover rates of Leucine and BCKAs. Whole body fasted turnover rates of (A) leucine (B) α-ketoisovalerate and (C) α-keto-β-methylvalerate. All the values are represented as mean ± SEM, with n=8-14/ group. Results were considered significant at $P < 0.05$ following one-way ANOVA (between 12-wk diet groups) and tukey's pairwise mean comparison which are represented by the following alphabets: "a"—LF vs LB; "b"—LF vs HF; "c"—LF vs HB; "d"—LB vs HF; "e"—LB vs HB; and "f"—HF vs HB. The significance between 24-wk HF and HB groups were analyzed following a t-test and is represented by "*.

Bibliography

1 Liu, X., Wang, H., Liang, X. & Roberts, M. in *Liver Pathophysiology* 391-400 (Elsevier, 2017).

2 McMichael, J. The oxygen supply of the liver. *Quarterly Journal of Experimental Physiology: Translation and Integration* **27**, 73-87 (1937).

3 Rogers, A. B. & Dintzis, R. Z. in *Comparative Anatomy and Histology (Second Edition)* (eds Piper M. Treuting, Suzanne M. Dintzis, & Kathleen S. Montine) 229-239 (Academic Press, 2018).

4 De Fabiani, E. *et al.* When food meets man: the contribution of epigenetics to health. *Nutrients* **2**, 551-571.

5 Rui, L. Energy metabolism in the liver. *Compr Physiol* **4**, 177-197, doi:10.1002/cphy.c130024 (2014).

6 Arner, P. Insulin resistance in type 2 diabetes: role of fatty acids. *Diabetes/metabolism research and reviews* **18**, S5-S9 (2002).

7 Biddinger, S. B. *et al.* Hepatic insulin resistance is sufficient to produce dyslipidemia and susceptibility to atherosclerosis. *Cell metabolism* **7**, 125-134 (2008).

8 Fabbrini, E., Sullivan, S. & Klein, S. Obesity and nonalcoholic fatty liver disease: biochemical, metabolic, and clinical implications. *Hepatology* **51**, 679-689 (2010).

9 Angulo, P. Nonalcoholic fatty liver disease. *New England Journal of Medicine* **346**, 1221-1231 (2002).

10 Clark, J. M., Brancati, F. L. & Diehl, A. M. Nonalcoholic fatty liver disease. *Gastroenterology* **122**, 1649-1657 (2002).

11 Matteoni, C. A. *et al.* Nonalcoholic fatty liver disease: a spectrum of clinical and pathological severity. *Gastroenterology* **116**, 1413-1419 (1999).

12 Mitra, S., De, A. & Chowdhury, A. Epidemiology of non-alcoholic and alcoholic fatty liver diseases. *Transl Gastroenterol Hepatol* **5**, 16-16, doi:10.21037/tgh.2019.09.08 (2020).

13 Browning, J. D. & Horton, J. D. Molecular mediators of hepatic steatosis and liver injury. *The Journal of clinical investigation* **114**, 147-152 (2004).

14 Browning, J. D. *et al.* Prevalence of hepatic steatosis in an urban population in the United States: impact of ethnicity. *Hepatology* **40**, 1387-1395 (2004).

15 Sunny, N. E., Bril, F. & Cusi, K. Mitochondrial adaptation in nonalcoholic fatty liver disease: novel mechanisms and treatment strategies. *Trends in Endocrinology & Metabolism* **28**, 250-260 (2017).

16 Sunny, N. E., Parks, E. J., Browning, J. D. & Burgess, S. C. Excessive hepatic mitochondrial TCA cycle and gluconeogenesis in humans with nonalcoholic fatty liver disease. *Cell metabolism* **14**, 804-810 (2011).

17 Noble, R. & Cocchi, M. Lipid metabolism and the neonatal chicken. *Progress in lipid research* **29**, 107-140 (1990).

18 Noble, R. & Moore, J. Studies on the lipid metabolism of the chick embryo. *Canadian journal of biochemistry* **42**, 1729-1741 (1964).

19 Hicks, J. A., Porter, T. E., Sunny, N. E. & Liu, H.-C. Delayed Feeding Alters Transcriptional and Post-Transcriptional Regulation of Hepatic Metabolic Pathways in Peri-Hatch Broiler Chicks. *Genes* **10**, 272 (2019).

20 Noble, R. & Ogunyemi, D. Lipid changes in the residual yolk and liver of the chick immediately after hatching. *Neonatology* **56**, 228-236 (1989).

21 Patterson, R. E. *et al.* Lipotoxicity in steatohepatitis occurs despite an increase in tricarboxylic acid cycle activity. *American Journal of Physiology-Endocrinology and Metabolism* **310**, E484-E494 (2016).

22 Gastaldelli, A. (Portland Press Limited, 2017).

23 Wei, Y., Rector, R. S., Thyfault, J. P. & Ibdah, J. A. Nonalcoholic fatty liver disease and mitochondrial dysfunction. *World journal of gastroenterology: WJG* **14**, 193 (2008).

24 Holeček, M. Branched-chain amino acids in health and disease: metabolism, alterations in blood plasma, and as supplements. *Nutrition & metabolism* **15**, 1-12 (2018).

25 Newgard, C. B. *et al.* A branched-chain amino acid-related metabolic signature that differentiates obese and lean humans and contributes to insulin resistance. *Cell metabolism* **9**, 311-326 (2009).

26 Sunny, N. E. *et al.* Cross-talk between branched-chain amino acids and hepatic mitochondria is compromised in nonalcoholic fatty liver disease. *American Journal of Physiology-Endocrinology and Metabolism* **309**, E311-E319 (2015).

27 Hutson, S. M., Sweatt, A. J. & LaNoue, K. F. Branched-chain amino acid metabolism: implications for establishing safe intakes. *The Journal of nutrition* **135**, 1557S-1564S (2005).

28 Kujala, U. M. *et al.* Branched-chain amino acid levels are related with surrogates of disturbed lipid metabolism among older men. *Frontiers in medicine* **3**, 57 (2016).

29 White, P. J. *et al.* Branched-chain amino acid restriction in Zucker-fatty rats improves muscle insulin sensitivity by enhancing efficiency of fatty acid oxidation and acyl-glycine export. *Molecular metabolism* **5**, 538-551 (2016).

30 Röder, P. V., Wu, B., Liu, Y. & Han, W. Pancreatic regulation of glucose homeostasis. *Exp Mol Med* **48**, e219-e219, doi:10.1038/emm.2016.6 (2016).

31 Bayol, S. A., Bruce, C. R. & Wadley, G. D. Growing healthy muscles to optimise metabolic health into adult life. *J Dev Orig Health Dis* **5**, 420-434, doi:10.1017/s2040174414000452 (2014).

32 Satake, S. *et al.* Direct and indirect effects of insulin on glucose uptake and storage by the liver. *Diabetes* **51**, 1663-1671 (2002).

33 Lauro, D. *et al.* Impaired glucose tolerance in mice with a targeted impairment of insulin action in muscle and adipose tissue. *Nature genetics* **20**, 294-298 (1998).

34 Rodnick, K. J., Haskell, W. L., Swislocki, A. L., Foley, J. E. & Reaven, G. M. Improved insulin action in muscle, liver, and adipose tissue in physically trained human subjects. *American Journal of Physiology-Endocrinology And Metabolism* **253**, E489-E495 (1987).

35 Hohlweg, A. *et al.* Hormonal effects on amino acids and related compounds in plasma, amniotic fluid, and allantoic fluid of the chicken embryo. *General and comparative endocrinology* **114**, 378-386 (1999).

36 Meshkani, R. & Adeli, K. Hepatic insulin resistance, metabolic syndrome and cardiovascular disease. *Clinical biochemistry* **42**, 1331-1346 (2009).

37 Malmström, R. *et al.* Defective regulation of triglyceride metabolism by insulin in the liver in NIDDM. *Diabetologia* **40**, 454-462 (1997).

38 Van, W. S. & Lanckmans, S. Liver disturbances in obesity and diabetes mellitus. *International journal of obesity and related metabolic disorders: journal of the International Association for the Study of Obesity* **19**, S27-36 (1995).

39 Romina Lomonaco, M. Non-alcoholic fatty liver disease (NAFLD) in diabetes: distraction or impending disaster? *Evidence-based Management of Diabetes*, 383 (2012).

40 Satapati, S. *et al.* Elevated TCA cycle function in the pathology of diet-induced hepatic insulin resistance and fatty liver. *Journal of lipid research* **53**, 1080-1092 (2012).

41 Guo, Z., Li, M., Han, B. & Qi, X. Association of non-alcoholic fatty liver disease with thyroid function: A systematic review and meta-analysis. *Digestive and Liver Disease* (2018).

42 Lomonaco, R., Sunny, N. E., Bril, F. & Cusi, K. Nonalcoholic fatty liver disease: current issues and novel treatment approaches. *Drugs* **73**, 1-14 (2013).

43 Neuschwander-Tetri, B. A. Hepatic lipotoxicity and the pathogenesis of nonalcoholic steatohepatitis: the central role of nontriglyceride fatty acid metabolites. *Hepatology* **52**, 774-788 (2010).

44 Lomonaco, R. *et al.* Metabolic impact of nonalcoholic steatohepatitis in obese patients with type 2 diabetes. *Diabetes care* **39**, 632-638 (2016).

45 Farrell, G. C. & Larter, C. Z. Nonalcoholic fatty liver disease: from steatosis to cirrhosis. *Hepatology* **43**, S99-S112 (2006).

46 Buzzetti, E., Pinzani, M. & Tsochatzis, E. A. The multiple-hit pathogenesis of non-alcoholic fatty liver disease (NAFLD). *Metabolism* **65**, 1038-1048, doi:10.1016/j.metabol.2015.12.012 (2016).

47 Gastaldelli, A. *et al.* Relationship between hepatic/visceral fat and hepatic insulin resistance in nondiabetic and type 2 diabetic subjects. *Gastroenterology* **133**, 496-506 (2007).

48 Strawford, A., Antelo, F., Christiansen, M. & Hellerstein, M. Adipose tissue triglyceride turnover, de novo lipogenesis, and cell proliferation in humans measured with 2H2O. *American Journal of Physiology-Endocrinology and Metabolism* **286**, E577-E588 (2004).

49 Perry, R. J., Samuel, V. T., Petersen, K. F. & Shulman, G. I. The role of hepatic lipids in hepatic insulin resistance and type 2 diabetes. *Nature* **510**, 84 (2014).

50 Turrens, J. F., Alexandre, A. & Lehninger, A. L. Ubisemiquinone is the electron donor for superoxide formation by complex III of heart mitochondria.

Arch Biochem Biophys **237**, 408-414, doi:10.1016/0003-9861(85)90293-0 (1985).

51 Genova, M. L. *et al.* The site of production of superoxide radical in mitochondrial Complex I is not a bound ubisemiquinone but presumably iron–sulfur cluster N2. *FEBS letters* **505**, 364-368 (2001).

52 Kushnareva, Y., Murphy, A. N. & Andreyev, A. Complex I-mediated reactive oxygen species generation: modulation by cytochrome c and NAD (P)+ oxidation–reduction state. *Biochemical Journal* **368**, 545-553 (2002).

53 Rimessi, A., Previati, M., Nigro, F., Wieckowski, M. R. & Pinton, P. Mitochondrial reactive oxygen species and inflammation: Molecular mechanisms, diseases and promising therapies. *Int J Biochem Cell Biol* **81**, 281-293, doi:10.1016/j.biocel.2016.06.015 (2016).

54 Takeuchi, O. & Akira, S. Pattern recognition receptors and inflammation. *Cell* **140**, 805-820 (2010).

55 Zhou, R., Yazdi, A. S., Menu, P. & Tschopp, J. A role for mitochondria in NLRP3 inflammasome activation. *Nature* **469**, 221-225 (2011).

56 Zhang, Q. *et al.* Circulating mitochondrial DAMPs cause inflammatory responses to injury. *Nature* **464**, 104-107 (2010).

57 Yu, J. *et al.* Inflammasome activation leads to Caspase-1–dependent mitochondrial damage and block of mitophagy. *Proceedings of the National Academy of Sciences* **111**, 15514-15519 (2014).

58 Shi, H. *et al.* TLR4 links innate immunity and fatty acid–induced insulin resistance. *The Journal of clinical investigation* **116**, 3015-3025 (2006).

59 Cherian, G. Nutrition and metabolism in poultry: role of lipids in early diet. *Journal of animal science and biotechnology* **6**, 28 (2015).

60 Moran, E. T., Jr. Nutrition of the Developing Embryo and Hatchling1. *Poultry Science* **86**, 1043-1049, doi:10.1093/ps/86.5.1043 (2007).

61 Nangsuay, A., Meijerhof, R., Ruangpanit, Y., Kemp, B. & Van den Brand, H. Energy utilization and heat production of embryos from eggs originating from young and old broiler breeder flocks. *Poultry science* **92**, 474-482 (2013).

62 Hicks, J. A., Porter, T. E. & Liu, H.-C. Identification of microRNAs controlling hepatic mRNA levels for metabolic genes during the metabolic transition from embryonic to posthatch development in the chicken. *BMC genomics* **18**, 687 (2017).

63 Zaefarian, F., Abdollahi, M. R., Cowieson, A. & Ravindran, V. Avian liver: The forgotten organ. *Animals* **9**, 63 (2019).

64 Romanoff, A. L. & Romanoff, A. J. The avian egg. *The avian egg.* (1949).

65 D'Alba, L. *et al.* What does the eggshell cuticle do? A functional comparison of avian eggshell cuticles. *Physiological and Biochemical Zoology* **90**, 588-599 (2017).

66 Li-Chan, E. C., Powrie, W. D. & Nakai, S. The chemistry of eggs and egg products. *Egg science and technology* **4**, 105-175 (1995).

67 Sunny, N. & Bequette, B. Gluconeogenesis differs in developing chick embryos derived from small compared with typical size broiler breeder eggs. *Journal of animal science* **88**, 912-921 (2010).

68 De Oliveira, J., Uni, Z. & Ferket, P. Important metabolic pathways in poultry embryos prior to hatch. *World's poultry science journal* **64**, 488-499 (2008).

69 Lu, J., McMurtry, J. & Coon, C. Developmental changes of plasma insulin, glucagon, insulin-like growth factors, thyroid hormones, and glucose concentrations in chick embryos and hatched chicks. *Poultry science* **86**, 673-683 (2007).

70 Hazelwood, R. L. Endocrine control of avian carbohydrate metabolism. *Poultry science* **50**, 9-18 (1971).

71 Pearce, J. Carbohydrate metabolism in the domestic fowl. *Proceedings of the Nutrition Society* **30**, 254-259 (1971).

72 Sunny, N., Adamany, J., Owens, S. & Bequette, B. The use of glutamine and glutamate for gluconeogenesis and non-essential amino acid synthesis in late term chicken embryos. *PUBLICATION-EUROPEAN ASSOCIATION FOR ANIMAL PRODUCTION* **124**, 475 (2007).

73 Sunny, N. & Bequette, B. Glycerol is a major substrate for glucose, glycogen, and nonessential amino acid synthesis in late-term chicken embryos. *Journal of animal science* **89**, 3945-3953 (2011).

74 Sato, M., Tachibana, T. & Furuse, M. Heat production and lipid metabolism in broiler and layer chickens during embryonic development. *Comparative Biochemistry and Physiology Part A: Molecular & Integrative Physiology* **143**, 382-388 (2006).

75 Nangsuay, A. *et al.* Differences in egg nutrient availability, development, and nutrient metabolism of broiler and layer embryos. *Poultry Science* **94**, 415-423, doi:10.3382/ps/pev007 (2015).

76 Speake, B. K., Noble, R. C. & Murray, A. M. The utilization of yolk lipids by the chick embryo. *World's Poultry Science Journal* **54**, 319-334 (1998).

77 Nangsuay, A., Ruangpanit, Y., Meijerhof, R. & Attamangkune, S. Yolk absorption and embryo development of small and large eggs originating from young and old breeder hens. *Poultry science* **90**, 2648-2655 (2011).

78 Speake, B. K., Murray, A. M. & Noble, R. C. Transport and transformations of yolk lipids during development of the avian embryo. *Progress in Lipid Research (United Kingdom)* (1998).

79 Rutter, G. A., da Silva Xavier, G. & Leclerc, I. Roles of 5′-AMP-activated protein kinase (AMPK) in mammalian glucose homoeostasis. *Biochemical Journal* **375**, 1-16 (2003).

80 Wu, G. & Li, Z. Rapid clearance of circulating protein by early chicken embryo blood cells. *Journal of Experimental Biology* **212**, 2176-2182 (2009).

81 Ohta, Y., Tsushima, N., Koide, K., Kidd, M. & Ishibashi, T. Effect of amino acid injection in broiler breeder eggs on embryonic growth and hatchability of chicks. *Poultry Science* **78**, 1493-1498 (1999).

82 Hu, Q., Agarwal, U. & Bequette, B. Gluconeogenesis, non-essential amino acid synthesis and substrate partitioning in chicken embryos during later development. *Poultry science* **96**, 414-424 (2016).

83 Noy, Y. & Sklan, D. Yolk utilisation in the newly hatched poult. *British poultry science* **39**, 446-451 (1998).

84 Swennen, Q. *et al.* Effect of macronutrient ratio of the pre-starter diet on broiler performance and intermediary metabolism. *Journal of animal physiology and animal nutrition* **94**, 375-384 (2010).

85 Lilburn, M. Practical aspects of early nutrition for poultry. *Journal of Applied Poultry Research* **7**, 420-424 (1998).

86 Shinde Tamboli, A. S. *et al.* Delayed post-hatch feeding affects the performance and immunocompetence differently in male and female broiler chickens. *Journal of Applied Animal Research* **46**, 306-313, doi:10.1080/09712119.2017.1299739 (2018).

87 Sklan, D. Fat and carbohydrate use in posthatch chicks. *Poultry Science* **82**, 117-122, doi:10.1093/ps/82.1.117 (2003).

88 Lamot, D. M. *et al.* Effects of moment of hatch and feed access on chicken development. *Poultry Science* **93**, 2604-2614, doi:10.3382/ps.2014-04123 (2014).

89 De pablo, F. *et al.* Insulin-like growth factor-I and insulin as growth and differentiation factors in chicken embryogenesis. *Poultry science* **70**, 1790-1796 (1991).

90 Picardo, M. & Dickson, A. Hormonal regulation of glycogen metabolism in hepatocyte suspensions isolated from chicken embryos. *Comparative biochemistry and physiology. B, Comparative biochemistry* **71**, 689-693 (1982).

91 Hazelwood, R. (Academic Press: San Diego, CA, 2000).

92 Elrick, H., Konigsberg, I. & Arai, Y. Effect of glucagon on growth of chick embryo. *Proceedings of the Society for Experimental Biology and Medicine* **97**, 542-544 (1958).

93 Jenkins, S. & Porter, T. Ontogeny of the hypothalamo–pituitary–adrenocortical axis in the chicken embryo: a review. *Domestic animal endocrinology* **26**, 267-275 (2004).

94 MASHALY, M. M. Effect of exogenous corticosterone on chicken embryonic development. *Poultry Science* **70**, 371-374 (1991).

95 Kubrusly, R. C. C. *et al.* Norepinephrine acts as D1-dopaminergic agonist in the embryonic avian retina: Late expression of β1-adrenergic receptor shifts norepinephrine specificity in the adult tissue. *Neurochemistry international* **50**, 211-218 (2007).

96 Hazelwood, R. in *Avian Physiology* 303-325 (Springer, 1986).

97 Zhang, L. *et al.* Changes of plasma growth hormone, insulin-like growth factors-I, thyroid hormones, and testosterone concentrations in embryos and broiler chickens incubated under monochromatic green light. *Italian Journal of Animal Science* **13**, 3266 (2014).

98 ROMSOS, D. R. & LEVEILLE, G. A. in *Advances in lipid research* Vol. 12 97-146 (Elsevier, 1974).

100 Feller, D. METABOLISM OF ADIPOSE TISSUE I. INCORPORATION OF ACETATE CARBON INTO LIPIDES BY SLICES OF ADIPOSE TISSUE. *Journal of Biological Chemistry* **206**, 171-180 (1954).

101 Leveille, G. A. In vivo fatty acid synthesis in adipose tissue and liver of meal-fed rats. *Proceedings of the Society for Experimental Biology and Medicine* **125**, 85-88 (1967).

102 O'hea, E. & Leveille, G. Lipid biosynthesis and transport in the domestic chick (Gallu domesticus). *Comparative Biochemistry and Physiology* **30**, 149-159 (1969).

103 Hermier, D. Lipoprotein metabolism and fattening in poultry. *The Journal of nutrition* **127**, 805S-808S (1997).

104 Shrago, E., Glennon, J. A. & Gordon, E. S. Comparative aspects of lipogenesis in mammalian tissues. *Metabolism* **20**, 54-62 (1971).

105 Gibson, W. & Nalbandov, A. Lipolysis and lipogenesis in liver and adipose tissue of hypophysectomized cockerels. *American Journal of Physiology-Legacy Content* **211**, 1352-1356 (1966).

106 O'hea, E. & Leveille, G. Lipogenesis in isolated adipose tissue of the domestic chick (Gallus domesticus). *Comparative biochemistry and physiology* **26**, 111-120 (1968).

107 Chen, K., ANDERSON, R. C. & MAZE, N. Susceptibility of birds to insulin as compared with mammals. *Journal of Pharmacology and Experimental Therapeutics* **84**, 74-77 (1945).

108 Langslow, D., Butler, E., Hales, C. & Pearson, A. The response of plasma insulin, glucose and non-esterified fatty acids to various hormones, nutrients and drugs in the domestic fowl. *Journal of Endocrinology* **46**, 243-260 (1970).

109 Jungas, R. L. & Ball, E. G. Studies on the metabolism of adipose tissue. XII. The effects of insulin and epinephrine on free fatty acid and glycerol production in the presence and absence of glucose. *Biochemistry* **2**, 383-388 (1963).

110 Langslow, D. & Hales, C. role of the endocrine pancreas and catecholamines in the control of carbohydrate and lipid metabolism. *Bell, David James Physiology and Biochemistry of the Domestic Fowl* (1971).

111 Heald, P., McLachlan, P. & Rookledge, K. The effects of insulin, glucagon and adrenocorticotrophic hormone on the plasma glucose and free fatty acids of the domestic fowl. *Journal of Endocrinology* **33**, 83-95 (1965).

112 Goodridge, A. G. Regulation of Fatty Acid Synthesis in the Liver of Prenatal and Early Postnatal Chicks HEPATIC CONCENTRATIONS OF INDIVIDUAL FREE FATTY ACIDS AND OTHER METABOLITES. *Journal of Biological Chemistry* **248**, 1939-1945 (1973).

113 Kompiang, I. P., Bensadoun, A. & Yang, M. Effect of an anti-lipoprotein lipase serum on plasma triglyceride removal. *Journal of lipid research* **17**, 498-505 (1976).

114 Wu, G. Functional amino acids in nutrition and health. *Amino Acids* **45**, 407-411, doi:10.1007/s00726-013-1500-6 (2013).

115 Wilcox, G. Insulin and insulin resistance. *Clinical biochemist reviews* **26**, 19 (2005).

116 Gannon, N. P., Schnuck, J. K. & Vaughan, R. A. BCAA Metabolism and Insulin Sensitivity - Dysregulated by Metabolic Status? *Mol Nutr Food Res* **62**, e1700756, doi:10.1002/mnfr.201700756 (2018).

117 Macotela, Y. *et al.* Dietary leucine-an environmental modifier of insulin resistance acting on multiple levels of metabolism. *PloS one* **6**, e21187 (2011).

118 Li, X. *et al.* Chronic leucine supplementation increases body weight and insulin sensitivity in rats on high-fat diet likely by promoting insulin signaling in insulin-target tissues. *Molecular nutrition & food research* **57**, 1067-1079 (2013).

119 Rozengurt, E., Soares, H. P. & Sinnet-Smith, J. Suppression of feedback loops mediated by PI3K/mTOR induces multiple overactivation of compensatory pathways: an unintended consequence leading to drug resistance. *Mol Cancer Ther* **13**, 2477-2488, doi:10.1158/1535-7163.MCT-14-0330 (2014).

120 Huffman, K. M. *et al.* Relationships between circulating metabolic intermediates and insulin action in overweight to obese, inactive men and women. *Diabetes care* **32**, 1678-1683 (2009).

121 Harris, R. A., Joshi, M., Jeoung, N. H. & Obayashi, M. Overview of the Molecular and Biochemical Basis of Branched-Chain Amino Acid Catabolism. *The Journal of Nutrition* **135**, 1527S-1530S, doi:10.1093/jn/135.6.1527S (2005).

122 Harris, R. A., Joshi, M. & Jeoung, N. H. Mechanisms responsible for regulation of branched-chain amino acid catabolism. *Biochemical and biophysical research communications* **313**, 391-396 (2004).

123 Ichihara, A. & Takahashi, H. Transaminases of branched-chain amino acids: V. Activity change in developing and regenerating rat liver. *Biochimica et Biophysica Acta (BBA)-Enzymology* **167**, 274-279 (1968).

124 Shinnick, F. & Harper, A. Branched-chain amino acid oxidation by isolated rat tissue preparations. *Biochimica et Biophysica Acta (BBA)-General Subjects* **437**, 477-486 (1976).

125 Harper, A., Miller, R. & Block, K. Branched-chain amino acid metabolism. *Annual review of nutrition* **4**, 409-454 (1984).

126 Hutson, S., Wallin, R. & Hall, T. Identification of mitochondrial branched chain aminotransferase and its isoforms in rat tissues. *Journal of Biological Chemistry* **267**, 15681-15686 (1992).

127 Suryawan, A. *et al.* A molecular model of human branched-chain amino acid metabolism. *The American journal of clinical nutrition* **68**, 72-81 (1998).

128 Zhou, M. *et al.* Targeting BCAA catabolism to treat obesity-associated insulin resistance. *Diabetes* **68**, 1730-1746 (2019).

129 Wang, J. H., Byun, J. & Pennathur, S. in *Seminars in nephrology.* 500-511 (Elsevier).

130 Tolstikov, V. V. in *Micro and Nano Technologies in Bioanalysis* 343-353 (Springer, 2009).

131 Zhang, A., Sun, H., Wang, P., Han, Y. & Wang, X. Modern analytical techniques in metabolomics analysis. *Analyst* **137**, 293-300 (2012).

132 Lee, D. Y., Bowen, B. P. & Northen, T. R. Mass spectrometry—based metabolomics, analysis of metabolite-protein interactions, and imaging. *Biotechniques* **49**, 557-565 (2010).

133 Kendall, C. & Doctor, D. Stable isotope applications in hydrologic studies. *Treatise on geochemistry* **5**, 605 (2003).

134 Katz, J., Lee, W., Wals, P. & Bergner, E. Studies of glycogen synthesis and the Krebs cycle by mass isotopomer analysis with [U-13C] glucose in rats. *Journal of Biological Chemistry* **264**, 12994-13004 (1989).

135 Klein, S. & Heinzle, E. Isotope labeling experiments in metabolomics and fluxomics. *Wiley Interdisciplinary Reviews: Systems Biology and Medicine* **4**, 261-272 (2012).

136 Fernandez, C. A., Des Rosiers, C., Previs, S. F., David, F. & Brunengraber, H. Correction of 13C mass isotopomer distributions for natural stable isotope abundance. *Journal of Mass Spectrometry* **31**, 255-262 (1996).

137 Comte, B. *et al.* A 13C mass isotopomer study of anaplerotic pyruvate carboxylation in perfused rat hearts. *Journal of Biological Chemistry* **272**, 26125-26131 (1997).

138 Poirier, M. *et al.* Probing the link between citrate and malonyl-CoA in perfused rat hearts. *American Journal of Physiology-Heart and Circulatory Physiology* **283**, H1379-H1386 (2002).

139 Reeds, P. *et al.* Integration of amino acid and carbon intermediary metabolism: studies with uniformly labeled tracers and mass isotopomer analysis. *European journal of pediatrics* 156, S50-S58 (1997).

140. Mantovani, A., Byrne, C. D., Bonora, E. & Targher, G. Nonalcoholic Fatty Liver Disease and Risk of Incident Type 2 Diabetes: A Meta-analysis. *Diabetes Care* **41**, 372-382 (2018).

141 Rinella, M. E. Nonalcoholic fatty liver disease: a systematic review. *JAMA* **313**, 2263-2273 (2015).

142 Lambert, J. E., Ramos-Roman, M. A., Browning, J. D. & Parks, E. J. Increased de novo lipogenesis is a distinct characteristic of individuals with nonalcoholic fatty liver disease. *Gastroenterology* **146**, 726-735 (2014).

143 Garcia-Berumen, C. I. *et al.* The severity of rat liver injury by fructose and high fat depends on the degree of respiratory dysfunction and oxidative stress induced in mitochondria. *Lipids Health Dis* **18**, 78 (2019).

144 Begriche, K., Massart, J., Robin, M. A., Bonnet, F. & Fromenty, B. Mitochondrial adaptations and dysfunctions in nonalcoholic fatty liver disease. *Hepatology* **58**, 1497-1507 (2013).

145 Koliaki, C. *et al.* Adaptation of hepatic mitochondrial function in humans with non-alcoholic fatty liver is lost in steatohepatitis. *Cell Metab* **21**, 739-746 (2015).

146 Sunny, N. E. *et al.* Progressive adaptation of hepatic ketogenesis in mice fed a high-fat diet. *Am J Physiol Endocrinol Metab* **298**, E1226-1235 (2010).

147 Cotter, D. G. *et al.* Ketogenesis prevents diet-induced fatty liver injury and hyperglycemia. *J Clin Invest* **124**, 5175-5190 (2014).

148 Fletcher, J. A. *et al.* Impaired ketogenesis and increased acetyl-CoA oxidation promote hyperglycemia in human fatty liver. *JCI Insight* **5** (2019).

149 Schmid, A. I. *et al.* Liver ATP synthesis is lower and relates to insulin sensitivity in patients with type 2 diabetes. *Diabetes Care* **34**, 448-453 (2011).

150 Satapati, S. *et al.* Mitochondrial metabolism mediates oxidative stress and inflammation in fatty liver. *The Journal of clinical investigation* **126**, 1605-1605 (2016).

151 Jelenik, T. *et al.* Mechanisms of Insulin Resistance in Primary and Secondary Nonalcoholic Fatty Liver. *Diabetes* **66**, 2241-2253 (2017).

152 Cappel, D. A. *et al.* Pyruvate-Carboxylase-Mediated Anaplerosis Promotes Antioxidant Capacity by Sustaining TCA Cycle and Redox Metabolism in Liver. *Cell Metab* **29**(6), 1291-1305 (2019).

153 Apostolopoulou, M. *et al.* Specific hepatic sphingolipids relate to insulin resistance, oxidative stress, and inflammation in nonalcoholic steatohepatitis. *Diabetes Care* **41**, 1235-1243 (2018).

154 Morris, E. M. *et al.* Aerobic capacity and hepatic mitochondrial lipid oxidation alters susceptibility for chronic high-fat diet-induced hepatic steatosis. *Am J Physiol Endocrinol Metab* **311**, E749-E760 (2016).

155 Smith, C. M., Bryla, J. & Williamson, J. R. Regulation of mitochondrial α-ketoglutarate metabolism by product inhibition at α-ketoglutarate dehydrogenase. *Journal of Biological Chemistry* **249**, 1497-1505 (1974).

156 Wu, N. *et al.* Alpha-Ketoglutarate: Physiological Functions and Applications. *Biomolecules & therapeutics* **24**, 1-8 (2016).

157 Holland, W. L. *et al.* Lipid mediators of insulin resistance. *Nutrition reviews* **65**, S39-S46 (2007).

158 Erion, D. M. & Shulman, G. I. Diacylglycerol-mediated insulin resistance. *Nat Med* **16**, 400-402 (2010).

159 García-Ruiz, C., Colell, A., Morales, A., Kaplowitz, N. & Fernández-Checa, J. C. Role of oxidative stress generated from the mitochondrial electron transport chain and mitochondrial glutathione status in loss of mitochondrial function and activation of transcription factor nuclear factor-kappa B: studies with isolated mitochondria and rat hepatocytes. *Molecular pharmacology* **48**, 825-834 (1995).

160 Zitka, O. *et al.* Redox status expressed as GSH:GSSG ratio as a marker for oxidative stress in paediatric tumour patients. *Oncol Lett* **4**, 1247-1253 (2012).

161 Hu, J., Dong, L. & Outten, C. E. The redox environment in the mitochondrial intermembrane space is maintained separately from the cytosol and matrix. *J Biol Chem* **283**, 29126-29134 (2008).

162 Szczepaniak, L. S. *et al.* Magnetic resonance spectroscopy to measure hepatic triglyceride content: prevalence of hepatic steatosis in the general population. *Am J Physiol Endocrinol Metab* **288**, E462-468 (2005).

163 Patel, M. S. & Owen, O. E. Lipogenesis from ketone bodies in rat brain. Evidence for conversion of acetoacetate into acetyl-coenzyme A in the cytosol. *The Biochemical journal* **156**, 603-607 (1976).

164 Endemann, G., Goetz, P. G., Edmond, J. & Brunengraber, H. Lipogenesis from ketone bodies in the isolated perfused rat liver. Evidence for the cytosolic activation of acetoacetate. *Journal of Biological Chemistry* **257**, 3434-3440 (1982).

165 Puchalska, P. & Crawford, P. A. Multi-dimensional roles of ketone bodies in fuel metabolism, signaling, and therapeutics. *Cell metabolism* **25**, 262-284 (2017).

166 Freed, L. E., Endemann, G., Tomera, J. F., Gavino, V. C. & Brunengraber, H. Lipogenesis from ketone bodies in perfused livers from streptozocin-induced diabetic rats. *Diabetes* **37**, 50-55 (1988).

167 Nakamura, S. *et al.* Palmitate induces insulin resistance in H4IIEC3 hepatocytes through reactive oxygen species produced by mitochondria. *J Biol Chem* **284**, 14809-14818 (2009).

168 Mailloux, R. J. *et al.* The tricarboxylic acid cycle, an ancient metabolic network with a novel twist. *PLoS One* **2**, e690 (2007).

169 Puntel, R. L. *et al.* Antioxidant properties of Krebs cycle intermediates against malonate pro-oxidant activity in vitro: a comparative study using the colorimetric method and HPLC analysis to determine malondialdehyde in rat brain homogenates. *Life Sci* **81**, 51-62 (2007).

170 Puntel, R. L., Nogueira, C. W. & Rocha, J. B. Krebs cycle intermediates modulate thiobarbituric acid reactive species (TBARS) production in rat brain in vitro. *Neurochem Res* **30**, 225-235 (2005).

171 Liu, S., He, L. & Yao, K. The Antioxidative Function of Alpha-Ketoglutarate and Its Applications. *Biomed Res Int* **2018**, 3408467 (2018).

172 Brand, M. D. & Nicholls, D. G. Assessing mitochondrial dysfunction in cells. *The Biochemical journal* **435**, 297-312 (2011).

173 Sunny, N. E. & Bequette, B. J. Glycerol is a major substrate for glucose, glycogen, and nonessential amino acid synthesis in late-term chicken embryos1,2,3. *Journal of Animal Science* **89**, 3945-3953 (2011).

174 Kalavalapalli, S. *et al.* Pioglitazone improves hepatic mitochondrial function in a mouse model of nonalcoholic steatohepatitis. *Am J Physiol Endocrinol Metab* **315**, E163-E173 (2018).

175 Lerin, C. *et al.* Defects in muscle branched-chain amino acid oxidation contribute to impaired lipid metabolism. *Molecular metabolism* **5**, 926-936 (2016).

176 Bai, J., Greene, E., Li, W., Kidd, M. T. & Dridi, S. Branched-chain amino acids modulate the expression of hepatic fatty acid metabolism-related genes in female broiler chickens. *Molecular nutrition & food research* **59**, 1171-1181 (2015).

177 Muyyarikkandy, M. S. *et al.* Branched chain amino acids and carbohydrate restriction exacerbate ketogenesis and hepatic mitochondrial oxidative dysfunction during NAFLD. *The FASEB Journal* **34**, 14832-14849 (2020).

178 Fabbrini, E., Sullivan, S. & Klein, S. Obesity and nonalcoholic fatty liver disease: biochemical, metabolic, and clinical implications. *Hepatology* **51**, 679-689 (2010).

179 Krebs, H. & Veech, R. Equilibrium relations between pyridine nucleotides and adenine nucleotides and their roles in the regulation of metabolic processes. *Advances in enzyme regulation* **7**, 397-413 (1969).

180 Go, S., Kramer, T. T., Verhoeven, A. J., Elferink, R. P. O. & Chang, J.-C. The extracellular lactate-to-pyruvate ratio modulates the sensitivity to oxidative stress-induced apoptosis via the cytosolic NADH/NAD+ redox state. *Apoptosis* **26**, 38-51 (2021).

181 Forrester, S. J., Kikuchi, D. S., Hernandes, M. S., Xu, Q. & Griendling, K. K. Reactive oxygen species in metabolic and inflammatory signaling. *Circulation research* **122**, 877-902 (2018).

182 Moore, M. C., Coate, K. C., Winnick, J. J., An, Z. & Cherrington, A. D. Regulation of hepatic glucose uptake and storage in vivo. *Advances in nutrition* **3**, 286-294 (2012).

183 Moore, M. C. *et al.* Nonesterified fatty acids and hepatic glucose metabolism in the conscious dog. *Diabetes* **53**, 32-40 (2004).

184 Palmquist, D., Learn, D. & Baker, N. Re-evaluation of effects of meal feeding on lipogenic activation by glucose in rats. *The Journal of nutrition* **107**, 502-509 (1977).

185 Mayes, P. & Felts, J. Regulation of fat metabolism in the liver. *Nature* **215**, 716-718 (1967).

186 Ratziu, V. *et al.* Elafibranor, an agonist of the peroxisome proliferator− activated receptor− α and− δ, induces resolution of nonalcoholic steatohepatitis without fibrosis worsening. *Gastroenterology* **150**, 1147-1159. e1145 (2016).

187 Anderson, E. J. *et al.* Mitochondrial H 2 O 2 emission and cellular redox state link excess fat intake to insulin resistance in both rodents and humans. *The Journal of clinical investigation* **119**, 573-581 (2009).

188 Circu, M. L. & Aw, T. Y. Reactive oxygen species, cellular redox systems, and apoptosis. *Free Radical Biology and Medicine* **48**, 749-762 (2010).

189 Kamata, H. & Hirata, H. Redox regulation of cellular signalling. *Cellular signalling* **11**, 1-14 (1999).

190 Menon, S. & Goswami, P. A redox cycle within the cell cycle: ring in the old with the new. *Oncogene* **26**, 1101-1109 (2007).

191 Gambino, R., Musso, G. & Cassader, M. Redox balance in the pathogenesis of nonalcoholic fatty liver disease: mechanisms and therapeutic opportunities. *Antioxidants & redox signaling* **15**, 1325-1365 (2011).

192 Spahis, S., Delvin, E., Borys, J.-M. & Levy, E. Oxidative stress as a critical factor in nonalcoholic fatty liver disease pathogenesis. *Antioxidants & redox signaling* **26**, 519-541 (2017).

193 Boudaba, N. *et al.* AMPK Re-Activation Suppresses Hepatic Steatosis but its Downregulation Does Not Promote Fatty Liver Development. *EBioMedicine* **28**, 194-209, doi:https://doi.org/10.1016/j.ebiom.2018.01.008 (2018).

194 Li, Y. *et al.* AMPK phosphorylates and inhibits SREBP activity to attenuate hepatic steatosis and atherosclerosis in diet-induced insulin-resistant mice. *Cell metabolism* **13**, 376-388 (2011).

195 Ruderman, N. B., Carling, D., Prentki, M. & Cacicedo, J. M. AMPK, insulin resistance, and the metabolic syndrome. *The Journal of clinical investigation* **123**, 2764-2772 (2013).

196 Hawley, S. A., Gadalla, A. E., Olsen, G. S. & Hardie, D. G. The antidiabetic drug metformin activates the AMP-activated protein kinase cascade via an adenine nucleotide-independent mechanism. *Diabetes* **51**, 2420-2425 (2002).

197 Kim, J., Yang, G., Kim, Y., Kim, J. & Ha, J. AMPK activators: mechanisms of action and physiological activities. *Exp Mol Med* **48**, e224-e224 (2016).

198 Zhou, G. *et al.* Role of AMP-activated protein kinase in mechanism of metformin action. *The Journal of clinical investigation* **108**, 1167-1174 (2001).

199 Garcia, D. *et al.* Genetic liver-specific AMPK activation protects against diet-induced obesity and NAFLD. *Cell reports* **26**, 192-208. e196 (2019).

200 Surugihalli, C. *et al.* Hepatic mitochondrial oxidative metabolism and lipogenesis synergistically adapt to mediate healthy embryonic-to-neonatal transition in chicken. *Scientific reports* **9**, 1-14 (2019).